Characterisation of ParH, a Novel Protein for Chromosome Organisation in the Filamentous Bacterium *Streptomyces coelicolor*

Mashael Naif Alanazi

100227843

A thesis submitted for the degree of Doctor of Philosophy

University of East Anglia

School of Biological Sciences

March 2023

Abstract

The replication and segregation of chromosomes are essential processes during bacterial cell division to ensure that each new cell receives a complete set of chromosomes. Chromosome segregation in bacteria is often controlled by the ATP-ase ParA and the DNA binding protein ParB. The dynamic interaction between ParA and ParB governs movement and positioning of the chromosomal origin of replication (*ori*) within the cell. In the filamentous bacterium *Streptomyces coelicolor,* the ParAB proteins have been shown to control both chromosome organisation and septum placement during the synchronous cell division event of sporulation. Intriguingly, both ParA and ParB were shown to interact with proteins involved in polar growth.

In addition to ParAB there are several ParA-like proteins in *S .coelicolor* that have not been fully characterised. One of these proteins, designated ParH, has 49% identity to Soj and 30% identity to MinD of *Bacillus subtilis.* The ParH is presumably co-translated with the downstream gene, which encodes a small hypothetical protein (Hyp). Through bioinformatic analysis, homologues of ParH and Hyp were found in numerous *Actinobacteria*. The knockout mutant of *parH* shows delayed sporulation and irregularities in septum placement suggesting that ParH might also contribute to correct chromosome organisation in *Streptomyces*.

In this work, we were building on preliminary in *vivo* data generated previously in our lab. Our aim was to complement the in *vivo* experiments with the in *vitro* characterisation of ParH and some of its interacting partners and to compare the gene expression pattern of the *parH* mutant compared to the wild type strain during morphological differentiation on solid media.

Contents

Acknowledgement

Dedicated to my dear father, the person I always wished could be by my side during my academic journey; the one who cleared the path for me and made higher education possible; and the image of whose proud eyes upon my previous degrees is etched in my mind.

To my wonderful mother, whose patience has been unwavering and who provided me with the determination to persevere. To my cherished sisters Ameera, Nouf, and Amjad, and to my brothers, your boundless love and unwavering support have meant the world to me, and I'm grateful for your belief in my aspirations. You are my unsung heroes.

To my cherished friends, thank you for being the source of laughter, encouragement, and companionship that carried me through the challenges of academia. To my best friend, Dina Alshareef, thank you for endless amount of support, love and encouragement, you cheered me up along the whole way.

To my wonderful friends who have supported me within the lab and beyond; Emily Alcock, Kavana Bywater- Brenna, and Gemma Cassettari. And a massive thanks must go to my hero friends in the lab; Daniel Moye, and Stefan Harper. I am so grateful for the time these people have given me throughout the writing up period. To Jude, thank you for all the giggles and fun days filled with lighthearted banter.

Last but certainly not least, to my supervisor; Gabriella Kelemen a big thank you for the support and guidance during my PhD journey in your laboratory.

CHAPTER 1

1. Introduction

1.1 Bacterial cell division

Cell division in bacteria appears quite simple when observed through time-lapse microscopy, a single bacterium turns into two. However, most biological processes are more complicated than they seem on the surface (Mahone and Goley, 2020). In prokaryotes, the process takes place through binary fission, where a single cell divides into two identical cells at a specific stage of cell development (Busiek and Margolin, 2015). In rod-shaped bacteria, the cell envelope layers (cell wall and the membrane) grow until a septum forms at the midpoint between two identical chromosomes. This septum growth is triggered by a multi-protein complex called the divisome, which localises at the division site before septal growth (Harry, 2001). For Gram-negative bacterial cells, the division into two identical daughter cells follows a sequence involving inner membrane invagination, remodeling of the peptidoglycan cell wall, and constriction of the outer membrane (Misra *et al.*, 2018).

Most components of the divisome are conserved across bacteria and can be found in every sequenced bacterial genome, though a small number are specific to the organism. To date, most bacteria studied have varying regulation of molecular processes during cell division. It has been studied in a large number of bacteria including *Escherichia coli, Bacillus subtilis*, *Caulobacter crescentus* and *Mycobacterium tuberculosis* (Nanninga, 1991). Proteins associated with cell division have been known as filamentation temperature sensitive (Fts) according to the filamentation phenotype condition of mutant that lacks them. The process of assembling cell division proteins in a divisome is highly ordered and organised manner (Misra *et al.*, 2018).

1.1.1 FtsZ a key protein for cell division

In most bacteria, many archaea, some chloroplasts, and a few primitive mitochondria, FtsZ shares structural and functional features with 40–50% sequence identity (Tripathy and Sahu, 2019). There are similarities between the three-dimensional structures of some bacterial FtsZ and α- and β- tubulin

(Erickson, 1998). In eukaryotes, tubulin is a crucial component of microtubules. The proteins FtsZ and tubulin are shown to play an important role in maintaining the shape and structure of living cells (Tripathy and Sahu, 2019). The FtsZ protein comprises two distinct enzymatic domains with unique structures. It includes an N-terminal domain linked to a C-terminal tail domain with varying extensions (as shown in Figure 1.1). Within bacterial cells, when FtsZ binds to GTP or GDP, it exists both as monomers and as higher-order polymers. The enzymatic domain consists of two sub-domains, referred to as the N-terminal subdomain and the C-terminal subdomain, separated by the H7 helix. Additionally, the elongated C-terminal domain is connected to the N-terminal enzymatic domain by the H5 helix (Löwe, Van Den Ent and Amos, 2004; Michie and Löwe, 2006). The N-terminal domain contains a nucleotide-binding pocket, while the C-terminal subdomain hosts a GTPase-activating site, which can be positioned between the two monomers (Tripathy and Sahu, 2019).

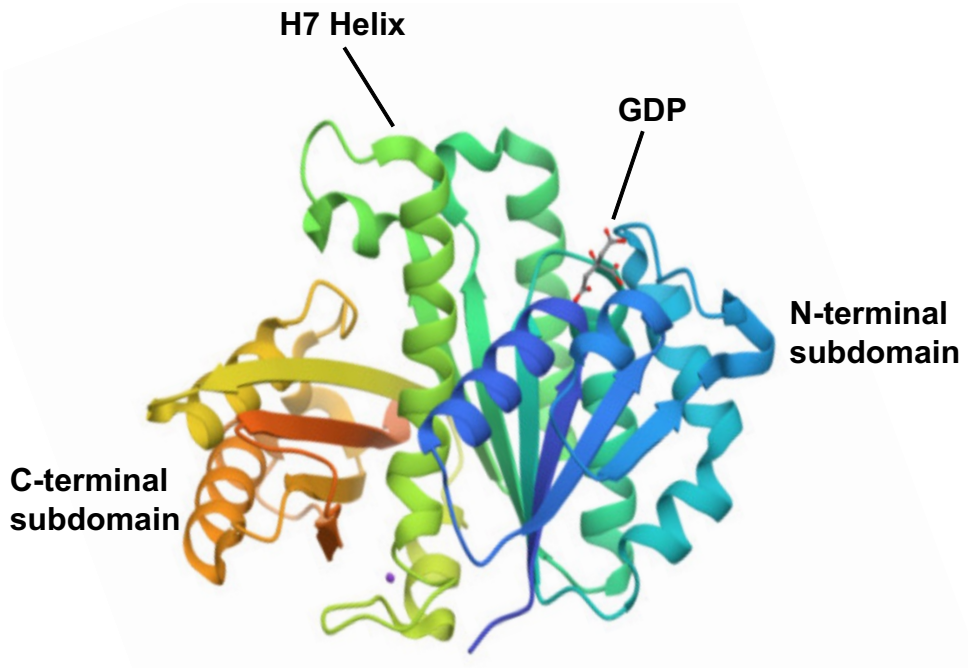

Figure 1.1 Structure of FtsZ of *B. subtilis*

The enzymatic domain of FtsZ consists of two distinct subdomains. On the right, the N-terminal subdomain houses the nucleotide-binding site. On the left, the C-terminal subdomain contains the GTPase activity site. The blue colour represents β-sheet. The H7 helix (highlighted in green) serves as a separator between these two subdomains. Taken from Brown *et al.*, 2008.

Formation of the Z-ring is the earliest event so far identified in bacterial cytokinesis and it is the Z ring that establishes where division will take place as well as transmitting cell division proteins into the nascent septum (Daniel *et al.*, 2006). In essence, FtsZ is a structural homologue of tubulin and, like tubulin, purified FtsZ both binds and hydrolyses GTP. FtsZ's self-assembly into protofilaments comprising a (head-to-tail) FtsZ linear polymer is induced by GTP binding (Mukherjee, Dai and Lutkenhaus, 2006). Lateral association of FtsZ protofilaments creates sheets or bundles, and this bundling can be induced by binding of partner proteins which include ZipA (Erickson, Anderson and Osawa, 2010).

Cell division driven by FtsZ has been studied most widely in *E. coli* where it is possible to divide bacterial cytokinesis into several phases (de Boer, 2010). The initial phase involves assembly of a polymeric FtsZ structure or 'Z ring' where cell division will take place (Bi and Lutkenhaus, 1991). GTP regulates FtsZ polymerisation in which GTP-bound FtsZ leads to the formation of filaments after which hydrolisation of GTP into GDP causes the polymers to disassemble (Figure 1.2) (Erickson, 1998).

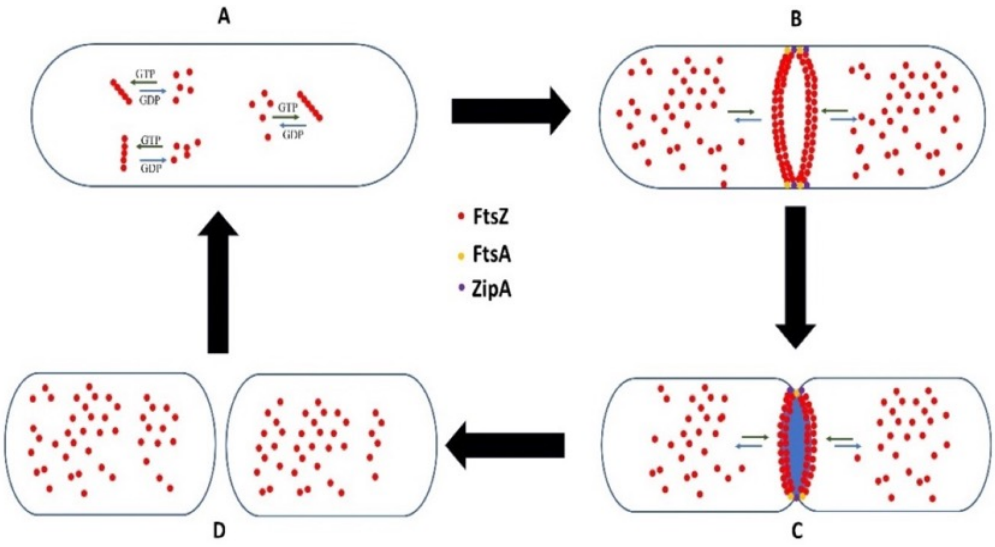

Figure 1.2 FtsZ polymerisation in bacteria

FtsZ monomer polymerised into protofilaments in GTP-bound state (A). At the mid-cell protofilaments laterally contact to form Z-ring, the Z-ring interact with FtsA and ZipA to attach to the cell membrane (B). The contraction of the Z-ring results in invagination of the membranes (C). Z-ring disassembled by GTP hydrolysis and cell division occurred (D). Taken from Sun and Wong, 2018.

After a lag, the Z ring maturation proceeds by recruiting downstream division proteins, of which many are essential for the formation of a complete divisome. Finally, the divisome begins to constrict simultaneously with the synthesis and splitting of septal peptidoglycan, resulting in invagination and division of the bacteria into two daughter cells (de Boer *et al.*, 2009; Fero *et al.*, 2011). Interestingly, within the liposome, it becomes apparent that FtsZ has the capacity to independently form the Z ring and produce force. This finding implies that the involvement of additional proteins is unnecessary for both the assembly process and the generation of force (Osawa, Anderson and Erickson, 2008).

1.1.2 Regulator of Fts Z-ring positioning

The Z-ring's formation is the first step in bacterial cytokinesis and becomes a scaffold for other proteins that link to form a divisome complex (Liu *et al.*, 2015). Extensive research has been conducted to investigate the spatial regulation of Z-ring assembly in three rod-shaped bacteria: *E. coli*, *B. subtilis* and *C. crescentus*. New reports are increasing involving other bacteria (Lutkenhaus, Pichoff and Du, 2012). Regulatory processes acting on the Z ring can be both negative and positive systems (Lutkenhaus, 2007; Monahan *et al.*, 2014). Positive systems include proteins positively regulating formation of the Z ring, while negative systems inhibit Z ring formation close to the poles or over chromosomes (Huang, Durand-Heredia and Janakiraman, 2013). Negative regulation of FtsZ positioning at the site of future cell division is by two separate systems: Min oscillation and nucleoid occlusion (Adams, Wu and Errington, 2015).

1.1.2.1 Min Oscillation System

Z-ring formation at the cell's midpoint is governed by a septum regulatory system (Lutkenhaus, 2007). Min oscillation has been extensively studied in *E. coli* and contributes to Z-ring positioning where division will occur (de Boer and Raskin, 1999). *E. coli* Min system comprises MinC, MinD and MinE proteins, and it is these that determine placement of FtsZ (de Boer, Crossley and Rothfield, 1989; Margolin, 2001). Oscillation causes MinC and MinD to

accumulate at one pole surrounded by MinE ring which, as it moves closer to the pole, releases MinD and MinC which reassemble at the other pole (Figure 1.3) (Hale, Meinhardt and De Boer, 2001; Fu *et al.*, 2012). MinC is an antagonist of FtsZ assembly and inhibits the lateral interactions between FtsZ filaments essential if the Z ring is to assemble with structural integrity (Hu *et al.*, 2002). Recruitment of MinC to the membrane occurs due to a membrane-associated ATPase MinD, which when bound to ATP binds to the membrane by its C-terminus. MinD distribution on the membrane is even and it activates MinC to inhibit FtsZ polymerization close to the cell poles (de Boer, Crossley and Rothfield, 1989; De Boer, Crossley and Rothfield, 1992). MinE regulates this MinCD complex and can locate the Z-ring assembly at the cell's mid-point by stimulating MinD's ATPase activity and by MinD's release from the membrane (Hu *et al.*, 2002). A pool of MinD proteins oscillates rapidly between poles and carries the division inhibiting MinC to dominate the formation of the Z-ring at the cell's mid-point. Continuous pole-to-pole oscillations mean that MinC division inhibitor concentration is at its lowest at the cell's midpoint, so that cells can divide only there (Laloux and Jacobs-Wagner, 2013).

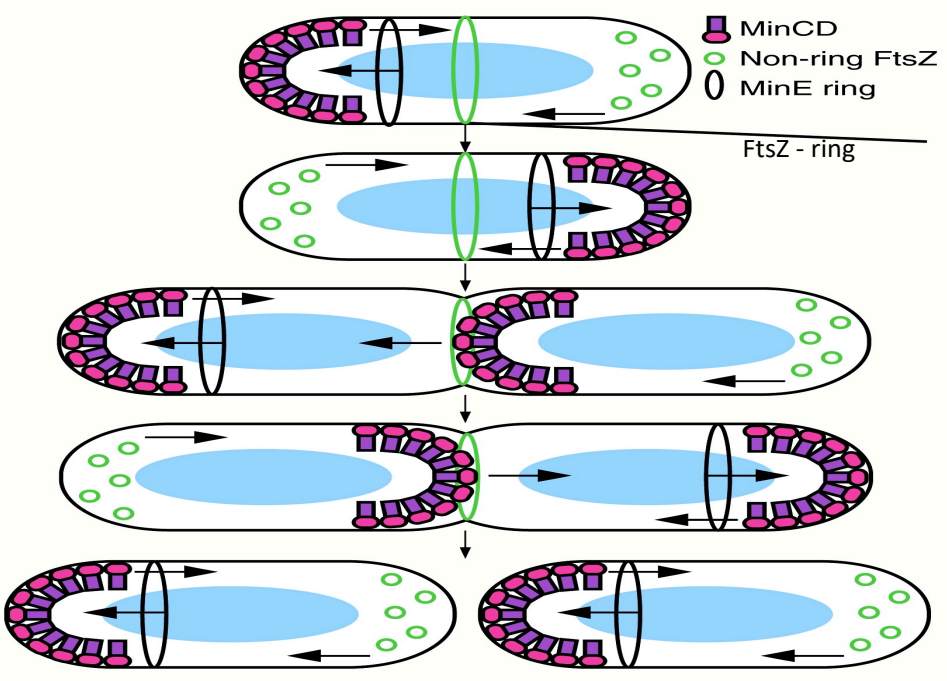

Figure 1.3 Min oscillation system in *E. coli*

ATPase activity of MinD is stimulated when MinE binds to complexes of MinC-MinD at one pole, causing both to cycle towards the opposite pole. Responding to MinC, Non-ring FtsZ oscillates as well. When the cell division is closed, MinC and MinD pause at the septum before oscillating again in both daughter cells.Taken from Rowlett and Margolin, 2013.

The oscillatory Min system's behaviour is multi-step and self-organizing (Figure 1.4) (Shih and Zheng, 2013). ATP-bound MinD dimers cooperate to bind the membrane in a zone from the pole towards the cell centre (Hu, Gogol and Lutkenhaus, 2002; Lackner, Raskin and De Boer, 2003). At the edge of that zone, the MinE protein binds to MinD and stimulates ATP hydrolysis (Hu and Lutkenhaus, 2001), releasing MinD monomers from the membrane into the cytoplasm. MinE then destabilises the next MinD dimer at the membrane (Holyoak *et al.*, 2011) and eventually reaches the pole where it dissociates and diffuses freely in the cytoplasm after which it starts a new cycle where MinD has re-assembled on the other side of the cell (Laloux and Jacobs-Wagner, 2013; Rowlett and Margolin, 2015)

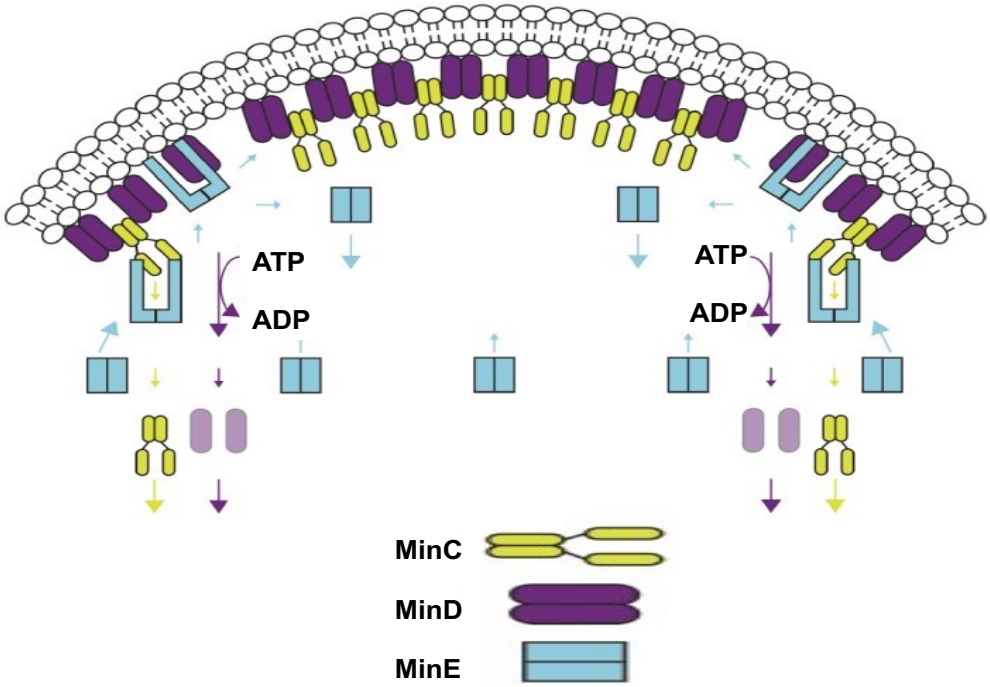

Figure 1.4 MinD-MinE interaction

ATP bound dimer of MinD bind to the cell membrane through a C-terminal at the pole accumulating until be closed to the mid-cell, MinE binding to MinD stimulate ATPase activity leading the release of MinD from the membrane. Adopted from Rowlett and Margolin, 2015.

The Min system of *B. subtilis* comprises MinC and MinD but instead of a MinE homologue has two proteins, MinJ and DivIVA, which determine the MinCD complex polar localisation (Edwards and Errington, 1997; Donovan *et al.*, 2008). In *B. subtilis*, the cell division site recognition mechanism must be different because no oscillation of the Min proteins has been observed. While the Min system in *B. subtilis* is less conspicuously dynamic than in *E. coli*, MinD molecule binding and dissociation at the membrane is rapid and it has been suggested that this is accompanied by MinD polymerisation and depolymerisation, respectively (Barák *et al.*, 2008). In *B. subtilis*, the polar positioning protein DivIVA is responsible for the static localisation of MinD to the poles and newly synthesized division septa (Cha and Stewart, 1997; El Karoui and Errington, 2001). MinD localisation to the pole depends on localisation of DivIVA facilitated by interaction of the intermediated protein MinJ with both DivIVA and MinD (Patrick and Kearns, 2008). Localisation of

DivIVA to the poles has been shown to result from the membrane negative curvature at these sites (Ramamurthi and Losick, 2009) and was originally thought to be to the result of interaction with the maturing divisome complex but has now been shown to result from the membrane's initial constriction during formation of the septum generating the negative curvature by which DivIVA is localised (Eswaramoorthy *et al.*, 2011). When MinDC is localised to the site at where the septum will form, aberrant secondary FtsZ ring formation close to the mid cell during or after division is inhibited.

1.1.2.2 Nucleoid Occlusion NO

The Min system as a negative regulator of FtsZ promotes the Z-ring's mid cell location but does not prevent guillotining of the chromosome during septum formation and not even chromosome segregation would be sufficient to prevent this as the DNA's terminator region is usually found in the closing septa and DNA translocases are need to carry these ends into the correct compartment before full septa closure (Touzain *et al.*, 2011). Nucleoid occlusion is the second system and depends on the protein Noc in *B. subtilis.* Noc is a DNA-binding protein associating with sites distributed widely over the chromosome. Noc also inhibits Z ring assembly near the nucleoid (Wu and Errington, 2004). SlmA is an unrelated but functionally equivalent protein in *E.coli* (Bernhardt and De Boer, 2005). Each bind to their own specific areas of the chromosome, SlmA binding sites (SBS) and Noc binding sites (NBS), both distributed everywhere in the chromosome except at the region surrounding the terminus (Cho *et al.*, 2011). In *E. coli*, SlmA interacts directly with FtsZ on the surface of each nucleoid, inhibiting nearby Z ring assembly and thus sparing the nucleoid from bisection (Cho *et al.*, 2011; Tonthat *et al.*, 2013), but in *B. subtilis* the nucleoid occlusion protein Noc performs a similar function without direct interaction with FtsZ (Figure 1.5) (Adams, Wu and Errington, 2015).

Two models have been suggested for SmlA action in *E. coli*. The first is that, when binding to SBS sites around the chromosomal DNA, SmlA binds to FtsZ's C-terminal tail and competes there for binding with such other FtsZ regulatory proteins as ZapD, MinC, FtsA and other FtsZ molecules. Not only

would this promote further SmlA interactions with FtsZ but it would lead to the eventual breakdown of FtsZ protofilaments (Du and Lutkenhaus, 2014). The second suggestion is that SlmA spreads along DNA as a dimer of dimers forming higher order nucleoprotein complexes that, by sequestering FtsZ, prevent it from forming Z-Rings (Tonthat *et al.*, 2013). Each of these models would imply that FtsZ polymerisation is negatively regulated independently of FtsZ's GTPase activity (Cabré *et al*., 2015). Unlike SmlA, it is not thought that Noc interacts directly with FtsZ; it acts instead by binding the chromosome to the membrane along the lateral wall and occupying the physical space FtsZ would need to occupy to polymerise into a Z ring (Adams, Wu and Errington, 2015). Noc is a protein whose DNA binding is site-specific and binds with recognition sites (NBS) distributed everywhere on the chromosome except near the replication terminus region (Wu and Errington, 2004; Wu *et al.*, 2009).

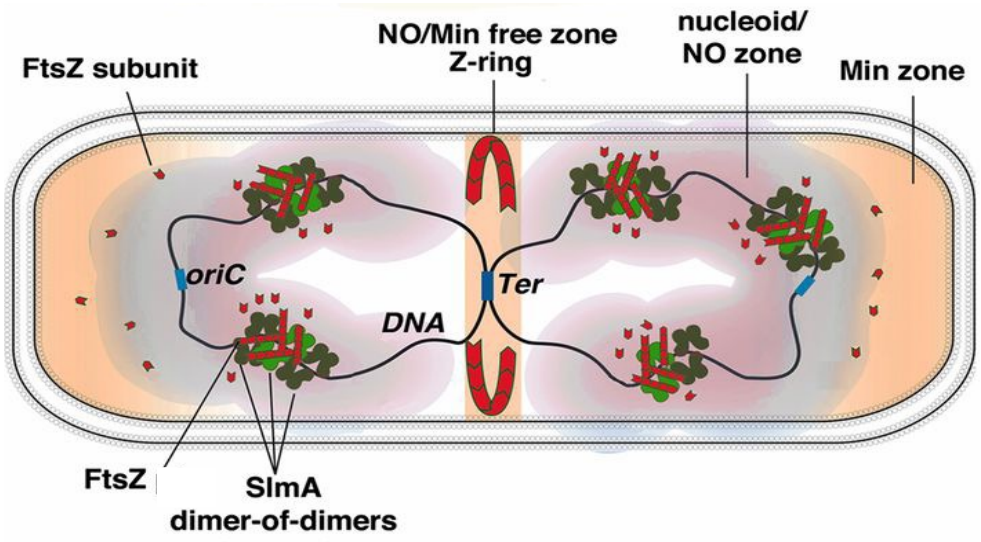

Figure 1.5 Nucleoid occlusion mechanism

The nucleoid occlusion proteins SlmA in *E. coli* and Noc in *B. subtilis* inhibit FtsZ ring formation from occurring over the chromosome. Taken from Schumacher, 2017.

1.1.3 Control of Fts Z-ring assembly

The FtsZ-ring is stabilised and connected to the membrane where cell division will take place at the prompting of positive regulator proteins. In *E. coli*, the proteins are FtsA and ZipA, both of which interact directly with FtsZ

and promote the membrane connection to complete division (Pichoff and Lutkenhaus, 2002). FtsA localises at the midcell and its FtsZ interaction is through the C- terminal end, after which it tethers FtsZ to the membrane (Ma and Margolin, 1999; Pichoff and Lutkenhaus, 2007). FtsA is a protein similar to actin and can form actin-like protofilaments (Szwedziak *et al.*, 2012). FtsA is involved in *E. coli's* self-interaction and in recruiting downstream division proteins (van den Ent, 2002; Pichoff and Lutkenhaus, 2005). In addition to FtsA, ZipA in *E. coli* can tether FtsZ to the membrane, stabilise it, and recruit downstream division proteins (Huang, Durand-Heredia and Janakiraman, 2013). FtsA plays a critical role in assembling divisome since *ftsA* mutant are able to bypass ZipA (Vicente *et al.*, 2002) which reduces FtsA self-interaction capability, leading to a model with FtsA monomers active in recruiting downstream proteins (Lutkenhaus, Pichoff and Du, 2012). ZipA overlaps functionally with FtsA in *E. coli* in tethering FtsZ to the membrane (Huang, Durand-Heredia and Janakiraman, 2013). In common with FtsA, ZipA binds conserved residues in the FtsZ C- terminal end and recruits downstream division proteins (Figure 1.6) (Ma and Margolin, 1999). ZipA's C-terminal domain can be localised to the midcell septum FtsZ-dependently (Hale, Rhee and De Boer, 2000). As well as tethering FtsZ to the membrane, there is genetic and cytological evidence for involvement of ZipA in Z ring stabilisation. Assembly of FtsZ rings is still possible in ZipA depleted filaments, but happens less often and with more variable results (Hale and De Boer, 1999). Nevertheless, a recently published study showed that in the absence of most of ZipA linker domains, oxidative stress sensitivity and resistance are not significantly affected (Schoenemann, Vega and Margolin, 2020).

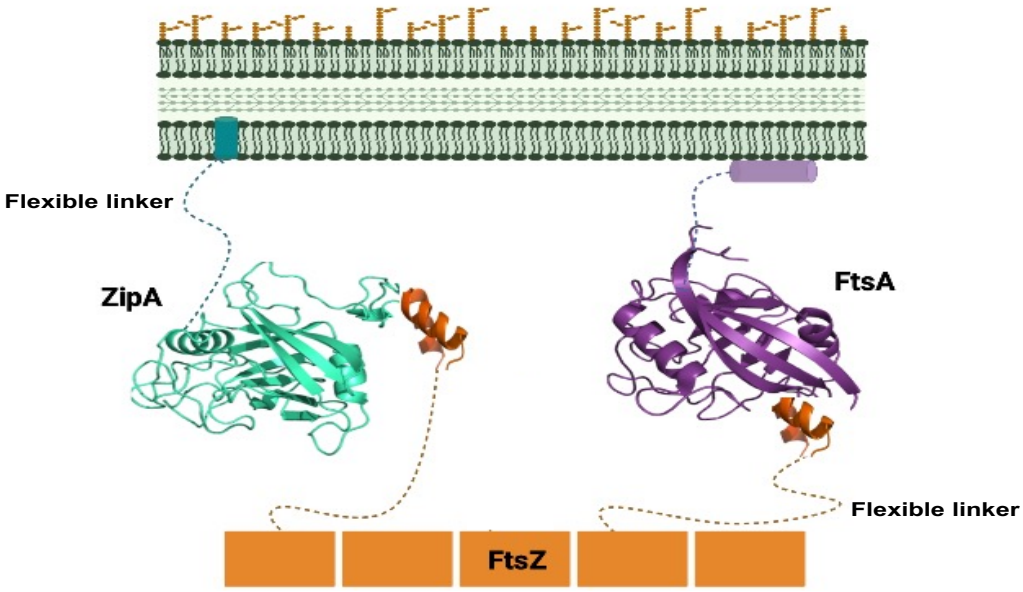

Figure 1.6 FtsA and ZipA tether the FtsZ filaments to the membrane

ZipA and FtsA bind to the highly conserved C-tail of FtsZ, which is connected to main body of FtsZ by a flexible linker. Both ZipA and FtsA are tethered to the membrane by a flexible linker that connects the membrane binding domains of these proteins to the main body of the protein. Adopted from Lutkenhaus, Pichoff and Du, 2012 (modified by biorender).

In *B. subtilis*, there is immediate conservation of FtsA location upstream of and near to FtsZ; it differs from *E. coli* in that *B. subtilis ftsA* mutants are viable, though their division is substantially deficient (Beall and Lutkenhaus, 1992). Conversely, in *B. subtilis*, mutations affecting *ftsA* self-interaction exhibit a phenotype characterised by the loss of function. This indicates that a certain degree of FtsA self-interaction contributes to the facilitation of cytokinesis (Szwedziak *et al*., 2012). This, in turn, introduces ambiguity regarding the precise contribution of FtsA self-interaction to polymerisation during cytokinesis. Moreover, the mechanism through which FtsA facilitates the recruitment of other proteins to the divisome remains uncertain (Huang, Durand-Heredia and Janakiraman, 2013).

Gram positive bacteria lack ZipA homologues and in these cases it has been suggested that the protein SepF carries out part of ZipA role. Yeast two hybrid screening has suggested that SepF-SepF self-interaction and

interaction with FtsZ take place, but with slightly defective cell production and aberrant septum formation (Hamoen *et al.*, 2006). SepF overexpression combats *ftsA* mutant division defects , suggesting function overlap, while *ftsA-sepF* double mutants are synthetically lethal and cannot form Z-rings (Ishikawa *et al.*, 2006). Dependent on its interaction with FtsZ, SepF in *B. subtilis* localises to the division site (Hamoen *et al.*, 2006; Ishikawa *et al.*, 2006). Recent research indicates that correct FtsZ polymer formation needed for proper cell division is promoted by SepF (Gündoğdu *et al.*, 2011). Transmission Electron Microscopy TEM has shown SepF assembling in *vitro* into large rings with a 50 nm diameter capable of bundling FtsZ protofilaments into long tubular structures (Figure 1.7) (Duman *et al.,* 2013).

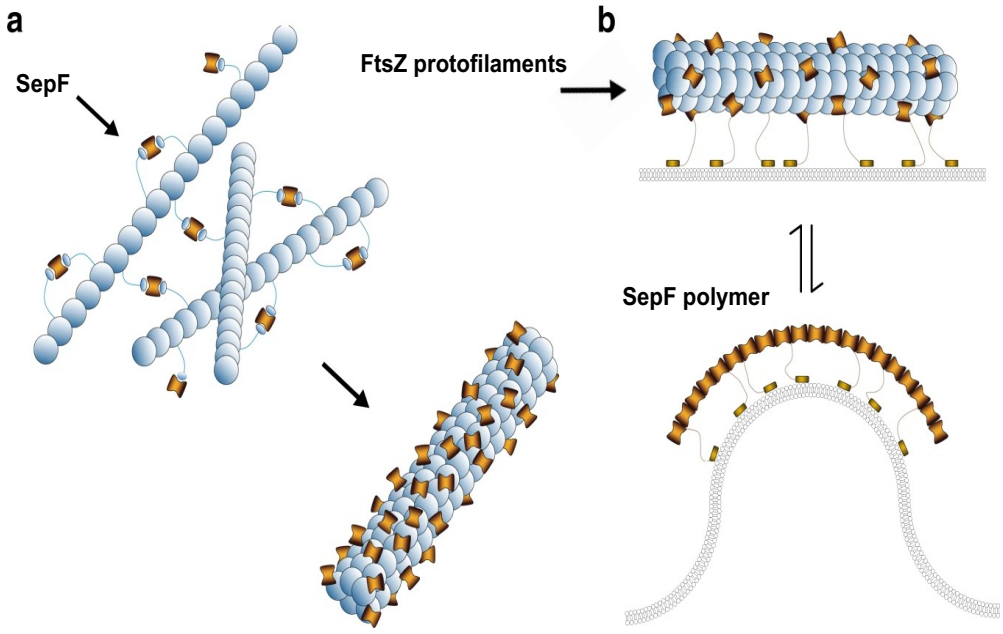

Figure 1.7 SepF bundling of FtsZ protofilaments

Bundling of FtsZ filaments occurs as a result of FtsZ-SepF complex formation in the cytoplasm **a.** At the membrane, SepF bound to FtsZ filaments leading to tether the membrane (top). Taken from Sogues *et al.*, 2020

The suggestion would seem to be that SepF rings bundle FtsZ protofilaments, most likely to aid FtsZ ring formation (Gündoğdu *et al.*, 2011).

1.1.3.1 Z-Ring Maturation

Z-ring maturation begins on successful establishment of the ring and its tethering to the membrane. The maturation pathways are slightly different in *E. coli* and *B. subtilis*, but many of the same proteins are involved. *E. coli* has a dependency pathway (Figure 1.8), with sequential localisation of each protein or protein complex. *B. subtilis*, however, can have two-phase divisome formation with independent formation of all maturation proteins (Harry *et al*., 2006).

FtsK in *E. coli* is a DNA translocase protein, with an essential role in FtsZ recruitment through the N-terminal region and recruitment of the next protein necessary if maturation is to occur (Begg, Dewar and Donachie, 1995; Wang and Lutkenhaus, 1998). FtsK is a chromosome partitioning protein with a smaller amino terminal domain comprising four transmembrane segments and a large carboxy terminal cytoplasmic domain using ATP to translocate DNA in a sequence pathway (Goehring and Beckwith, 2005; Pease *et al.*, 2005). In *B. subtilis*, the SpoIIIE protein – a FtsK homologue – is involved in DNA translocation during sporulation (Sharp and Pogliano, 2003).

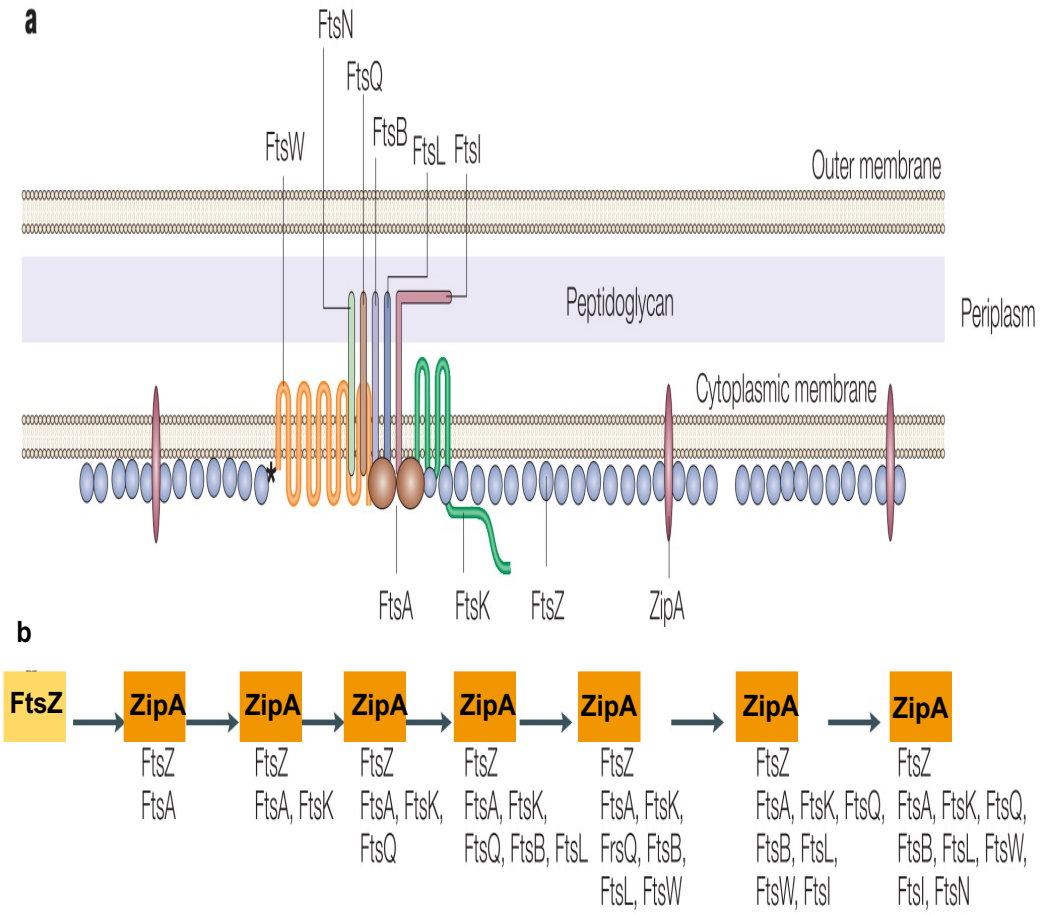

Figure 1.8 The assembly pathway for the divisome *in E. coil*

FtsZ appears as single protofilaments at the membrane. Both ZipA and FtsA interact with FtsZ and the membrane in *E. coli*. A transmembrane subassembly associated with an FtsA dimer is depicted due to the low levels of essential integral membrane proteins. These proteins, such as FtsQ, FtsB, FtsL, FtsI, and FtsN, are bitopic with a single transmembrane and periplasmic domain. FtsW and FtsK are polytopic with multiple domains. Protein associations are suggested by their proximity in the diagram. Proteins stabilizing the ring are labeled below, while those involved in later stages like septum synthesis are labeled above. The order of recruiting essential cell-division proteins to the Z ring is shown in section b based on their mutual localization requirement. Late divisome proteins finalize septum formation, with FtsN triggering constriction. Modified from Margolin, 2005.

FtsQ, FtsL and FtsB proteins form the protein complex FtsQLB in *E. coli,* and this is involved in maturation of the Z-ring. The FtsQLB complex forms

before localisation of the septum as was shown by use of co-immunoprecipitation of FLAG-tagged proteins (Buddelmeijer and Beckwith, 2004). Recruitment of the FtsQLB complex to the division site can be through FtsQ action. In *B. subtilis* FtsQ, FtsL and FtsB proteins are respectively represented by their homologues DivIB, FtsL and DivIC, which depend on each other for localisation (Goehring and Beckwith, 2005). Further FtsL data suggests a possible role in Z ring constriction regulation in *B. subtilis* by recruiting the regulation of division proteins which act later to allow constriction (Kawai and Ogasawara, 2006). Although FtsB/DivIC function is as yet unknown, proteins essential for cell survival exist in their respective bacteria (Levin and Losick, 1994; Buddelmeijer and Beckwith, 2004).

The next protein recruited to the *E. coli* division site is FtsW. Some biochemical studies have suggested that FtsW transports lipids needed to synthesise peptidoglycan synthesis, such as lipid II (Mohammadi *et al*., 2011). The action of FtsW localises FtsI to the division site (Mercer and Weiss, 2002). FtsI in *E. coli* encodes penicillin binding protein 3 which is involved in synthesising peptidoglycan and is thought to be the only PBP that must be present for cell division to take place (Goehring and Beckwith, 2005). The final protein whose recruitment to the site of septation is FtsN (Chen and Beckwith, 2001), which can be recruited by direct interaction with FtsI to the division site. Screening of FtsI-FtsN interaction has confirmed the possibility of disruption of FtsN localisation by a number of point mutations in *ftsL* (Di Lallo *et al.*, 2003; Wissel and Weiss, 2004; Karimova, Dautin and Ladant, 2005). AmiC, an amidase, is the last protein recruited to *E.* coli maturing Z ring and is an enzyme linked in cleaving murein (peptidoglycan) required to degrade the cell wall before cell division (Weiss, 2004).

1.1.4 Chromosome segregation- ParAB system

Chromosome segregation must be synchronised with formation of the division septum for the two daughter cells each to receive a full genome copy (Donczew *et al.*, 2016). Bacterial chromosome segregation is regulated by molecular mechanisms involving specific proteins (Badrinarayanan and Laub, 2016). The ParABS portioning system is the fundamental chromosome segregation machinery. There are *parABS* homologues in over 50% of bacteria as facilitators of chromosome segregation (Livny, Yamaichi and Waldor, 2007).

The majority of bacterial chromosomes have partitioning (Par) proteins encoded near their origins *oriC* (Gerdes, Moller-Jensen and Jensen, 2000). The loci in plasmids encoded Par comprise three components: ParA protein, an ATPase; ParB, a DNA-binding protein; and a site like a centromere known as ParS. ParB protein binds ParS and spreads along the DNA to form a large nucleoprotein complex. It is stimulated immediately by ATPase activity, since ParA proteins have weak ATPase activity (Easter and Gober, 2002; Leonard, Butler and Löwe, 2005a). The ParB/ParS complex binds to ParA in an interaction essential for efficient segregation of plasmids (Ebersbach and Gerdes, 2005).

Partition systems are encoded by most bacterial chromosomes as well as plasmids. Plasmid partition systems typically comprise a pair of proteins and one or more partition sites, termed par sites, that dictate the operation of the segregation mechanism. These *par* sites serve as prokaryotic centromeres since they are crucial for plasmid stability within the same genetic region (*cis*) and function as the assembly sites for the segregation machinery. One of the partition proteins is a specific DNA-binding protein that identifies the par site; it is commonly referred to as the centromere-binding protein (CBP). The second protein is either an ATPase or GTPase, employing the energy derived from nucleotide binding and hydrolysis to facilitate the intracellular movement of plasmid DNA. Typically, the genes are organised into an operon, and the proteins autonomously govern their expression. The positioning of the *par* site exhibits diversity; it can be directly downstream of the *par* genes, positioned

upstream near the operon's promoter, or distributed across several locations on the plasmid (Baxter and Funnell, 2015). In plasmid, three Par systems have been categorized based on their specific NTPase enzymes: a P loop ATPase with a modified Walker A motif (Type I), an ATPase resembling actin (Type II), and a GTPase resembling tubulin (Type III) (Gerdes, Moller-Jensen and Jensen, 2000; Bignell and Thomas, 2001). Many bacterial chromosomes encode plasmid-likepartition systems, which have been shown to contributeto bacterial chromosome segregation (Baxter and Funnell, 2015).

1.2 Bacterial Growth

Peptidoglycan synthesis (PG) is the crucial mechanism governing both bacterial cell shape and vitality. For bacterial growth, the incorporation of new PG into the cell wall is imperative. For lateral growth, exhibited by most rod-shaped bacteria including *E. coli* and *B. subtilis*, PG are inserted into the lateral cell wall causing extension at the mid-cell (Margolin, 2009; Cameron *et al.*, 2014). In *B. subtilis* and *E. coil,* the lateral growth is driven by MreB, the bacterial homologue of eukaryotic actin. The polar growth model is driven by DivIVA and mainly found in *Actinomycetes* (Flärdh, 2003).

MreB proteins are the first proteins identified to contribute to the mechanism of lateral growth, which were initially described in *E. coli* and *B. subtilis* (Isolation *et al.*, 1987; Figge, Divakaruni and Gober, 2004). MreB is essential for cell shape formation and maintenance, and depletion through drug treatment or genetic mutations lead to loss of rod shape gradually and transformed into spherical cells (Bendezú and De Boer, 2008). Although most rod-shaped bacteria consist only a single MreB locus, *B. subtilis* has three genes encoding actin-like proteins, MreB, MbI and MreBH (Kawai, Asai and Errington, 2009). Most importantly that the three *B. subtilis* actin-like proteins interact with each other in vivo and affect each other's localisation. Localisation of MreB and MbI using GFP revealed that formation helical filaments which wrap around the cell longitudinally from pole to pole (Defeu Soufo and Graumann, 2006). The mutation of MreB lead to direct effect of localisation MbI filaments, hence defect the synthesis of cell wall (Joël, Soufo and Graumann, 2005; Defeu Soufo and Graumann, 2006). Localisation of the sites of cell wall insertion in *B. subtilis* showed that this also occurs in a helical pattern suggesting that MreB proteins contribute to the control of location of cell wall synthesis in bacteria (Daniel and Errington, 2003; Errington, 2015).

Summing up these aspects results in the prevailing MreB model (Figure 1.9). MreB proteins forming helix-like structure through filaments associate to the membrane and rotate around the long axis of the cell, where they recruit multiple cell wall synthetic complexes. These complexes create new

peptidoglycan strands which are guided by the motion of the MreB helices (Errington, 2015).

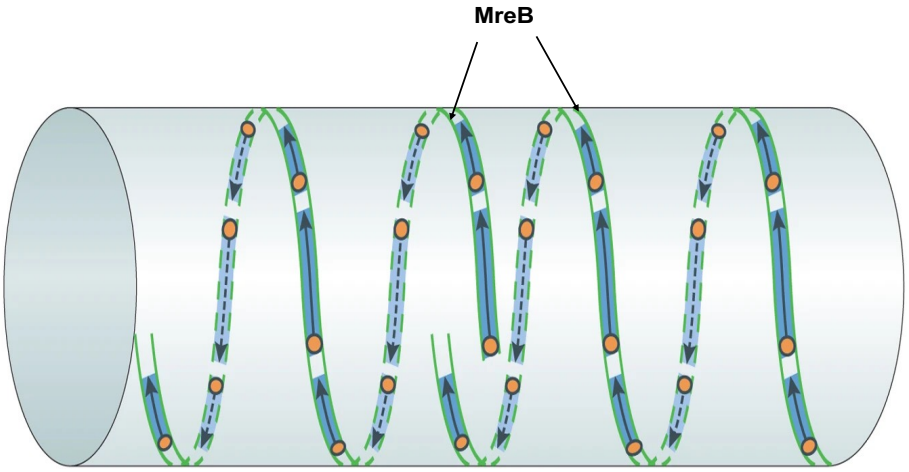

Figure 1.9 The role of MreB model in determination of cell shape

In dashed and solid green lines MreB filaments interact to the membrane and wrap around the long axis. Recruitment of peptidoglycan synthetic complexes (orange circles) leading to create new strands of PG (blue shading) then directed by MreB filaments orientation. Taken from Errington, 2015.

Moreover, through electron cryotomography (ECT) suggested that MreB assembles as discreet disconnected patches that follow a helical path through the cell and are moved through interacting to the cell wall synthetic machinery (Dominguez-Escobar *et al.*, 2011; Garner *et al.*, 2011; Tocheva *et al.*, 2011). Recently, observation data *in vitro* of MreB showed the model of MreB localisation back towards the initial helical filaments. MreB has been shown to form antiparallel filaments that interact extensively with membranes (van den Ent *et al.*, 2014). In addition, observations of MreB localisation using high-superresolution microscopy methods such as structured illumination microscopy (3D Sim) have shown helical filaments in live bacterial cells (Olshausen *et al.*, 2013; Reimold *et al.*, 2013).

Although lateral growth is the prevalent mechanism of growth in the bacteria that have been characterised, a considerable number of bacteria provide an alternative mechanism of polar growth. This mechanism of growth

is especially prevalent in the Gram-positive *Actinomycetales* and in the other different Gram-negative bacteria including *Agrobacterium* and *Rhizobium* (Daniel and Errington, 2003; Brun *et al.*, 2012). The polarity growth driven by essential protein DivIVA, which was found in both *S. coelicolor* and *Brevibacterium lactofermentum* (Flärdh, 2003a). Basically, DivIVA protein was initial identified in *B. subtilis*, where it implicated in cell division (Edwards and Errington, 1997). In *B. subtilis*, DivIVA localises to the poles, facilitating the recruitment of MinD through the intermediary protein MinJ (Min system explained above) (Patrick and Kearns, 2008). While DivIVA functionally has two roles in different bacteria; polarity growth in *S. coelicolor* and cell division in *B. subtilis*, in all cases the protein is localised to the poles (Flärdh, 2003).

Amongst the *Actinomycetales* DivIVA functions as an essential polarity protein for localisation of cell wall synthesis at the poles in *Mycobacterium* and *Corynebacterium* (Nguyen *et al.*, 2007; Kang *et al.*, 2008; Letek *et al.*, 2008) or at the growing tips and at the sites of new tip formation, then branching, in *S. coelicolor* (Flärdh, 2003a; Hempel *et al.*, 2008). DivIVA is essential in all these three genera and changes in the DivIVA levels have effects on cell shape. Decresing the amount of DivIVA in *Mycobacterium* and *Corynebacterium* leads to coccoidal cells, where synthesis of cell wall becomes limited to the division septum. On the other hand, the high level of DivIVA create club-shaped cells in *Mycobacterium* or *Corynebacterium* (Kang *et al.*, 2008; Letek *et al.*, 2008). The excessive amount of DivIVA not only accumulates at existing poles triggering their expansion, but it also assembles at ectopic locations, where new polarity centres are established and produce branching both in *Streptomyces* and *Mycobacterium* (Flärdh, 2003a; Kang *et al.*, 2008).

Until recently, it was assumed that all polar growth in bacteria occurred at the cell tip, and data from microscopy studies appeared to support this model. However, re-examination of *Mycobacterium* cell growth by super-resolution microscopy revealed subpolar addition of nascent peptidoglycan (Baer *et al.*, 2014) and it is now unclear whether subpolar growth occurs in other *Actinomycetales*. DivIVA has no homologues in Gram-negative bacteria

that display polar growth (Oliva *et al.*, 2010). Therefore In Gram-negative bacteria that exhibit polar growth, there is no mechanism identified that controls polar growth (Oliva *et al.*, 2010). Across bacteria that have polar growth there diversity in how growth at different poles is regulated to generate a variety of shapes and nuances to growth (Figure 1.10), with the filamentous *Streptomyces*, the bi-directional growth of *Corynebacterium*, the asymmetrical bi-directional growth of *Mycobacterium* and the unidirectional growth of *Agrobacterium* (Brun *et al.*, 2012; Sieger *et al.*, 2013; Baer *et al.*, 2014).

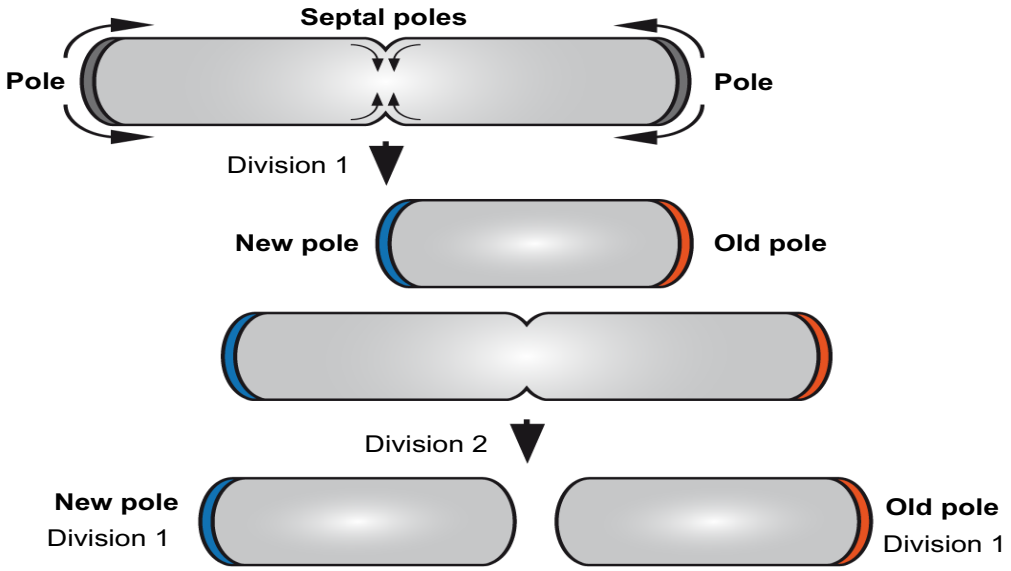

Figure 1.10 Model of polar growth in bacteria

Mycobacterium exhibits bipolar growth. Two division cycles (Division 1 and Division 2) are presented. The active biosynthesis of lateral peptidoglycan at the poles and biosynthesis of septal peptidoglycan at the future pole (septal poles) are illustrated with curved arrows. The old pole (in red) and the new pole (in blue); are both represented and refer to the first division event (Division 1). Taken from Carel *et al.*, 2014.

1.3 *Streptomyces coelicolor*

S. coelicolor is a high G-C content, Gram-positive, soil dwelling, filamentous bacterium, which belongs to a genus of the phylum *Actinobacteria* , and is the model organism for a genus that produces many biologically active secondary metabolites. Unlike most other bacteria *Streptomyces* have linear chromosomes (Chen *et al.*, 1993), with *S. coelicolor* containing 7,825 genes and 20 possible gene clusters coding for secondary metabolites within its 8Mbp chromosome (Bentley *et al.*, 2002). The chromosome consists of a central core region containing many of the primary metabolic genes and the replication origin (*oriC*) which is flanked by two unstable terminal arm regions containing non- essential genes, often implicated in secondary metabolism. *S. coelicolor* is the most studied *Streptomyces,* and it has unique mycelial and sporulating life cycle involving complex regulation of gene expression resembling that of other differentiated and multicellular organisms (Bentley *et al.*, 2002).

1.3.1 Life cycle of *S. coelicolor*

S. coelicolor exhibits a more complex life cycle than most other bacteria, as it does not divide by binary fission, but by filamentous growth. The germinating spore develops one or two germ tubes which elongate by apical tip extension during germination (Figure 1.11) (Zakrzewska-Czerwinska *et al.*, 2011). This develops into a network of vegetative mycelium allowing for the uptake of nutrients and grow in a polar manner through tip extension and branching events that occur along the lateral wall of the hyphae in a similar fashion to filamentous fungi (Errington *et al*., 2003). These branching events allow for the increase in growth rate which is also proportionate to the rate of DNA replication (Ptomyces and Chater, 1993; Flärdh, 2003). During vegetative growth in *S. coelicolor,* cell division is suspended with the placement of cross walls. These cross walls separate the hyphae into connected compartments rather than full cell-cell separation and each compartment contains multiple copies of the chromosome. This stage of growth is characterised by colonies which appear shiny and bald which is the classic phenotype for mutants which are blocked at this stage of development on nutrient medium. In response to

nutrient depletion and other signals, both production of secondary metabolites and morphological differentiation are initiated. Aerial hyphae break the surface tension, escaping the aqueous environment of the vegetative mycelium, and grow into the air (Kelemen *et al.*, 1998; Flärdh *et al.*, 2012). Aerial mycelium grow as multi-genomic hyphae with less branching than in vegetative hyphae. Colonies at this stage of development appear fuzzy and white which is the classic appearance for mutants blocked at this stage of development. After the aerial hyphae have stopped growing, septa are placed at equal spacing along the length of the unbranched hyphae, such that each individual chromosome is packed into a single compartment, the pre-spore compartment. The spore chain then matures into uni-genomic spores with the production of a grey polyketide pigment, and thus the life-cycle is complete (Ptomyces and Chater, 1993; Kelemen *et al.*, 1998; Flärdh and Buttner, 2009).

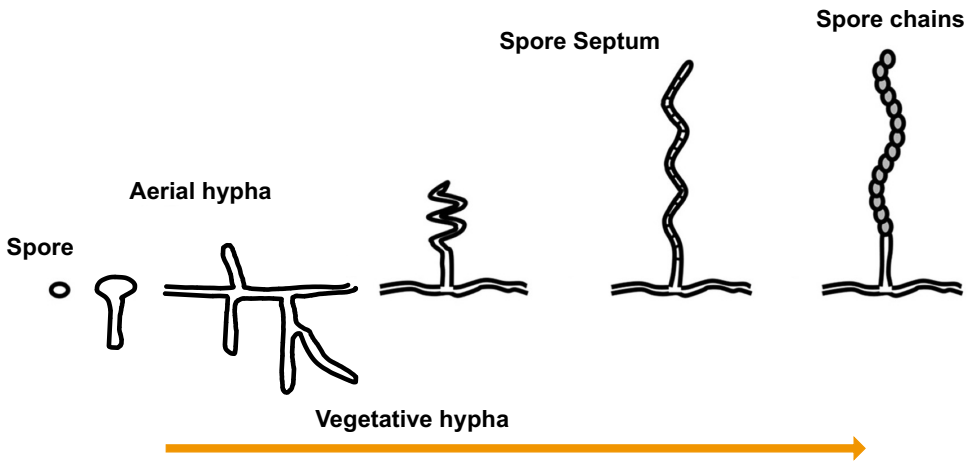

Figure 1.11 *S. coelicolor* life cycle

The life cycle of *S. coelicolor* begins with a single uni-genomic spore, which upon favorable conditions germinates with the protrusion of either one or two germ tubes. *S. coelicolor* then grows and branches forming a network of vegetative hyphae which stretch into the media in order to uptake nutrients. Upon nutrient depletion, aerial hyphae are erected above the surface of the media. After the cessation of aerial growth, septa are formed along the length of the aerial hyphae creating pre-spore compartments. These compartments then mature into spores from which the life cycle can begin again. Modified from Nodwell, 2019.

1.3.2 Growth in *S. coelicolor* – TIPOC

The growth of *S. coelicolor* is characterised by an apical growth pattern, whereby vegetative hyphal tips extend and initiate branches (Fuchino *et al.*, 2013). This contrasts with the growth seen in many bacterial species, representing an extreme version of cell polarisation to yield offspring (spores). Central to this apical growth is the formation of a polarisome-like complex TIPOC (tip organising center) comprising the polarity protein DivIVA, as well as other proteins associated with cell growth and structural integrity (Flärdh *et al.*, 2012). These proteins provide essential signalling gradients to initiate and support growth through hyphae, while providing support to the cell wall during this process (Holmes *et al.*, 2013).

The DivIVA protein forms large oligomeric complexes, which are essential for growth of the bacteria (Wang *et al*., 2009). Molecular analyses of the DivIVA protein have shown a 22-amino acid sequence that determines the role of the protein in *S. coelicolor*, although it is recognised that other molecules and proteins determine the polarity of DivIVA during the initiation and completion of cell division (Wang *et al*., 2009). *Streptomyces* cytoskeletal element (Scy) is a coiled-coil protein that has been shown to play an important role in determining polarised growth in *S. coelicolor* acting as a polarity determinant of DivIVA (Holmes *et al*., 2013). Together, DivIVA and Scy form an apical complex of proteins that govern growth in the hyphal tip.

FilP is another coiled-coil protein associated with the development of the polarisome in Streptomyces species (Sigle *et al*., 2015). Identification of FilP (Ausmees, 2013) noted similarities between this protein and intermediate filament proteins, suggesting that FilP adds stability and rigidity to the extending hyphal tip (Figure 1.12). Apical accumulation of FilP is dependent on interactions with DivIVA, suggesting that the essential protein in initiating hyphal growth recruits a structural protein to support the growth process (Ausmees, 2013). Apical assemblies of FilP have been shown to be dynamic in nature, independent of Scy activity/location, and may determine the position and size of DivIVA in Streptomyces venezuelae, suggesting complexity in the interactions between these three proteins across species (Fröjd and Flärdh,

2019). The vegetative hyphae exhibit a meandering morphology in the absence of *filP*, suggesting the polymerisation of FilP is important for the strengthening the hyphae cell walls (Alcock, 2019; Bagchi *et al.,* 2008; Fuchino *et al*., 2013).

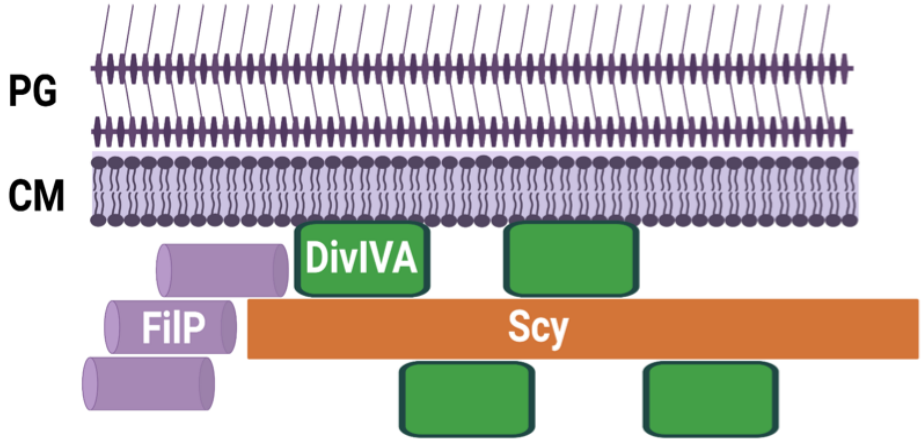

Figure 1.12 The tip organising centre proteins (TIPOC) in *S. coelicolor*

The TIPOC Scy, DivIVA and FilP are the coiled-coil intermediate filament-like proteins. At hyphal tips, the coiled-coil protein Scy interacts directly with DivIVA and FilP. DivIVA directly interact with the cell wall synthesis machinery and FilP strengthens the hyphae walls. Cell wall machinery synthesis organised by DivIVA, whereas FilP controls the hyphae walls. (CM: cell membrane and PG: peptidoglycan. Modified from Holmes *et al.*, 2013. (Biorender)

The growth phase of *S. coelicolor* is similar in nature to that of filamentous fungi, whereby the formation of branched hyphae leads to the development of aerial hyphae, predecessors of long-chain spores (Cameron, Zupan and Zambryski, 2015). When bacteria reproduce, the division of chromosomes in daughter cells typically relies on an active system of partitioning, leading to chromosomal segregation long of the hyphae (Ausmees, 2013). However, in *S. coelicolor* the unique features of the hyphal extension and vegetative mycelium formation require further examination of mechanisms and proteins involved in DNA replication and segregation,

particularly as chromosomal segregation is not obvious within the mycelium (Sigle *et al.*, 2015).

1.3.3 DNA replication and segregation - ParAB system

Two key proteins are typically associated with DNA replication and chromosomal segregation in bacterial species: ParA, and ParB (Donczew *et al.*, 2016). ParA is a cytoskeletal ATPase that generates the energy for the segregation of chromosomes, while ParB serves as an organiser of nucleo-protein complexes. Mutations in the ParAB promoter, which controls the expression of *parA* and *parB* genes, resulted in chromosome segregation abnormalities in 13% of Streptomyces spores (Kim *et al.*, 2000). Although the mechanisms are incompletely understood, ParA and Par B interact to drive filament formation and chromosomal segregation and this activity needs to be coordinated with cell elongation and daughter cell partitioning to ensure successful spore formation (Donczew *et al.*, 2016).

A dynamic interplay between the ParAB system and the Scy protein has been noted during the growth phase and chromosome segregation of *S. coelicolor* (B. Ditkowski *et al.*, 2013). Specifically, Scy recruits ParA to the hyphal tip and plays a role in regulating ParA polymerisation, key mechanisms in sporulation (B. Ditkowski *et al.*, 2013). Evidence in *Mycobacteria* also suggests that ParA interacts with Wag31 (the DivIVA homologue), further supporting interactions between polarity-associated proteins and the ParAB system (Ginda *et al.*, 2013). Furthermore, one comprehensive study (Kois-Ostrowska *et al*., 2016) provides further insights into the mechanisms of chromosomal segregation in *Streptomyces* during vegetative growth. In this study, labelling of the chromosomal replication initiation region (*oriC*) was coupled with time-lapse photography to track chromosome segregation relative to ParA and ParB localisation and interactions with other proteins. The findings suggested that ParB complexes with every chromosome copy, while ParA interacts with the polarisome and anchors only one chromosome at the extending hyphal tip. During replication, the ParA anchor persists during binding with an *oriC*, while branching and sporulation are reliant on ParA targeting chromosomal copies to the hyphal tip (Kois-Ostrowska *et al.*, 2016).

Taken together, these data suggest that the protein-protein interactions of the ParAB system and the polarisome govern the transition from cell elongation and growth to sporulation in *S. coelicolor* (B. Ditkowski *et al.*, 2013).

1.3.4 Cell division in *S. coelicolor* - FtsZ

Bacteria undergo cell division as part of a process governed by a tubulin-like protein, termed FtsZ (Rioseras *et al.*, 2018). Exceptions are limited to bacteria with limited genomes or unique species, while it has been noted that FtsZ is dispensable for proliferation and viability in only two bacteria: *Mycoplasma* species, and *S. coelicolor* (B. Ditkowski *et al.*, 2013). It is thought that the formation of branching hyphae during reproduction and cell division account for this anomaly in *S. coelicolor*, as this type of reproduction does not require the formation of FtsZ-dependent cross-walls (Ausmees, 2013). However, the role of FtsZ is apparent during sporulation in aerial hyphae, where the formation of FtsZ rings (Z rings) in a ladder-like pattern facilitates septation events leading to spore formation (Figure 1.13). The Z ring has been described as a series of single-stranded protofilaments of FtsZ, essential for compartmentalisation of tends of spores during active replication.

Consistent with the roles of FtsZ in *S. coelicolor*, FtsZ mutant bacteria demonstrate vegetative growth but do not produce spores (Schwedock *et al.*, 1997; Santos-Beneit *et al.*, 2017). Interestingly, mutants of FtsZ (affecting the beta-strand of the protein) have been shown to interfere with Z ring formation, producing a spiral pattern that remains capable of cell constriction during replication in *S. coelicolor* and *S. venezuelae* although assembly of the FtsZ complex is impaired in these mutants (Sen *et al.*, 2019). Furthermore, the role of FtsZ in Z ring formation and sporulation may be dependent on phosphorylation events based on the recent identification of a key phosphorylation site on the protein that is differentially activated during cellular replication stages (Rioseras *et al.*, 2018).

Overall, the data suggest that the roles of key proteins during bacterial division and growth may be uniquely assigned in *S. coelicolor.* One of the curiosities of the reproductive process of *S. coelicolor* is the reliance on

relatively static intermediate filament proteins (coiled-coil proteins) for vegetative hyphal tip growth (Ausmees, 2013). In most bacterial species, tubulin and actin components of the cytoskeleton govern reproductive cell division, based on their active dynamic processes in cellular transport, division and constriction (Donczew *et al.*, 2016). However, the tubulin-like protein FtsZ and the actin-like protein MreB can be deleted in mutant *S. coelicolor*, yielding bacteria that are able to successfully grow via hyphal tip extension (McCormick *et al.*, 1994; Mazza *et al.*, 2006). The emerging model of DivIVA-Scy-FilP aggregation and polarisation during cell division and growth accounts for the lack of reliance on FtsZ during cell growth (tip extension) in *S. coelicolor*, while supporting the importance of this protein during sporulation.

1.3.4.1 Cell division site regulation in *S. coelicolor*

S. coelicolor carries the proteins SsgA and SsgB, which play important roles in regulation of the Z-ring in a positive manner (Willemse *et al.*, 2011; Monahan and Harry, 2013). In the absence of negative regulation system in *S. coelicolor,* sporulating cells use two proteins system SsgA/SsgB to regulate Z-ring positioning (Willemse *et al.*, 2011). The progression towards fully formed FtsZ rings (Figure 1.13) begins with the localisation of SsgA starting at the hyphal tips followed by evenly spaced distinct foci which occur the length of the hyphae (young aerial). SsgA then recruits SsgB to the side wall in an evenly spaced manner alternating between the two sides of the hyphae (early division stage IIA). FtsZ then forms long spiral-like filaments along the length of the hyphae interacting with the alternately placed SsgB (early division). At this point small SsgB foci are seen on the opposite side wall of the hyphae from the SsgA recruited SsgB. FtsZ then co-localises with SsgB as distinct foci along the hyphal length forming foci on opposite sides of the hyphae (pre-division). FtsZ and SsgB then co-localise as rings both forming the classical laddering seen in FtsZ localisation (Z-rings) (Barka *et al.*, 2016).

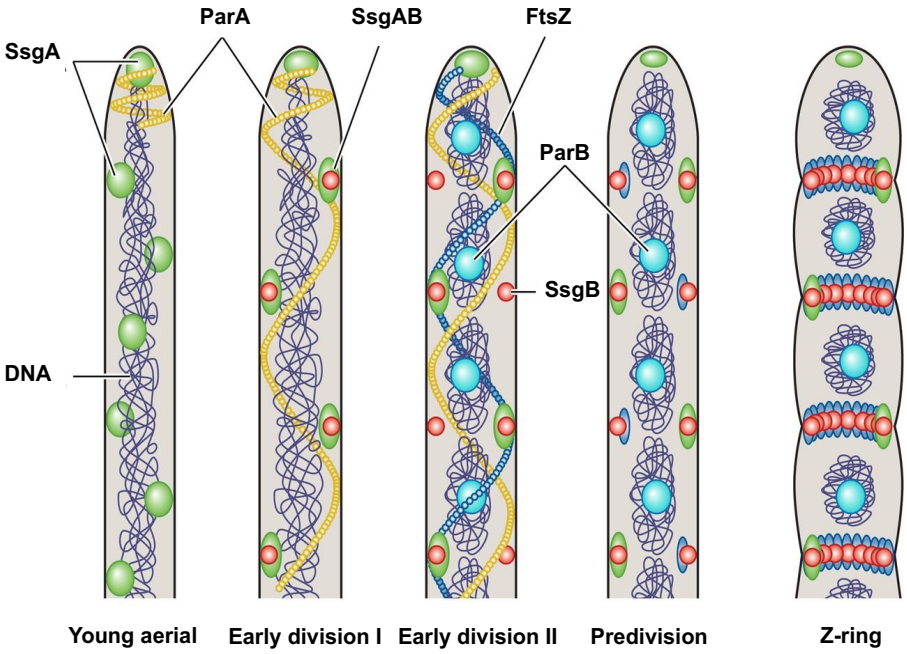

Figure 1.13 Positive regulation of FtsZ ring localisation by SsgA and SsgB in *S. coelicolor*

In young aerial SsgA in the beginning localises as distinct regular foci along the aerial hyphae, while SsgB and FtsZ are still diffuse at this stge. At this point, ParA is constrained to the hyphal tip. At early division I: SsgB recruited by SsgA to the side wall in an evenly spaced alternating fashion with ParA extending downward as filaments along the aerial hypha. ParB complexes are then formed over the uncondensed chromosomes. Early division II: FtsZ forms spiral like filaments attaching at alternating sides to the assembled SsgB foci. Predivision: Further co-localisation of FtsZ and SsgB occurs whereby SsgB interacts with the membrane tethering FtsZ. Z-ring: FtsZ rings are formed then followed by chromosome condensation and segregation and formation of the sporulation septa. Taken from Barka *et al*., 2016.

SsgA localises before the appearance of the other two proteins suggesting that its localisation is not dependent on FtsZ or SsgB. Indeed, SsgA was shown to correctly localise in an *ftsZ* mutant background. FtsZ on the other hand failed to localise correctly in either the *ssgA* or *ssgB* null mutants suggesting that its localisation is dependent on both of these proteins. Interestingly, in these mutant strains, FtsZ forms sparsely spaced ring structures similar to the distribution of septa in vegetative hyphae and show

the same lack of constriction associated with these non-dividing septa suggesting that at least part of the difference in septa formation between vegetative and aerial hyphae is the presence of SsgA and SsgB. SsgB while not able to localise correctly in a *ssgA* mutant background, does form regular foci on the lateral wall to Z ring formation. What SsgB is not able to do it is correctly form the rings associated with the formation of Z rings. Interaction between FtsZ and SsgB was confirmed *in vivo* in *S. coelicolor* using Forster resonance energy transfer and in a heterologous host *E. coli* using a bacterial-two hybrid assay. In addition, electron microscopy of FtsZ protein samples showed that filament length substantially increased in the presence of SsgB *in vitro* (Willemse *et al.*, 2011)

1.3.5 ParA- like proteins in *S. coelicolor* - ParH & Hyp

Previously in the Kelemen lab several novel ParA-like proteins were identified in *S. coelicolor.* One of these proteins was designated ParH has 49% identity to *B. subtilis* Soj and 30% identity to MinD in *B. subtilis.* The *parH* gene is presumably co-translated with the downstream gene, which encodes a small hypothetical protein (Figure 1.14). Through bioinformatic analysis, homologues of ParH and Hyp were found in numerous *Actinobacteria* (Figure 1.16). Interestingly, most *Actinobacteria* have ParH but not all of them have Hyp.

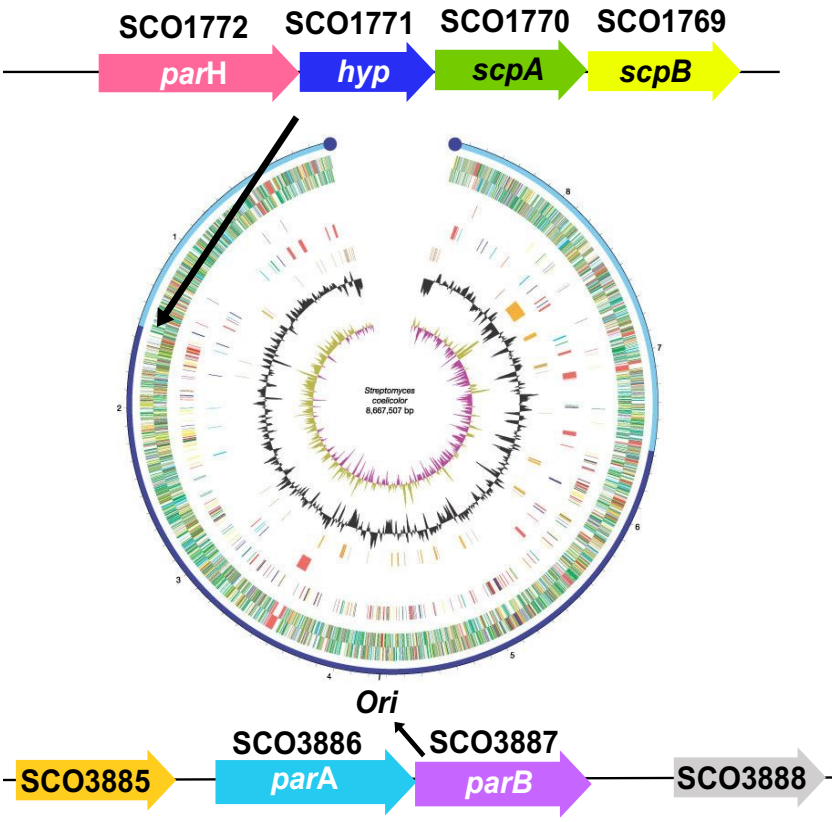

Figure 1.14 Chromosomal location of ParA and ParH

ParH is encoded by a gene found halfway between the origin of replication and the terminator region to the left of the origin while ParA is encoded on the *parAB* operon located near the origin. Taken from Gillespie, Unpublished, 2017

Despite ParH is a ParA-like protein and its homologous to many other ParA-like and MinD-like proteins, the identification other ParA-like proteins that are located alongside similar genes were determined. Thorough the searching found that there are similar gene arrangements throughout *Actinobacteria*, but not outside this phylum (Figure 1.15). This suggested that this Par-A like protein is specific to *Actinobacteria*. Interestingly, while the gene encoding hyp is found throughout *Streptomyces* species, it is not found in all *Actinobacteria*, notably being absent from the genomes of *Mycobacteria* and *Corynebacteria*. Also of note is the presence of a gene encoding the protein

XerD, which is found upstream if the gene encoding ParH in many organisms, although not in *Streptomyces* species. XerD is a site specific tyrosine recombinase involved in the resolution of circular chromosomes after replication. The linear chromosomes of *Streptomyces* species mean that they are not required to resolve replicated chromosomes and so the absence of this protein is expected (Gillespie, Unpublished 2017).

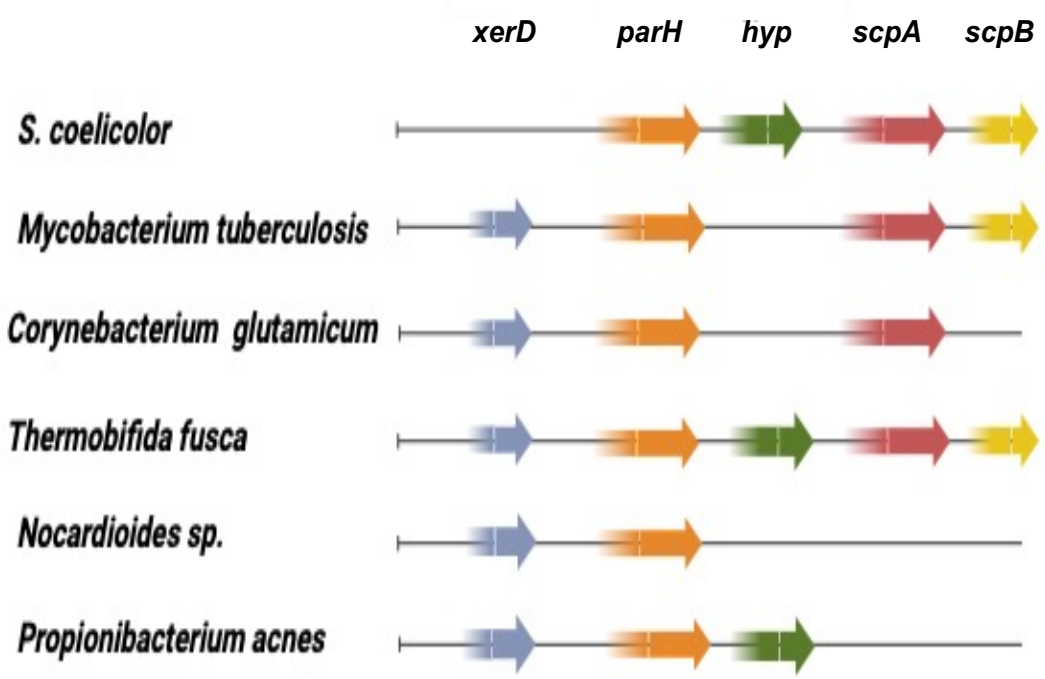

Figure 1.15 Similar gene arrangements throughout *Actinobacteria* around ParH

The orange arrows indicate genes similar to ParH. While the green arrows indicate genes similar to Hyp, illustrating that it is not present in all *Actinobacteria.* Modified from Gillespie, Unpublished 2017 (Biorender)

The *parH* null mutant generated showed delayed sporulation phenotype compared to the wild type when grown on solid medium. Moreover, fluorescent microscopy revealed that the mutant strain of *parH* showed irregular septation compared to the wild type strain as well as aberrant branching in the aerial hyphae. These observations suggested that ParH plays

a role both during cell growth and cell division. Further analysis of the mutant strain of *parH* revealed that it developed smaller colonies that the wild-type strain as well as producing fewer viable spores. While the *parH-hyp* double mutant showed similarity with the phenotype of the *parH* mutant strain, the analysis of the *hyp* mutant had not revealed a significant phenotype under the conditions tested.

1.3.5.1 ParH and Hyp

ParH and Hyp were overexpressed as His-tagged proteins, His-ParH and His-Hyp in *E. coli* and purified using Ni-affinity chromatography (Gillespie, Unpublished 2017). Interestingly, purified His-ParH showed oligomerisation when run using native-PAGE gel. Analytical gel filtration, chemical cross linking, and a Ferguson plot led to demonstrate that ParH assemblies into multiple oligomers and that ATP had no effect on this oligomerisation (Gillespie, Unpublished 2017). However, the investigation made for other ParA-like proteins revealed that dimerisation and oligomerisation were dependent on ATP binding. Interestingly, when Hyp was added to ParH, ParH-Hyp interaction was detectable but the interaction between ParH and Hyp occurred only between higher oligomers of ParH and Hyp, demonstrated that the ParH oligomeric state is necessary for interaction with Hyp. Moreover, this possibly suggests that the regulation mechanism could exist which would regulate ParH oligomerisation and in turn regulate ParH-Hyp interaction.

Further investigations of interaction between ParH and Hyp are confirmed in *vitro* using pelleting assay and in *vivo* using bacteria two-hybrid assay. The interaction in *vitro* revealed that is not dependent on, nor is it effected by the presence of ATP, suggesting that interaction occurs independently of ATP. Although we cannot rule out that ATP hydrolysis plays a role in the presence of a third molecule, perhaps DNA.

Hyp was shown to be a DNA binding protein in *vitro* through pelleting assay and electrophoretic mobility shift assay. Therefore, while Hyp is not a ParB

homologue, it is also a DNA binding partner of a ParA-like protein. Hyp has not yet shown a specific DNA target sequence, but it is a possibility that one exists (more details in the next section 1.3.6) (Gillespie, Unpublished 2017).

1.3.6 Hyp is a ribbon-helix-helix DNA binding protein

When sequences of Hyp proteins from different *Actinomycetes* were compared, it was clear that high conservation was shown at a short N-terminal sequence and the C-terminal ~72 amino acid fragment. When the structure of Hyp was solved using X-ray crystallography, it was revealed that the C-terminal domain had a β-strand followed by three α-helices that form a tetramer consisting of a dimer of dimers (Figure 1.16). Using analytical gel filtration shown that the N-terminal domain of Hyp has a capability to form a tetramer while the C-terminal domain is monomeric (Gillespie, Unpublished 2017). While the N-terminal domain is responsible for tetramerization it does not rule out the possibility that the C-terminal domain could form a dimer of a tetramer in the absence of N-terminal domain. During searching for structural homologues of Hyp revealed that the C-terminal domain consisted of a ribbon-helix-helix DNA (RHH) binding domain. These domains are widely spread in bacteria and have been implicated in diverse functions such as anti-toxicity and controlling plasmid segregation. A key feature of RHH domains is the specificity to the DNA target that the ribbon motif provides. Across RHH domain the residues in positions 2, 4 and 6 of the ribbon all provide a specific interaction to their target DNA bases. The target DNA sequence could be specific, but short and there might be very large number of short target sequences in the *Streptomyces* genome, suggesting that Hyp binding sites might be abundant.

Figure 1.16 Structure of C-terminal domain of Hyp

The structure of C-terminal domain as revealed by X-ray crystallography has four subunits, each contain β-strand followed by three α-helices. Taken from Gillespie, Unpublished 2017

1.4 Aims

In the context of this thesis, the objectives have been set to expand upon the foundational insights previously generated by (Gillespie, Unpublished 2017) and to further elucidate the roles played by ParH and Hyp in the developmental processes of *Streptomyces*. The outlined objectives are structured to comprehensively investigate the interactions and functions of ParH within the broader framework of chromosome partitioning and its interrelation with cell division.

To achieve this, the following objectives have been defined:

1. Exploring Protein Interactions

This objective seeks to delve into the intricate web of protein interactions that underlie Streptomyces development. By employing Bacterial Two Hybrid assays, we aim to investigate how ParH interacts with key partner proteins. This includes examining its interaction with proteins governing critical aspects such as cell division (SepF), polar growth regulation (Scy and Dia), and chromosome segregation (ParB). Through these interactions, we anticipate uncovering insights into how ParH is intricately linked to the larger context ofn chromosome organisation and division.

2. Deciphering Oligomerisation Dynamics

The second objective involves investigating the oligomerisation behavior of ParH. By overexpressing and purifying these proteins, we intend to recreate native PAGE experiments. This approach will allow us to unravel the oligomerisation patterns of ParH and how they are influenced by partner proteins. Furthermore, we will employ gel shift assays to assess ParH DNA binding affinity and how this interaction is modulated by the presence of

partner proteins. These experiments are designed to shed light on the mechanistic underpinnings of ParH role in chromosome organisation.

3. Unraveling Gene Expression Patterns

Our third objective aims to discern the gene expression landscape of *parH* mutant strain in comparison to the wild type. Utilizing RNA-Seq, we will systematically analyze and compare gene expression profiles between these two strains. This investigation will provide valuable insights into how the absence of ParH impacts the cellular transcriptome, thereby revealing its broader influence on *Streptomyces* development.

As we embark on these research endeavors, it is crucial to place our work within the broader context of chromosome partitioning and its symbiotic relationship with cell division. By focusing on ParH multifaceted role in interacting with proteins associated with both chromosome organization and cell division, we aspire to contribute to a deeper understanding of the fundamental mechanisms governing *Streptomyces* development. This exploration stands to uncover new dimensions of the intricate coordination that underlies the life cycle of *Streptomyces*, ultimately advancing our knowledge of these complex cellular processes.

CHAPTER 2

2. Material and Methods

2.1 Bacterial strains and plasmids

E. coli Strains Used in this Study

Table 2.1 The *Escherichia coli* strains used throughout the current study.

Strains	Genotype	Standard Growing Temp (°C)	Reference or Source
BL21 (DE3) pLysS	*F-, dcm, ompT, lon, hsdSB(rB⁻ mB⁻), gal, λ (DE3), pLysS(cm^R)*	37	(Studier and Moffatt, 1986)
DH5α	F- endAI hsdRJ7 (r-, mit) supE44 thi-J ArecAI gyrA96 relAI deoR A(lacZYA-argF)-U169 480dlacZAM15	37	Grant *et al*., 1990
BTH101	F′, *cya-99, araD139, galE15, galK16, rpsL1 (StrR), hsdR2, mcrA1, mcrB1, relA1*	37	Karimova *et al.,* 1998

S. coelicolor Strains used in the present study

Table 2.2 *Streptomyces* strains used in this study

Strain	Genotype	Reference or Source
M145	*Chromosome*: SCP1-, SCP2-	Bentley *et al*., 2002
parH	M145 parH::aac(3)IV	Kelemen Lab, UEA
hyp	M145 hyp::aac(3)IV	Kelemen Lab, UEA
dia		Kelemen Lab, UEA
sepf	*Chromosome*: Δ*scy*::*apraR* SCP1-, SCP2-	Kelemen Lab, UEA
scy	*Chromosome*: Δ*scy*::*apraR* SCP1-, SCP2-	Holmes *et al.,* 2013

Plasmids used throughout the present study.

Table 2.3 Plasmid/Cosmid DNA used in this study.

Plasmid	Genotype	Reference or Source
pMS82	ori pUC18, hyg, oriT RK2, int ΦBT1, attP	(Gregory et al., 2003)
pET28a	*ori* pBR322, T7 Promoter, His•Tag coding sequence, *lacI, kan, ori* f1	Novagen
pET28a-ParH	pET28a with ParH	Current work
pET28a-Hyp	pET28a with Hyp	Current work

Table 2.4 The bacterial two hybrid assay plasmids used in the current study.

Plasmid	Genotype	Reference or Source
pUT18C	Generates the T18-protein fusions in the bacterial two hybrid assay	Euromedex
pUT18	Generates the protein-T18 fusions in the bacterial two hybrid assay	Euromedex
pKT25	Generates the T25-protein fusions in the bacterial two hybrid assay	Euromedex
pKNT25	Generates protein-T25 fusions in the bacterial two hybrid assay	Euromedex
pUT18C-ParH	T18-ParH Expression	Kemelen *et al*.(unpublished)
pUT18-ParH	ParH-T18 Expression	Kemelen *et al*.(unpublished)
pKT25-ParH	T25-ParH Expression	Kemelen *et al*.(unpublished)
pKNT25-ParH	ParH-T25 Expression	Kemelen *et al*.(unpublished)
pUT18C-SepF	T18-SepF Expression	Kemelen *et al*.(unpublished)
pUT18-SepF	SepF-T18 Expression	Kemelen *et al*.(unpublished)
pKT25-SepF	T25-SepF Expression	Kemelen *et al*.(unpublished)
pKNT25-SepF	SepF-T25 Expression	Kemelen *et al*.(unpublished)
pUT18C-Dia	T18-Dia Expression	Kemelen *et al*.(unpublished)
pUT18-Dia	Dia-T18 Expression	Kemelen *et al*.(unpublished)
pUT18-Dia	T25-Dia Expression	Kemelen *et al*.(unpublished)
pKNT25-Dia	Dia-T25 Expression	Kemelen *et al*.(unpublished)

2.2 Media

Table 2.5 The media used throughout the current study.

Media	Components / Descriptions
Soya Flour Mannitol (SFM) **(For general growth and phenotypic analysis of *S. coelicolor* strains)**	Components*:* 2% agar, 2% soya flour and 2% mannitol. Dissolved in hard tap water. The 60 g of mannitol was dissolved in 3000 ml of tap water while 6 g soya flour and 6 g agar were measured into 500 ml Duran bottles. The dissolved mannitol media was dispensed in 300 ml aliquots into 500 ml Duran bottles and twice autoclaved.
Lennox Broth (LB) Agar (Kieser et al., 2000) **(For growing of E. coli strains and spore titres of S. coelicolor strains)**	Components: Tryptone 16 g, Yeast extract 8 g, NaCl 8 g, and 16 g of Glucose. All components were dissolved in 1600 ml dH_2O, while 4 g of agar was measured into 500 ml Duran bottles. Then the dissolved media was dispensed in 400 ml aliquots into Duran bottles and autoclaved.
Minimal Media Mannitol (MMM) **(For general growth and phenotypic analysis of *S. coelicolor* strains)**	For 4 x 400 ml MMM, into 1.6 L dH2O was dissolved 0.8 g L- Asparagine (anhydrous) or 0.91 g L-asparagine (monohydrate), 0.8 g K2HPO4, 0.32 g MgSO4·7H2O, 0.016 g FeSO4·7H2O, and 8 g mannitol. The media was then adjusted to pH 7-7.2 using orthophosphoric acid. This was equally divided into 4 x 500 ml Duran bottles contains 4 g agar. The media was autoclaved once
Lennox Broth (LB) (Kieser et al., 2000) **(For growing of *E. coli* strains)**	Components: Tryptone 10 g, Yeast Extract 5 g, NaCl 5g, and Glucose 1g. All components were dissolved in 1000 ml dH_2O. Once dissolved, the media was dispensed, either in 10 ml aliquots into universal or in 50 ml aliquots into 250 ml conical flasks, and autoclaved.

2.3 Bacterial growth conditions and storage

S. coelicolor strains

S. coelicolor strains were grown on SFM containing the appropriate antibiotics and incubated at 30°C until the required developmental stage. For storage (spore preparation), S. coelicolor spores were streaked on a single SFM plate to generate a confluent lawn and incubated at 30°C until mature spores developed. Spores were harvested by rubbing spores in a layer of water using a cotton bud. The spore suspension was collected in a 15 ml falcon tube using a pastor pipette. The spores were centrifuged for 10 minutes at 4500 g at 4°C and the supernatant removes. The spores were re-suspended in approximately 1 ml 20% glycerol and stored at -20°C in a 2 ml microcentrifuge tube with a screw cap. The viable spore concentration was determined by plating out a dilution series on LB agar plates containing the appropriate antibiotics.

E. coli strains

E. coli strains were grown in either LB solid or liquid media and incubated at 37°C, except for BW25113/pIJ790, which was grown at 30°C due to the presence of a temperature sensitive plasmid (pIJ790). Glycerol stocks were generated by making a 1:1 mixture of culture to 100% glycerol, and stored at -20°C.

Table 2.6 The antibiotics used throughout the current study.

Antibiotics	Stocks (mg/ml)	SFM media (final concentrations µg/ml)	LB media (final concentrations µg/ml)
Apramycin	100	50	50
Chloramphenicol	25	25	25
Kanamycin	100	50	50
Hygromycin	50	25	25
Ampicillin	100	-	100
Nalidixic acid	25	25	25
X-gal	20	-	40
IPTG	1M	-	0.5mM

2.4 General Biomolecular Methods

Plasmid DNA isolation from *E. coli*

A single colony of DH5α (or BW25113 for cosmids after cassette targeting) with the desired plasmid DNA was inoculated into 50 ml LB supplemented with appropriate antibiotics. Inoculums were grown overnight at 37°C (shaking 250 rpm). In a 50 ml falcon, overnight growth was centrifuged for 5 minutes at 5000 g at 4°C. Afterwards, 40 ml of Solution 1 was added to the cells, and they were centrifuged at 5000 g for 5 minutes at 4°C. After discarding the supernatant, cells were resuspended in 1 ml Solution 1 before adding 2 ml Solution 2. Cells were gently mixed and incubated for 4 minutes on ice after being turned in a falcon tube. The lysate was shaken vigorously after 1.5 ml of Solution 3 was added after incubation. Afterwards, the lysate was centrifuged at 4°C for 10 minutes for 10 minutes at 5000 g after being incubated for 10 minutes on ice. In a 15 ml falcon, the supernatant was mixed with 500 ml of 1:1 phenol:chloroform. A vortex was applied to the extract for thirty seconds, followed by 5 minutes of centrifugation at 5000 g. An aqueous phase was collected after centrifugation and was added to a fresh 15 ml falcon with 7 µl of 30 mg/ml RNase. The extract was incubated at 37°C for 1 hour. As before, phenol:chloroform extract was performed after incubation. To precipitate the DNA, the aqueous phase was mixed 1:1 with isopropanol kept at -20°C, then the solution was mixed by inversion and incubated on ice for 30 minutes. DNA precipitated at 4°C was centrifuged for 15 minutes at 5000 g. After discarding the supernatant, the DNA pellet was washed with 2 ml 70% ethanol and stored at -20°C. The DNA was centrifuged for 5 minutes at 5000 g at 4°C and the supernatant was discarded. DNA pellets were allowed to air dry for five minutes before being re-suspended in 200-400 µl of sterile water. Then, DNA was stored at -20°C.

Solution I: 50 mM Tris/HCl, 10 mM EDTA pH8

Solution II: 200 mM NaOH, 1% SDS

Solution III: 3 M potassium acetate pH5.5

Agarose gel electrophoresis of DNA

Agarose gels of 1x TAE buffer (40 mM Tris acetate, 1 mM EDTA, pH8), 0.5 µg/ml ethidium bromide were cast using the Bio-Rad Mini-Sub and Sub-cell trays. Gels were made in a range between 0.7% and 1% agarose . DNA was mixed with 1x loading dye (5 mM Tris, 5 mM EDTA, 5 % Glycerol , 0.005% Xylene Cyanol, 0.005% Bromophenol Blu, pH7.4) and run in gels submerged in 1x TAE buffer. Gels were imaged with UV light using a Bio-Rad trans- illuminator. For estimating band sizes, a size marker of λ DNA digested with *HindIII*, and *EcoRI* was applied.

Polymerase Chain Reaction

PCR reactions were performed using a BioRad T100 Thermo Cycler.

Oligonucleotide Sequences used in this Study

Table 2.7 Oligonucleotide sequences

Primer	5’ to 3’ primer sequences
ParH P EgFp*BamHI* FRW	GGATCAGGATCCTATGGTCACTTTGCGATTCTCG
ParH SQcrsp REV	GCTCCATGAGCAGGTTGTAGACGG
Dia 5569 XbaNde FRW	GGATCATCTAGAGCATATGGTGGACGTGCAGAACAAGCTCG
Dia 5569 Eco UT REV	GCTACGAATCCCTAGAGCCCGCGGCCCTGTTCG
SepF2 Xbal Bgl FRW	GATCACTCTAGATCTGACCGTGGCCCCGCTCAGCGG
mCherryHind REV	CAGTCAAGCTTTTACTTGTACAGCTCGTCCATGCC

In the present study the low fidelity PCR was applied under the following conditions: Go Tag polymerase buffer x1, 200 μM of each dNTP, 2.5 mM $MgCl_2$, 5 % DMSO, 1 μM of each primer and 0.02 U/ μl Invitrogen Go Tag DNA polymerase. The applied cycles were presented in the following Table (Table 2.8). The extension times were calculated as 30 seconds per 0.5 kpb for the desired PCR product.

Table 2.8 The PCR cycles completed during the present study.

Base cycles		
1. Initial Denaturing	96° C for 300 sec	
2. Denaturing	92° C for 60 sec	32 cycles
3. Primer Annealing	55° C for 30 sec	
4. Extension	72° C for 51 sec	
5. Final Extension	72° C for 300 sec	
6. Cool Down	20° C for 300 sec	

Transformation of Competent *E. coli* Cells

i) Electroporation

A single colony of the appropriate strain of *E. coli* was inoculated into 10 ml of LB containing appropriate antibiotics and incubated overnight at 37°C or 30°C depending on the strain while shaking at 250 rpm. This overnight culture was subcultured, using 1% of the new volume, into either 10 ml or 50 ml fresh LB with appropriate antibiotics. The culture was incubated at the appropriate temperature until the OD600 reached around 0.7. After centrifugation for five minutes at 5000 g at 4°C, the cells were collected. After removing the supernatant, the cells were centrifuged at 5000g for 5 minutes at 4°C twice in 10% glycerol. Following the second wash, the pellet was resuspended in a final volume of approximately 100 μl per 10 ml of initial culture 10% glycerol. The transformation was performed by mixing 45 μl of cells with 1 μl of plasmid or cosmid DNA. Using a BioRad Gene Pulser 2 set to 200 Ω, 25 μF and 2.5

kV, the electroporation was conducted in an ice cold 0.2 cm electroporation cuvette. After electroporation, cells were mixed with 500 µl ice cold LB and incubated for 1 hr at either 30°C or 37°C before plating onto LB agar plates with appropriate antibiotics. Plates were incubated overnight at either 30°C or 37°C.

ii) **Chemical Transformation**

The appropriate strain of *E. coli* was inoculated into 10 ml of LB with appropriate antibiotics and grown either at 30°C or 37°C overnight. These overnights were subcultured, 500 µl into 50 ml fresh LB with appropriate antibiotics and incubated at the appropriate temperature until the culture reached an OD600 of around 0.4- 0.6. The cells were centrifuged at 4°C for 5 minutes at 5000 g. The supernatant was discarded, and the cells washed with 10 mM NaCl centrifuging in the same way as before. The supernatant was removed, and the pellet resuspended in 30 mM $CaCl_2$, 10 mM $RbCl_2$ and incubated on ice for 1 hr at 4°C. After this incubation, the cells were centrifuged as before and the pellet resuspended in 500 µl 30 mM $CaCl_2$, 10 mM $RbCl_2$. For transformation, 50 µl cells were mixed with 1 µl plasmid or cosmid DNA or 5 µl ligation mix and incubated for 30 minutes on ice. The cells were then heat shocked at 42°C for 1 minute, 1 ml ice cold LB was added and placed in ice to cool after heat shock. After plating on LB agar plates with appropriate antibiotics, this was placed at 30°C or 37°C for one hour. Incubation was carried out overnight at 30°C or 37°C.

Conjugation into *S. coelicolor*

The *E. coli* strain ET12567/pUZ8002 was used to conjugate vectors containing oriT into *S.coelicolor*. Inoculation of a single ET12567/pUZ8002 colony containing the desired plasmid or cosmid for conjugation in 10 ml of LB containing kanamycin, chloramphenicol, and the antibiotic for which the plasmid or cosmid confers resistance was carried out. These were grown overnight at 37°C, 250 rpm. These overnight cultures were subcultured by transferring 100 µl into fresh 10 ml LB with the appropriate antibiotics. Fresh

cultures were incubated at 37°C with shaking until OD600 0.4-0.6 was achieved. After centrifugation for 5 minutes at 5000 g at 4°C, the cells were collected. As before, the supernatant was removed, and the cells were centrifuged twice in 10 ml LB. The pellet was re-suspended in 250 µl LB and kept on ice. Approximately 10^8 spores of the desired *S. coelicolor* strain were added to 500 µl of LB and allowed to germinate for 10 minutes at 50°C before cooling on ice. After cooling, the germinating spores were mixed with the ET12567/pUZ8002 cells containing the plasmid/cosmid and centrifuged for 2 minutes at 16,000 g at 4°C. The supernatant was removed, and the pellet re-suspended in 300 µl sterile water. A dilution series was carried out in which three 10x dilutions were made. Onto SFM containing 10 mM MgCl2 and incubated at 30°C, the stock and 3 dilutions were then plated. The plates were then overlaid with 500 ml of sterile water containing nalidixic acid and antibiotics after overnight incubation. Incubation was continued at 30°C until colonies had developed mature spores (5-8 days). Successful ex-conjugants were selected and streaked for single colonies on SFM supplemented with nalidixic acid and the appropriate antibiotics and grown at 30°C until spores were produced. After that, spore preparations were generated from a single colony of the streaked plate.

Spore prep generation

Single colonies were generated by streaking strains on SFM media that contained antibiotics and growing them at 30°C. To generate a confluent plate, a single colony was then streaked on SFM containing the appropriate antibiotics. On SFM media containing a layer of cellophane, non-sporulating strains were streaked for confluency. Plates were grown until confluent at 30 °C. Once confluent, spores were liberated using a dampened cotton bud and ≈5 mL dH2O. It was centrifuged (4000 rpm, 5 minutes, 4°C) after the spore solution was removed. The resulting supernatant was discarded, and the spores re-suspended in 1 ml 20% glycerol. For non-sporulating strains, the confluent area was removed with a sterile spatula and deposited into 1 ml storage medium.

2.5 Microscopy of *S. coelicolor*

Cells were grown on solid SFM medium and samples were taken by excising a piece of agar block containing a colony and attaching it to a copper stub. After quick freezing in nitrogen slush the sample was transferred onto a Quorum Technologies PP3010T Cyro-SEM Preparation system attached to a Zeiss Gemini 300 scanning electron microscope. After 15-minute sublimation of surface frost the samples were sputter-coated with platinum for 1 minute at 10 mA at -140 degrees, where they were viewed at 2 kV, and digital TIF files were stored.

2.6 Protein Purification

Cell Lysis

Protein expression was performed according to the optimal conditions as performed in the results section. Once cells with over production of the target protein were generated, for large scale purification they were collected in a 500 ml Beckmann centrifuge tube and centrifuged for 7 minutes at 7000 g using a Beckmann Avanti J20 centrifuge and a Beckmann JA 10 500 rotor. For small scale purification, they were collected in a 50 ml falcon tube and centrifuged at 4000 g for 10 minutes. The supernatant was discarded, and the cells were re- suspended in approximately 50 ml (or 5 ml) of the appropriate binding buffer. The cells that contain protein to be purified under denaturing conditions were re-suspended in Tris binding buffer and native lysis was performed first. Cell lysis was achieved using a high pressure homogeniser french press at a pressure of 1000 psi for large scale, or sonicated for the small scale. After lysis, the lysate was deposited in a 50 ml Beckmann centrifuge tube and centrifuged for 30 minutes at 20000 g using a Beckmann Avanti J20 centrifuge and a Beckmann JLA 25 50 rotor or at g in a benchtop centrifuge for 30 minutes at 4°C. For proteins that were purified under native conditions the supernatant was collected and used for purification. For proteins purified under denaturing conditions, the supernatant was discarded, and the pellet was re-suspended using denaturing binding buffer.

Protein Purification Under Native Conditions

Binding buffer	50 mM Tris, 300 mM NaCl, 20 mM $MgCl_2$, 10 mM imidazole pH8
Washing buffer	50 mM Tris, 300 mM NaCl, 20 mM $MgCl_2$, 20 mM imidazole pH8
Elution buffer	50 mM Tris, 300 mM NaCl, 20 mM $MgCl_2$, 300 mM imidazole pH8
Cleaningbuffer	50 mM Tris, 300 mMNaCl, 20 mM $MgCl_2$, 500mM imidazole pH8

Large scale purification was achieved using a 2 ml Ni-Sepharose pre-packed gravity column from Novagen. The column was washed with 5 column volumes of first deionised water and then binding buffer to equilibrate. After centrifugation the supernatant was applied to the column and allowed to drip through, with the flow through collected in a single fraction. The column was then washed with 10 ml binding buffer which was collected in a single fraction.

After the initial wash the column was washed with 10 ml washing buffer which was collected in a single fraction. The protein was then eluted with 12 ml elution buffer which was collected in twelve 1 ml fractions. The column was then cleaned to ensure all protein had passed through using 12 ml cleaning buffer collected first as two 1 ml fractions then the subsequent 10 ml as one fraction. Fractions containing purified protein were identified using SDS-PAGE.

Protein Purification Under Denaturing Conditions

Denaturing binding buffer	8 M Urea, 0.1 M NaH2PO4, 0.01 M Tris-HCl, pH 8.0
Denaturing washing buffer	8 M Urea, 0.1 M NaH2PO4, 0.01 M Tris-HCl, pH 6.3
Denaturing elution buffer	8 M Urea, 0.1 M NaH2PO4, 0.01 M Tris-HCl, pH 4.5

The pellet was re-suspended in approximately 20 ml of denaturing binding buffer, after removing soluble proteins using the native cell lysis protocol as described above. To solubilise the target protein, the suspension was gently stirred for one hour. As a next step, the lysate was placed in a Beckmann Avanti J20 centrifuge tube and centrifuged for 30 minutes at 20000 g with the Beckmann JLA 25 50 rotor. Purification was performed using a 2 ml Ni-Sepharose pre-packed gravity column from Novagen. In order to equilibrate the column, 5 column volumes of first deionised water and then denaturing binding buffer were used. After centrifugation the supernatant was applied to the column and allowed to drip through, with the flow through collected in a single fraction. The column was then washed with 10 ml denaturing binding buffer which was collected in a single fraction. After the initial wash the column was washed with 10 ml denaturing washing buffer which was collected in a single fraction. A denaturing elution buffer of 22 ml was then used to elute the protein, which was fractionated into twelve 1 ml fractions and a 10 ml fraction. Using SDS-PAGE gel, purified protein fractions were identified.

Dialysis

Dialysis was accomplished using Spectra/Por® molecularporous membrane tubing with a molecular weight cut off of 3500 Da. Dialysis was performed in either a small scale for volumes less than 1 ml. For small scale the tubing was cut open and 5 cm^2 squares were cut and equilibrated in the target buffer for 10 minutes. The protein was aliquoted into a 2 ml microcentrifuge tube with the lid removed. The O-ring from the lid was removed and used to secure the membrane over the top of the microcentrifuge tube by fixing it to the underside of the lip. The membrane was pulled tight across the opening to ensure a flat surface. In the target buffer, the tube was placed upside down in a float so that the membrane separated the internal solution from the buffer used for dialysis. For at least two hours at a time, the buffer was gently stirred. The buffer was replaced twice so that three dialysis sessions were performed.

Determining the concentration of protein solutions

The Bradford assay was performed for measuring protein concentration. A standard curve was generated using known concentration of reactions containing BSA. Tubes were set up in 200 µl volume such that the final concentration of BSA in a 1 ml volume was as follows: 0 µg/ml, 1 µg/ml, 2.5 µg/ml, 5 µg/ml, 7.5 µg/ml and 10 µg/ml. Bio-Rad protein assay reagent was diluted in a1:3 ratio with deionised water and mixed .The reagent was then used to make the standard curve reactions 1 ml in volume. The reactions were incubated for 5 minutes at room temperature before their absorbance measured at 595 nm in a Jenway 7205 spectrophotometer. The protein of unknown concentration was measured first by diluting a small volume (1-5 µl) to 200 µl with deionised water. This was then treated the same way as the reactions used to generate the standard curve. The absorbance of the unknown protein was then compared to the standard curve and protein concentration estimated.

SDS-PAGE

SDS-PAGE gels were casted using the ATTO system. In the resolving gel, the acrylamide percentage were varied between 8 and 15% depending on the size of the protein that was being analysed. The protein loading dye was added to protein samples such that it diluted to a 1x buffer. In order to denature protein, the protein was heated at 95°C for 5 minutes before being cooled on ice. The gel was placed in the ATTO tank and submerged with 1x SDS-PAGE running buffer. An electrophoresis at 200 volts was conducted for 45 minutes to 1 hour after samples were loaded. With gentle agitation, the gels were stained for a minimum of 1 hour with Colloidal Coomassie blue R250 after running. Gels were de-stained in 50% ethanol, 2% acetic acid for 2 x 1 hr. Using a Bio-Rad trans-illuminator, the gels were illuminated with white light.

CHAPTER 3

3. Establishing a link between ParH and possible Partner Proteins

3.1 Introduction

Preliminary studies by a PhD student in the Kelemen lab indicated that the ParH protein plays an important role during sporulation, based on the phenotype of the *parH* knockout mutant, which stayed white even after 5 days of growth on solid medium (Gillespie, Unpublished 2017). The *parH* gene is not conserved among all *Actinobacteria*. In *S. coelicolor*, the *parH* gene is located within an operon containing the gene encoding the hypothetical protein called *hyp* (Chapter 1, Figure 1.14). In both macroscopic and microscopic analysis, *parH* mutant strains displayed defects in septum placement during sporulation (Gillespie, Unpublished 2017).

Similar to rod-shaped bacteria, in *Streptomyces* the ParAB proteins are responsible for segregating multiple chromosomes in sporogenic hyphal compartments (Jakimowicz, Chater and Zakrzewska-Czerwínska, 2002). In accordance with previously published data, two other proteins interact with ParA in *S. coelicolor*: ParJ, the Actinomycete-specific protein, which promotes the disassembly of ParA polymerisation prior to sporulation septation; and ParB which induces the ATPase activity of ParA (Chater *et al.*, 2007; Ditkowski *et al.*, 2010). In vegetative hyphae of *S. coelicolor*, ParA proteins are mostly associated with the tips, followed by ParA filaments extending along the sporulating aerial hyphae and trigger the regularly spaced distribution of the ParB complex (Donczew *et al.*, 2016).

In *S. coelicolor,* the chromosome organising protein, ParA, interacts with the tip polarity protein, Scy. Data analysis of previous studies showed that ParA binds to Scy through the C-terminal domain of Scy. ParA is likely inhibiting the assembly of Scy into higher order organisation, whereas Scy blocks the polymerisation of ParA and persuades its depolymerisation. As part of the TIPOC, Scy is essential for assembly and organisation of this polarity centre and can recruit ParA to the growing tip. In the hyphae of a *scy* knockout

mutant, ParA filamentation was observed along the hyphae and chromosomes were unevenly distributed (B. Ditkowski *et al.*, 2013; Holmes *et al.*, 2013).

In the current chapter, we investigate proteins involved in polar growth and cell division for possible interaction with ParH in *vivo*, in the heterologous host *E. coli,* using the bacterial two hybrid system. Initially, we characterise the link between ParH and the cell division protein SepF. Here we utilize the C-terminal of SepF which consistent with the truncated construct used for characterisation the interaction of SepF from *B. subtilis* (Duman *et al.*, 2013). In *B. subtilis* deletion of the 63 amino acid N-terminus of SepF did not the interaction between SepF and FtsZ or self- interaction. Therefore the C-terminal of SepF from *B. subtilis* is sufficient to form circular polymers with a ~50 nm diameter (Duman *et al.*, 2013). Then we also conducted further investigations aimed to examine the effect of deleting important residues in ParH on the ParH-sepF interaction. These residues are involved in dimerisation, ATP binding, and hydrolysis. Furthermore, using the similar technique we search for the link between ParH and a key component TIPOC protein Scy, then ParH with chromosome segregation protein ParB. Finally, bacterial two hybrid evidence also attempts to investigate the interaction with the polar growth protein Dia (SCO5569).

3.2 Results

The phenotype of the *parH* mutant implies that it is delayed in sporulation. Sporulation is cell division of the aerial hyphae, and therefore we have evidence from this phenotype that ParH has an effect on cell division. Therefore, this justifies checking whether ParH has been directly linked to cell division. To accomplish this we used bacterial two hybrid technique. The principle of this technique is testing protein-protein interaction *in vivo* in the heterologous host *E. coli.* This method relies on interaction-mediated reconstitution of two complementary fragments, T18 and T25, of the catalytic domain of the adenylate cyclase from *Bordetella pertussis* (Karimova, Ullmann and Ladant, 2000). A reaction takes place when these two fragments are fused to interacting polypeptides, X and Y, heterodimerization of these hybrid proteins results in functional complementation between T25 and T18

fragments and, therefore, cAMP synthesis occurs (Figure 3.1, A). The T25 and T18 are not active when separated and not in contact (Figure 3.1, B). The cAMP binds to catabolite activator protein CAP, forming the cAMP-CAP complex which binds to the *lac* promoter and activate gene transcription. It turns on the expression on several resident genes, including *lac* which is involved in lactose catabolism (Figure 3.1, A). One of these genes that are activated when the T18 and T25 domains reconstitute the functioning adenylate cyclase enzyme is *lacZ*, encoding the beta-galactosidase enzyme that can hydrolyse X-Gal into a blue coloured compound.

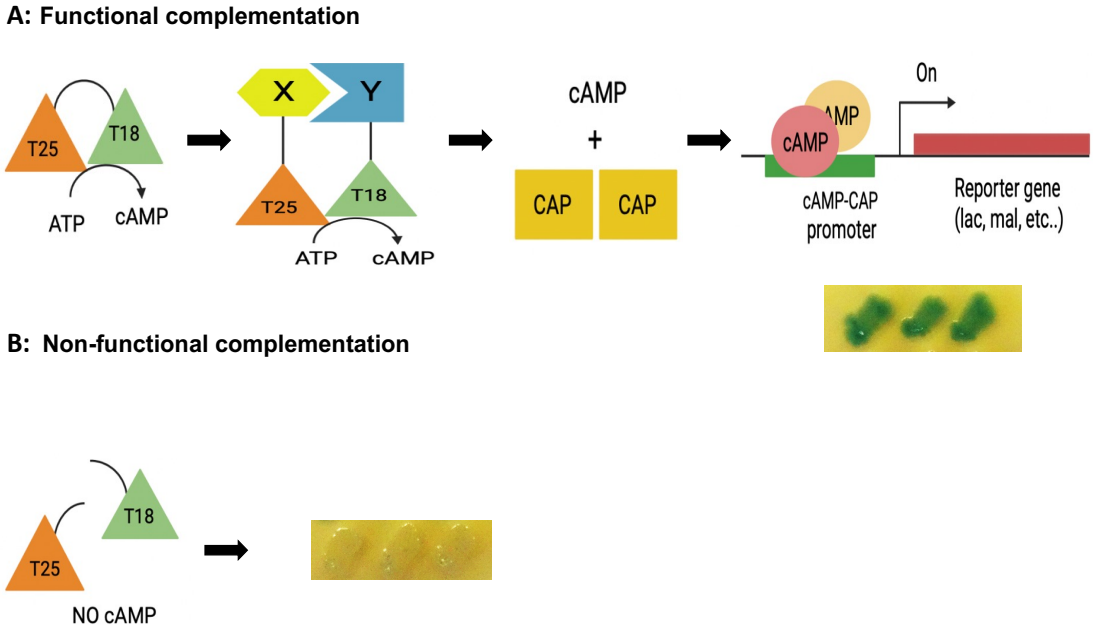

Figure 3.1 Bacterial Two Hybrid assays

The diagram represents the mechanism of the bacterial two hybrid system. (A) The fusion of T25 and T18 produces cAMP. Fusion of interacting proteins X and Y to T25 and T18 produces cAMP. (B) When T25 and T18 are not in contact – no cAMP is produced. Modified from (Euromedex BACTH System Kit, Bacterial Adenylate Cyclase Two Hybrid System protocol, 2016.

Four different vectors (Figure 3.2 A and B) are used to fuse proteins of interest to the T25 and T18 fragments, one of which expresses the T25 fusion (pKT25 and pKNT25), and one which expresses the T18 fusion

(pUT18 and pUT18C). The T25 and T18 tags can be used to tag the N-terminus or C-terminus of the protein tested. These four different vectors that were used for BTH assay are shown in Figure 2. In the T25 plasmids, there is a kanamycin resistance gene, while in the T18 plasmids, there is an ampicillin resistance gene, allowing for selection of two different constructs in a single bacterial cell. On each plasmid, the gene sequence for the protein was inserted between *XbaI* and *EcoRI* restriction enzyme sites. The two plasmids T25 and T18 are co-transformed in *E. coli* cells and are grown on LB-X-gal plates containing both antibiotics: ampicillin and kanamycin. When proteins interact and T25 and T18 fragments are brought together, cAMP is produced, as the positive activator for the *lacZ* gene encoding β-galactosidase. Therefore, this enzyme β-galactosidase breaks the X-gal substrate and bacterial colonies appear blue. On the other hand, when the two tags T18, T25 no interact, then the cAMP is not produced and the transcription of β-galactosidase gene cannot be promoted, as a result, X-gal substrate cannot be hydrolysed, leading to the white colonies.

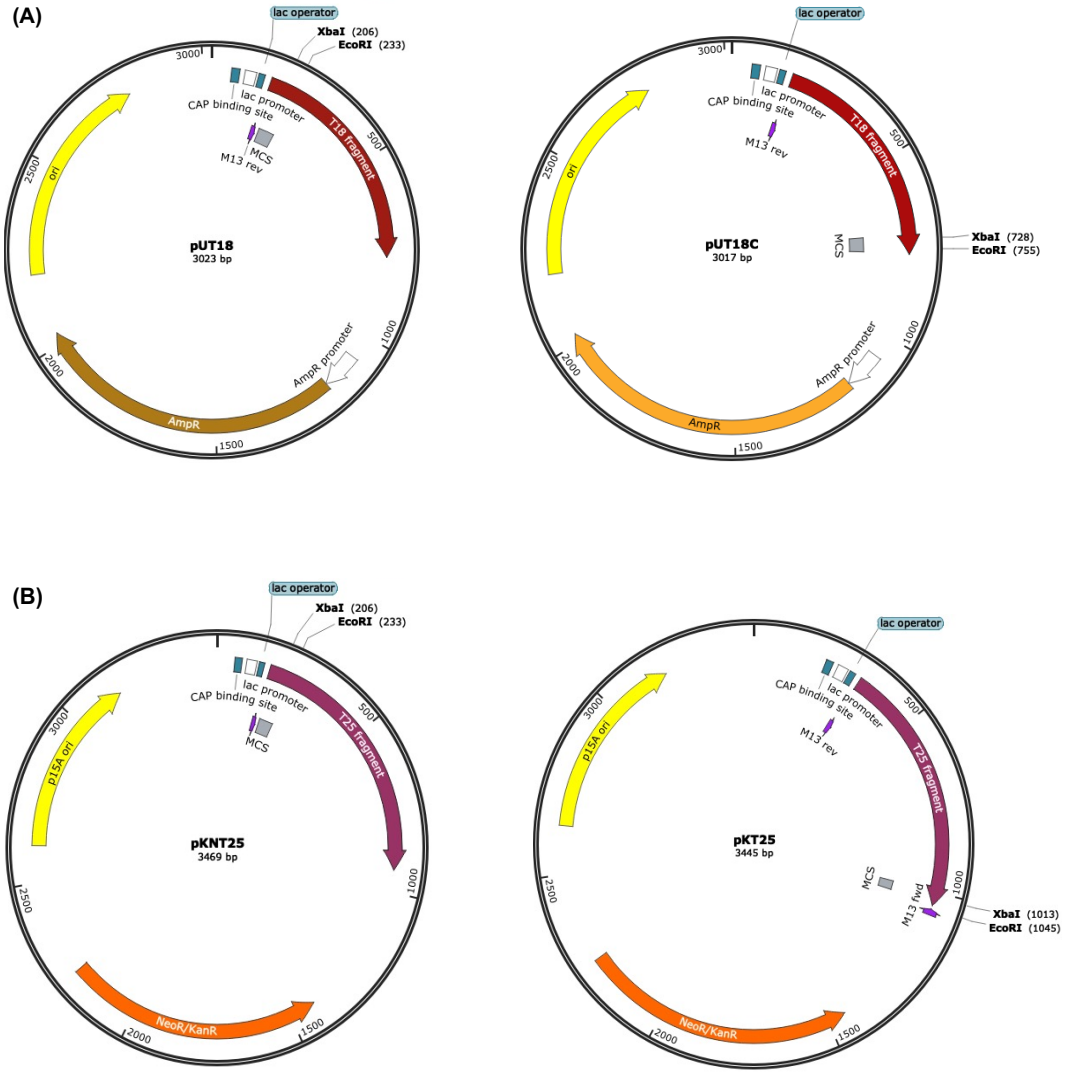

Figure 3.2 Bacterial Two Hybrid vectors pUT18C, pUT18, pKNT25, and pKT25

The vectors used to generate plasmids used in bacterial two hybrid assays pUT18, pUTC18 pKNT25, and pKT25, all of them contain DNA fragment encoding a domain of adenylate cyclase. (**A**) The vectors pUT18c and pUT18 express the T18 domain which is driven by the *lac* promoter, containing an origin of replication and ampicillin resistance gene. (**B**) The vectors pKNT25 and pKT25 express the T25 domain which is driven by the *lac* promoter, containing an origin of replication and kanamycin resistance gene. Vector maps were designed using Snap Gene.

The interactions between ParH and partner proteins were accomplished *in vivo* using bacterial two-hybrid technique. The appropriate genes for *parH*, *parH* mutants, *sepF*, *sepF* mutants and *dia* were cloned into the bacterial two-

hybrid vectors pUT18, pKT25, pUT18c, and pKNT25, by previous members of the Kelemen lab. A list of constructs that was used to analyse interactions between proteins are shown in the table 3.1, 3.2, 3.3, 3.4, and 3.5.

Table 3.1: The recombinant plasmid combinations that were used to co-transform BTH cells. The table represents the combinations testing ParH and SepF or ParH and SepF mutants

	Interaction tested ParH-SepF	
Recombinant Plasmids	T18 ParH - T25 SepF	T18 ParH-SepF T25
	ParH T18-SepF T25	ParH T18-T25 SepF
	T18 SepF -T25 ParH	T18 SepF -ParH T25
	SepF T18-ParH T25	SepF T18-T25 ParH
	Interaction tested ParH – SepF K46A	
Recombinant Plasmids	T18ParH-T25SepF K46A	T18 ParH-SepF K46A T25
	ParH T18-SepF K46A T25	ParH T18-T25 SepF K46A
	T18 SepF K46A-T25 ParH	T18SepF K46A-ParH T25
	SepF K46AT18-ParH T25	SepF K46A T18-T25 ParH
	Interaction tested ParH - SepF F71A	
Recombinant Plasmids	ParH T18-T25 SepF F71A	T18 ParH- SepF F71A T25
	ParH T18- SepF F71A T25	ParH T18-T25 SepF F71A
	T18 SepF F71A- T25 ParH	T18 SepF F71A- ParH T25
	SepF F71A T18- ParH T25	SepF F71A T18-T25 ParH

Table 3.2 The recombinant plasmid combinations that were used to co-transform BTH cells. The table represents the combinations testing interactions between ParH mutants and SepF.

Interaction tested ParHG95A – SepF		
Recombinant Plasmids	T18 ParH G95A - T25 SepF	T18ParH G95A – SepF T25
	ParH G95AT18 – SepF T25	ParHG95AT18 - T25 SepF
	T18 SepF - T25 ParH G95A	T18 SepF - ParH G95AT25
	SepF T18 - ParH G95A T25	SepF T18 - T25 ParH G95A
Interaction tested ParH K99A - SepF		
Recombinant Plasmids	T18 ParH K99A - T25 SepF	T18 ParH K99A – SepF T25
	ParH K99A T18 – SepF T25	ParH K99A T18 - T25 SepF
	T18 SepF - T25 ParH K99A	T18 SepF - ParH K99A T25
	SepF T18 - ParH K99A T25	SepF T18 - T25 ParH K99A
Interaction tested ParH D121A - SepF		
Recombinant Plasmids	T18 ParH D121A-T25 SepF	T18 ParH D121A – SepF T25
	ParH D121A T18-SepF T25	ParH D121A T18 - T25 SepF
	T18 SepF -T25 ParH D121A	T18 SepF - ParH D121A T25
	SepF T18- ParH D121A T25	SepF T18 - T25 ParH D121A
Interaction tested ParH K94A - SepF		
Recombinant Plasmids	T18 ParH K94A-T25 SepF	T18 ParH K94A – SepF T25
	ParH K94A T18-SepF T25	ParH K94A T18 - T25 SepF
	T18 SepF -T25 ParH K94A	T18 SepF - ParH K94A T25
	SepF T18- ParH K94A T25	SepF T18 - T25 ParH K94A

Table 3.3: The recombinant plasmid combinations that were used to co-transform BTH cells. The table represents the combinations testing ParH and Scy or ParH mutants and Scy.

Interaction tested ParH-Scy		
Recombinant Plasmids	T18 Scy -T25 ParH	T18 Scy-ParH T25
	T18 ParH-T25 Scy	ParH T18-T25 Scy
Interaction tested ParH G95A-Scy		
Recombinant Plasmids	T18 Scy - T25 ParH G95A	T18 Scy- ParH G95A T25
	T18 ParH G95A - T25 Scy	ParH G95A T18-T25 Scy
Interaction tested ParH K99A-Scy		
Recombinant Plasmids	T18 Scy - T25 ParH K99A	T18 Scy - ParH K99A T25
	T18 ParH K99A-T25 Scy	ParH K99A T18 - T25 Scy
Interaction tested ParH D121A - Scy		
Recombinant Plasmids	T18 Scy - T25 ParH D121A	T18 Scy - ParH D121A T25
	T18 ParH D121A - T25 Scy	ParH D121A T18 - T25 Scy

Table 3.4: The recombinant plasmid combinations that were used to co-transform BTH cells. The table represents the combinations testing ParH and ParB or ParH mutants and ParB.

Interaction tested ParH-ParB		
Recombinant Plasmids	T18 ParB -T25 ParH	T18 ParB -ParH T25
	T18 ParH-T25 ParB	ParH T18-T25 ParB
Interaction tested ParH G95A- ParB		
Recombinant Plasmids	T18 ParB - T25 ParH G95A	T18 ParB - ParH G95A T25
	T18 ParH G95A - T25 ParB	ParH G95A T18-T25 ParB
Interaction tested ParH K99A- ParB		
Recombinant Plasmids	T18 ParB - T25 ParH K99A	T18 ParB - ParH K99A T25
	T18 ParH K99A-T25 ParB	ParH K99A T18 - T25 ParB
Interaction tested ParH D121A - ParB		
Recombinant Plasmids	T18 ParB - T25 ParH D121A	T18 ParB - ParH D121A T25
	T18 ParH D121A - T25 ParB	ParH D121A T18 - T25 ParB

Table 3.5: The recombinant plasmid combinations that were used to co-transform BTH cells. The table represents the combinations testing interactions between ParH mutants and Dia.

Interaction tested ParH-Dia		
Recombinant Plasmids	T18 ParH -T25 Dia	T18 ParH - Dia T25
	ParH T18 - Dia T25	ParH T18 - T25 Dia
	T18 Dia -T25 ParH	T18 Dia - ParH T25
	Dia T18 - ParH T25	Dia T18 - T25 ParH
Interaction tested ParH G95A - Dia		
Recombinant Plasmids	T18 Dia - T25 ParHG95A	T18 Dia - ParH G95A T25
	Dia T18 - ParH G95A T25	DiaT18 - T25 ParH G95A
	T18 ParH G95A - T25 Dia	T18 ParHG95A - Dia T25
	ParH G95AT18 - Dia T25	ParH G95AT18 - T25 Dia

Table 3.5 : continued

Interaction tested ParH D121A - Dia		
Recombinant Plasmids	T18 Dia - T25ParH D121A	T18 Dia - ParH D121AT25
	Dia T18 - ParH D121AT25	Dia T18 - T25 ParH D121A
	T18 ParH D121A - T25 Dia	T18 ParH D121A - Dia T25
	ParH D121A T18 - Dia T25	ParH D121A T18 - T25 Dia
Interaction tested ParH K99A - Dia		
Recombinant Plasmids	T18 Dia - T25 ParHK99A	T18 Dia - ParH K99A T25
	Dia T18 - ParH K99A T25	DiaT18 - T25 ParH K99A
	T18 ParH K99A - T25 Dia	T18 ParHK99A - Dia T25
	ParH K99AT18 - Dia T25	ParH K99AT18 - T25 Dia

To test the interaction, the *E. coli* strain BTH101 competent cells were co-transformed with all different combinations of constructs (table 3.1, 3.2, and 3.3). The transformed cells were selected on LB plates containing both ampicillin and kanamycin antibiotics. Then the plates were incubated overnight at 37°C. In the following step, three randomly picked colonies were selected for each combination along with positive and negative controls and streaked onto LB agar plates without glucose, containing ampicillin, kanamycin, IPTG and X gal. The plates were incubated in the dark room at 30°C for 24 to 48 hours. This was followed by visual inspection of the colour of the streaks, with photo of the plates was taken by camera.

3.2.1 ParH interacts with the cell division protein SepF

In the aerial hyphae of *S. coelicolor* ParA filamentation is followed by the formation of a FtsZ ring regularly leading to evenly spaced pre-spore compartments with a single chromosome. In addition to connecting polar scaffolds and chromosomal organization through dynamic ParA and Scy interactions, other components of the division machinery could also be organised through tips in *Streptomyces* (Jakimowicz *et al*. 2007; Holmes *et al*. 2013). Furthermore, SepF functions as a membrane anchor for the FtsZ ring (Duman *et al.*, 2013). According to Cassettari data 2021, a bacterial two hybrid assay has been confirmed that the C-terminal of FtsZ, spanning the last 74 amino acids, interacts with SepF and the sporulation positive regulator, SsgB (Cassettari, Unpublished 2021).

Macroscopic analysis confirmed that the phenotype of the *parH* mutant strain had delayed sporulation compared to the wild type. Likewise, the *parH* mutant strain had irregular septation compared to the wild type M145 (Gillespie, Unpublished 2017). This evidence supports the expected role of ParH in both growth and division. Given the homology that exists between ParA and ParH, the current chapter involved further investigation to determine whether ParH has a possible interaction with partner proteins. Potential binding partners of ParH were investigated using bacterial two hybrid assay *in vivo* in the heterologous host *E. coli*.

Initially, the current project performed the interactions between ParH and SepF then ParH and SepF mutants, K46A and F71A. According to the Clustal Omega analysis of the SepF sequences (Cassettari, Unpublished 2021) the residues K101 and F126 of the *B. subtilis* SepF are well conserved. The F126S mutation of the *B. subtilis* SepF abolished the interaction with FtsZ but did not affect self-interaction or interaction with wild type SepF (Duman *et al.*, 2013). In *Mycobacterium* the K190A mutation did not affect the self-interaction of SepF but abolished the SepF-FtsZ interaction (Gupta *et al.,* 2005). While the F215S mutation greatly reduced both the self-interaction of SepF and the SepF-FtsZ interaction. Based on the mutant analysed in *B. subtilis* and in *M. tuberculosis* the equivalent mutants were generated in SepF. The numbering

of the mutants, K46A and F71A, relate to the position of these amino acids in the truncated SepF (Cassettari, Unpublished 2021). The utilization of truncated SepF due to its self-interaction behavior (dimerisation). Truncation targeted the self-interaction regions, resulting in separation and independence (Duman *et al.*, 2013). Also, for bacterial two hybrid screening, truncated version of *sepF* gene were employed, as earlier studies it was showed that full length proteins interfere with *E. coli* cell division machinery which can affect results (Kelemen *et al)*.

Here, the bacterial two hybrid assay confirmed that ParH interacts with SepF cell division protein (Figure 3.3). This result is surprising because up to date there is no direct interaction established between a ParA like protein and cell division. Hence, this is the first time where a ParA like protein is directly linked to cell division. On the other hand, a link between cell division and chromosome organisation is likely.

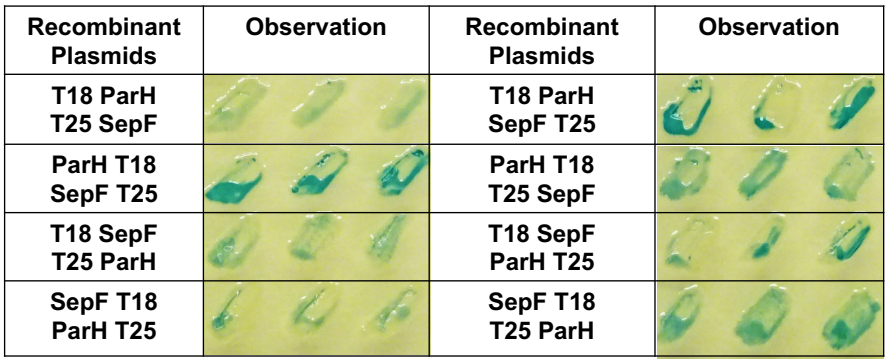

Figure 3.3 Bacterial two-hybrid assay testing the ParH-SepF interaction

E. coli BTH 101 competent cells were co-transformed with combinations of the appropriate bacterial two hybrid plasmid pairs (Table 3.1). Three colonies from each transformation were picked and streaked onto an LB plate with no glucose but supplemented with IPTG, X-gal, ampicillin, and kanamycin. Photo of the plates incubated for 48 hours at 30°C is shown.

To further investigate the interactions between ParH and cell division protein SepF, we tested the effect of the mutations of K46A and F71A on ParH-SepF interaction. As we mentioned above, the numbering of these mutations is based on the position of amino acids in the truncated SepF.

However, the K46A mutation did not alter the positive interaction of ParH-SepF through bacterial two hybrid assay. Most of colonies appeared blue which confirmed that ParH and SepF interacts (Figure 3.4).

Recombinant Plasmids	Observation	Recombinant Plasmids	Observation
T18 ParH T25 SepF K46A		T18 ParH SepF K46A T25	
ParH T18 SepF K46A T25		ParH T18 T25 SepF K46A	
T18 SepF K46A T25 ParH		T18 SepF K46A ParH T25	
SepF K46A T18 ParH T25		SepF K46A T18 T25 ParH	

Figure 3.4 Effect of the SepF K46A mutation on ParH-SepF interaction

E. coli BTH 101 competent cells were co-transformed with combinations of the appropriate bacterial two hybrid plasmid pairs (Table 3.1). Three colonies from each transformation were picked and streaked onto an LB plate with no glucose but supplemented with IPTG, X-gal, ampicillin, and kanamycin. Photo of the plates incubated for 48 hours at 30°C is shown.

3.2.1.1 SepF F71 residue is important for interaction with both ParH and FtsZ

Previous research in our lab investigated the effect of the mutations, K46A and F71A, on the interaction of SepF with FtsZ (Cassettari, Unpublished 2021). Both mutations inhibited interactions between FtsZ and SepFTR. Here, the interaction between SepF and ParH was not affected by the K46A mutation, as positive interaction was detected (Figure 3.4). This might indicate that the SepF protein interacts with ParH protein in different manner than it does with FtsZ protein. Interestingly, the SepF F71A mutation abolished the ParH-SepF interaction, (Figure 3.5), suggesting that the phenylalanine at the position 71 of SepF is important for the interaction with both ParH and FtsZ. This raises the possibility that SepF switches between ParH and FtsZ for binding.

Recombinant Plasmids	Observation	Recombinant Plasmids	Observation
ParH T18 T25 SepF F71A		T18 ParH SepF F71A T25	
ParH T18 SepF F71A T25	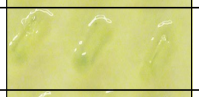	ParH T18 T25 SepF F71A	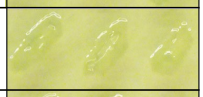
T18 SepF F71A T25 ParH		T18 SepF F71A ParH T25	
SepF F71A T18 ParH T25		SepF F71A T18 T25 ParH	

Figure 3.5 Effect of the SepF F71A mutation on ParH-SepF interaction

E. coli BTH 101 competent cells were co-transformed with combinations of the appropriate bacterial two hybrid plasmid pairs (Table 3.1). Three colonies from each transformation were picked and streaked onto an LB plate with no glucose but supplemented with IPTG, X-gal, ampicillin, and kanamycin. Photo of the plates incubated for 48 hours at 30°C is shown.

3.2.2 Testing the effect of ParH mutations on the ParH-SepF interaction

According to the Clustal Omega analysis of sequence alignment of ParH and ParA homologues (Figure 3.6), ParH consists of significant residues and motifs that are necessary for ParA function (Gillespie, Unpublished 2017). This involves both Walker A and Walker B motifs, which are essential for nucleotide binding and ATPase hydrolysis, respectively (Motallebi-Veshareh *et al*., 1990; Koonin, 1993). Furthermore, ParH homologues contain essential preserved residues that have been characterised in ParA homologues. This includes the arginine residues R189 and R218 which are important for DNA binding in *B. subtilis* Soj (Hester and Lutkenhaus, 2007); the lysine residue K20 that is essential for ATP binding (Fung *et al*., 2001); the glycine residue (G16) that allows dimerisation of ParA to arise (Leonard *et al*., 2005); and the aspartate residue (D44) which is essential for ATP hydrolysis (Lutkenhaus and Sundaramoorthy, 2003) (Figure 3.6). We have identified the corresponding residues in the ParH sequence to K20 of the Walker A motif for ATP binding

that is ParH K99 residue, the G16 residue for ParA dimerisation corresponds to G95 residue in ParH. Finally, the D44 residue for ATP hydrolysis corresponds to D121 in ParH. We have designed and synthesised DNA encoding the following ParH mutants: G95A, K99A and D121A. In addition, we included a mutation not tested in other organisms, a Lysin residue at the beginning of the Walker A motif, K94A. The synthetic clones were subcloned into the appropriate pUT18 or pKT25 vectors (Nikolai Kovzel, Unpublished) and were used here to test the effect of these mutations on the ParH-SepF interaction.

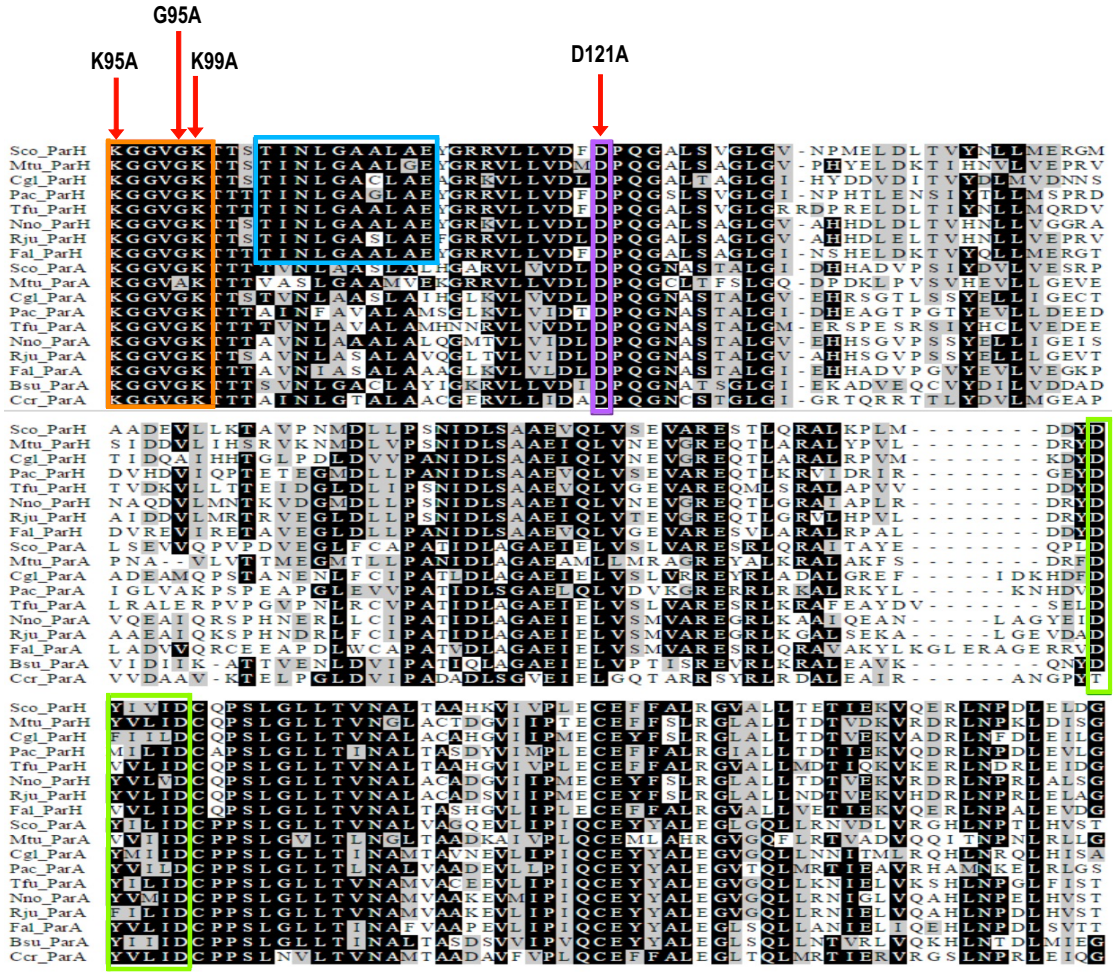

Figure 3.6 Sequence alignment of ParH and ParA homologues

Clustal omega (https://www.ebi.ac.uk/Tools/msa/clustalo/) performed the sequence alignment of ParA and ParH homologues. The orange box shows Walker A motif containing K20 lysine residue that is important for ATP binding and G16 glycine residue that allows the dimerisation of ParA. While the green box shows Walker B motif. The purple box shows D44 aspartate residue that is important for ATP hydrolysis; Residues conserved in ParH but absent in ParA are highlighted in blue box. Taken and modified from Gillespie, Unpublished 2017.

3.2.2.1 ATP binding residue of ParH and ATP hydrolysis might be important for ParH-SepF interaction

To explore the effect of abolishing ATP binding, ATP hydrolysis, and dimerisation residues of ParH in *S. coelicolor* on the interaction with SepF, a bacterial two hybrid assay was performed. As discussed in section (3.2.2) the G16 residue for ParA dimerisation corresponds to G95 residue in ParH. Here we wished to investigate the effect of ParH G95 mutant on interaction of ParH and SepF (Figure 3.7). The G95A mutation did not influence the ParH-SepF interaction. This is interesting, as it might suggest that ParH might not generate dimers in the same way as ParA.

Recombinant Plasmids	Observation	Recombinant Plasmids	Observation
T18 ParH G95A T25 SepF TR		T18 ParH G95A SepF T25	
ParH G95A T18 SepF T25		ParH G95A T18 T25 SepF	
T18 SepF T25 ParH G95A		T18 SepF ParH G95A T25	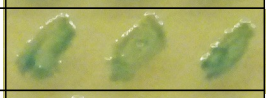
SepF T18 ParH G95A T25	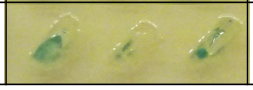	SepF T18 T25 ParH G95A	

Figure 3.7 Effect of the ParH G95A mutation on ParH-SepF interaction

E. coli BTH 101 competent cells were co-transformed with combinations of the appropriate bacterial two hybrid plasmid pairs (Table 3.2). Three colonies from each transformation were picked and streaked onto an LB plate with no glucose but supplemented with IPTG, X-gal, ampicillin, and kanamycin. Photo of the plates incubated for 48 hours at 30°C is shown.

However, the bacterial two hybrid assay did not detect any positive combinations involving the ParH K 94A, the K99A mutants or the ParH D121A mutants with SepF, most of the colonies were white. This result revealed that the K99A and D121A mutations altered the ParH-SepF interaction (Figure 3.8 and Figure 3.9). The novel mutation, K94A also abolished interaction

between ParH and SepF, supporting the idea that Walker A motif and ATP binding is important for the interaction between ParH and SepF (Figure 3.10). The Walker A motif's significance lies in its role as a conserved sequence that enables ATP binding and hydrolysis, driving conformational changes essential for protein interactions. Deletion or alteration of this motif, as seen with the K94A mutation, hinders the ATPase activity and thus inhibits the proper conformational adjustments needed for effective protein-protein interactions. In the context of ParH and SepF, this disruption prevents their functional partnership, underlining the importance of the Walker A motif and ATP binding for their interaction to occur.

Recombinant Plasmids	Observation	Recombinant Plasmids	Observation
T18 ParH K99A T25 SepF		T18 ParH K99A SepF T25	
ParH K99A T18 SepF T25		ParH K99A T18 T25 SepF	
T18 SepF T25 ParH K99A		T18 SepF ParH K99A T25	
SepF T18 ParH K99A T25		SepF T18 T25 ParH K99A	

Figure 3.8 Effect of the ParH K99A mutation on ParH-SepF interaction

E. coli BTH 101 competent cells were co-transformed with combinations of the appropriate bacterial two hybrid plasmid pairs (Table 3.2). Three colonies from each transformation were picked and streaked onto an LB plate with no glucose but supplemented with IPTG, X-gal, ampicillin, and kanamycin. Photo of the plates incubated for 48 hours at 30°C is shown.

Recombinant Plasmids	Observation	Recombinant Plasmids	Observation
T18 ParH D121A T25 SepF		T18 ParH D121A SepF T25	
ParH D121A T18 SepF T25		ParH D121A T18 T25 SepF	
T18 SepF T25 ParH D121A		T18 SepF ParH D121A T25	
SepF T18 ParH D121A T25	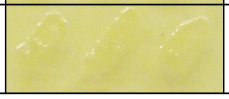	SepF T18 T25 ParH D121A	

Figure 3.9 Effect of the ParH D121A mutation on the ParH-SepF interaction

E. coli BTH 101 competent cells were co-transformed with combinations of the appropriate bacterial two hybrid plasmid pairs (Table 3.2). Three colonies from each transformation were picked and streaked onto an LB plate with no glucose but supplemented with IPTG, X-gal, ampicillin, and kanamycin. Photo of the plates incubated for 48 hours at 30°C is shown.

Recombinant Plasmids	Observation	Recombinant Plasmids	Observation
T18 ParH K94A T25 SepF		T18 ParH K94A SepF T25	
ParH K94A T18 SepF T25		ParH K94A T18 T25 SepF	
T18 SepF T25 ParH K94A		T18 SepF ParH K94A T25	
SepF T18 ParH K94A T25		SepF T18 T25 ParH K94A	

Figure 3.10 Effect of the ParH K94A mutation on the ParH-SepF interaction

E. coli BTH 101 competent cells were co-transformed with combinations of the appropriate bacterial two hybrid plasmid pairs (Table 3.2). Three colonies from each transformation were picked and streaked onto an LB plate with no glucose but supplemented with IPTG, X-gal, ampicillin, and kanamycin. Photo of the plates incubated for 48 hours at 30°C is shown.

3.2.3 Identifying interaction of ParH and the TIPOC protein Scy

Previous study confirmed the interaction of ParA with a key component TIPOC Scy (Bartosz Ditkowski *et al.*, 2013). Here we aimed to test the possible interaction between ParH and Scy *in vivo* using the bacterial two technique. Interestingly we were able to detect positive interaction between ParH and Scy (Figure 3.11), suggesting that both ParA and ParH are linked to the TIPOC, via Scy.

Recombinant Plasmids	Observation
T18 Scy T25 ParH	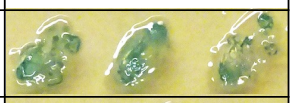
T18 ParH T25 Scy	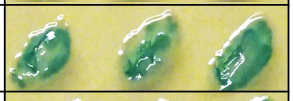
T18 Scy ParH T25	
ParH T18 T25 Scy	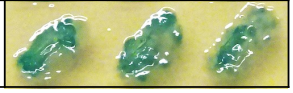

Figure 3.11 Bacterial two-hybrid assay testing the ParH-Scy interaction

E. coli BTH 101 competent cells were co-transformed with combinations of the appropriate bacterial two hybrid plasmid pairs (Table 3.3). Three colonies from each transformation were picked and streaked onto an LB plate with no glucose but supplemented with IPTG, X-gal, ampicillin, and kanamycin. Photo of the plates incubated for 48 hours at 30°C is shown.

To validate and confirm the preliminary results of ParH-Scy interaction obtained from bacterial two-hybrid assays, we need employ several complementary techniques, for example affinity co-elution, surface plasmon resonance and co-crystallisation for structural studies using X-ray crystallography. These techniques help ensure the reliability of the observed interactions by providing additional evidence.

3.2.3.1 Exploring the effect of ParH mutations on the ParH-Scy interaction

Further *in vivo* investigations, interaction between Scy and the different ParH mutations were performed using bacterial two hybrid assays. We tested three mutant version of ParH, ParH G95A that is impaired in the potential dimerisation of ParA; ParH K99A affecting ATP binding of ParA and finally ParH D121A, which is involved in ATP hydrolysis of ParA. Similarly to interactions between ParH and SepF, this assay detected positive interaction between Scy and ParH, which confirms the hypothesis that the G95A is not important for ParH assembly (Figure 3.12 A).

Interestingly, unlike the interaction between ParH and SepF, the ParH and Scy interaction was not affected by the ParH K99A mutation suggesting that the K99A residue (for ATP binding) not important for ParH-Scy interaction (Figure 3.12 B). However, the Walker A motif D121A mutation impaired the ParH-Scy interaction (Figure 3.12 C).

(A)

Recombinant Plasmids	Observation
T18 Scy T25 ParH G95A	
T18 ParH G95A T25 Scy	
T18 Scy ParH G95A T25	
ParH G95A T18 T25 Scy	

(B)

Recombinant Plasmids	Observation
T18 Scy T25 ParH K99A	
T18 ParH K99A T25 Scy	
T18 Scy ParH K99A T25	
ParH K99A T18 T25 Scy	

(C)

Recombinant Plasmids	Observation
T18 Scy T25 ParH D121A	
T18 ParH D121A T25 Scy	
T18 Scy ParH D121A T25	
ParH D121A T18 T25 Scy	

Figure 3.12 Testing the effect ParH G95A, ParH K99A, and ParH D121A mutation on ParH-Scy interaction

A ,B, and C: *E. coli* BTH 101 competent cells were co-transformed with combinations of the appropriate bacterial two hybrid plasmid pairs (Table 3.3). Three colonies from each transformation were picked and streaked onto an LB plate with no glucose but supplemented with IPTG, X-gal, ampicillin, and kanamycin. Photo of the plates incubated for 48 hours at 30°C is shown.

Overall, these observations suggested a link between ParH and the TIPOC; the assembly of the multiprotein complex that is essential for polar growth in *S. coelicolor.*

3.2.4 Interaction between ParH and the chromosome segregation protein ParB

We sought to explore the possible link between ParH and chromosome segregation in *S coelicolor* after showing a link between ParH and Scy in previous section. The similarity of ParH and ParA raises the question whether in addition to the ParA-ParB interaction, ParH might also be able to interact with ParB. In order to examine a ParH-ParB interaction *in vivo*, a bacterial two hybrid assay was used. The positive interaction between ParH and ParB was observed through the blue colonies (Figure 3.13). This interaction suggests a crosstalk between the ParH and the ParA system. Additionally, a direct ParH-ParB interaction through bacterial two hybrid might be dependent on the integrity of the Walker A motif.

Recombinant Plasmids	Observation
T18 ParB T25 ParH	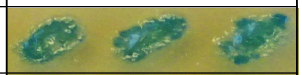
T18 ParH T25 ParB	
T18 ParB ParH T25	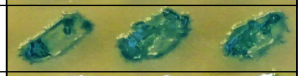
ParH T18 T25 ParB	

Figure 3.13 Bacterial two-hybrid assay testing the ParH-ParB interaction

E. coli BTH 101 competent cells were co-transformed with combinations of the appropriate bacterial two hybrid plasmid pairs (Table 3.4). Three colonies from each transformation were picked and streaked onto an LB plate with no glucose but supplemented with IPTG, X-gal, ampicillin, and kanamycin. Photo of the plates incubated for 48 hours at 30°C is shown.

We also tested the interaction between the different ParH mutations with ParB (Figure 3.14 A and B). The ParH G95A and K99A mutants failed to

abolish the ParH-ParB interaction (Figure 3.14 A and B). However, the ParH D121A mutant impaired the two-hybrid interaction (Figure 3.14 C), suggesting that similarly to the ParH-Scy interaction, the D121A and ATP hydrolysis residues might be essential for the ParH-ParB interaction.

(A)

Recombinant Plasmids	Observation
T18 ParB T25 ParH G95A	
T18 ParH G95A T25 ParB	
T18 ParB ParH G95A T25	
ParH G95A T18 T25 ParB	

(B)

Recombinant Plasmids	Observation
T18 ParB T25 ParH K99A	
T18 ParH K99A T25 ParB	
T18 ParB ParH K99A T25	
ParH K99A T18 T25 ParB	

(C)

Recombinant Plasmids	Observation
T18 ParB T25 ParH D121A	
T18 ParH D121A T25 ParB	
T18 ParB ParH D121A T25	
ParH D121A T18 T25 ParB	

Figure 3.14 Testing the effect of ParH G95A, ParH K99A, and ParH D121A mutation on ParH-ParB interaction

A, **B, and C**: *E. coli* BTH 101 competent cells were co-transformed with combinations of the appropriate bacterial two hybrid plasmid pairs (Table 3.4). Three colonies from each transformation were picked and streaked onto an LB plate with no glucose but supplemented with IPTG, X-gal, ampicillin, and kanamycin. Photo of the plates incubated for 48 hours at 30°C is shown.

3.2.5 ParH interaction with the coiled-coil protein Dia

A recent study in the Kelemen lab established that the Dia protein (SCO5569) is a novel TIPOC component. Preliminary data revealed that Dia protein plays an important role in controlling the width of the hypha and the positioning of the sporulation septa in *S. coelicolor*.

We aimed to test the potential interaction between ParH and coiled-coil protein Dia in *vivo* using bacterial two hybrid screening. The constructs of four plasmids expressing Dia with the T18 or T25 tags were made in the Kelemen

lab (A Hutchinson, Unpublished 2023) and were used in combinations shown in Table 3.3. First we tested interaction between ParH and Dia and we found that three out of the eight combinations gave blue streaks (Figure 3.15), indicating that the ParH and Dia proteins did interact.

Recombinant Plasmids	Observation	Recombinant Plasmids	Observation
T18 ParH T25 Dia	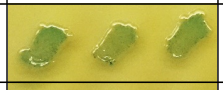	T18 ParH Dia T25	
ParH T18 Dia T25	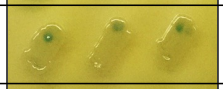	ParH T18 T25 Dia	
T18 Dia T25 ParH		T18 Dia ParH T25	
Dia T18 ParH T25	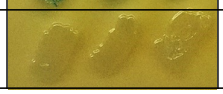	Dia T18 T25 ParH	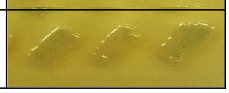

Figure 3.15 Bacterial two-hybrid assay testing the ParH-Dia interaction

E. coli BTH 101 competent cells were co-transformed with combinations of the appropriate bacterial two hybrid plasmid pairs (Table 3.5). Three colonies from each transformation were picked and streaked onto an LB plate with no glucose but supplemented with IPTG, X-gal, ampicillin, and kanamycin. Photo of the plates incubated for 48 hours at 30°C is shown.

3.2.5.1 Exploring ParH mutations effect on ParH-Dia interaction

Furthermore, in our research, we sought to examine the interaction between ParH and Dia. Additionally, we aimed to assess how mutations in ParH residues, which have been associated with dimerisation, ATP binding, and ATP hydrolysis, might impact the interaction with Dia. First we tested the ParH G95A mutation that could affect how ParH dimerises, based on what was established for the ParA/ Soj protein in *B. subtilis*. The data indicate that the two-hybrid interaction was not affected by the G95A mutation (Figure 3.16). When the interaction investigated with ParH G95A mutant, the same sets of combinations turned blue as with the wild type ParH.

Recombinant Plasmids	Observation	Recombinant Plasmids	Observation
T18 DIA T25 ParH G95A	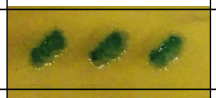	T18 DIA ParH G95A T25	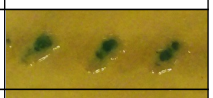
DIA T18 ParH G95A T25		DIA T18 T25 ParH G95A	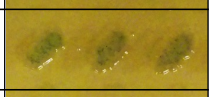
T18 ParH G95A T25 DIA		T18 ParH G95A DIA T25	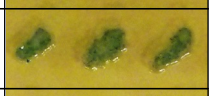
ParH G95A T18 DIA T25	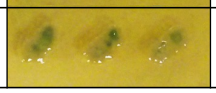	ParH G95A T18 T25 DIA	

Figure 3.16 Effect ParH G95A mutation on ParH-Dia interaction

E. coli BTH 101 competent cells were co-transformed with combinations of the appropriate bacterial two hybrid plasmid pairs (Table 3.5). Three colonies from each transformation were picked and streaked onto an LB plate with no glucose but supplemented with IPTG, X-gal, ampicillin, and kanamycin. Photo of the plates incubated for 48 hours at 30°C is shown.

3.2.5.2 The ATP binding and hydrolysis residues of ParH are crucial for its interaction with Dia.

Two hybrid assays were also sought for the possible effect of ATP binding and ATP hydrolysis on the interaction between ParH and Dia. The ParH K99A mutation, which corresponds to a ParA mutation that abolishes ATP binding, did affect the interaction, but it was not completely abolished (Figure 3.17 A). The D121A mutant, which corresponds to a ParA mutation that abolishes the ability of ParA to hydrolyse ATP, was impaired the two-hybrid interaction (Figure 3.17 B). This finding indicates that ATP hydrolysis and to some extent, ATP binding might be necessary for the ParH-Dia interaction.

(A)

Recombinant Plasmids	Observation	Recombinant Plasmids	Observation
T18 DIA T25 ParH K99A	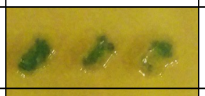	T18 DIA ParH K99A T25	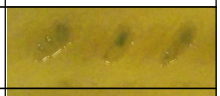
DIA T18 ParH K99A T25		DIA T18 T25 ParH K99A	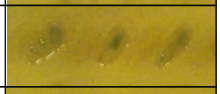
T18 ParH K99A T25 DIA		T18 ParH K99A DIA T25	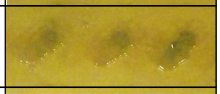
ParH K99A T18 DIA T25	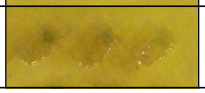	ParH K99A T18 T25 DIA	

(B)

Recombinant Plasmids	Observation	Recombinant Plasmids	Observation
T18 DIA T25 ParH D121A		T18 DIA ParH D121A T25	
DIA T18 ParH D121A T25		DIA T18 T25 ParH D121A	
T18 ParH D121A T25 DIA		T18 ParH D121A DIA T25	
ParH D121A T18 DIA T25		ParH D121A T18 T25 DIA	

Figure 3.17 Testing effect of ParH mutations on ParH-Dia interaction

(**A**) Dia and ParH K99A mutant: *E. coli* BTH 101 competent cells were co-transformed with combinations of the appropriate bacterial two hybrid plasmid pairs (Table 3.5). Three colonies from each transformation were picked and streaked onto an LB plate with no glucose but supplemented with IPTG, X-gal, ampicillin, and kanamycin. Photo of the plates incubated for 48 hours at 30°C is shown.

(B)Dia and ParH D121A mutant: : *E. coli* BTH 101 competent cells were co-transformed with combinations of the appropriate bacterial two hybrid plasmid pairs (Table 3.5). Three colonies from each transformation were picked and streaked onto an LB plate with no glucose but supplemented with IPTG, X-gal, ampicillin, and kanamycin. Photo of the plates incubated for 48 hours at 30°C is shown.

3.3 Summary

Cell division in rod-shaped bacteria occurs by binary fission, chromosomes are segregated into two halves of the elongating cell. However, in *Streptomyces*, the segregation of chromosomes during sporulation requires the accurate positioning of tens of chromosomes along the aerial hyphae. In Kelemen's lab we have established that ParH is a ParA homologue that is essential for the correct and efficient positioning of the septa during the sporulation of *S. coelicolor.*

In the current chapter, we have investigated the link between ParH and potential partner proteins with the aim to understand how some of the classical mutations established for the ParA protein influenced the interactions.

- We have tested the cell division protein SepF, the TIPOC component Scy that is involved in polar growth, the novel, possibly TIPOC component Dia and finally ParB the partner protein of ParA controlling chromosome organisation. We have found that all of these proteins interacted with ParH, suggesting direct links amongst these fundamental processes (Figure 3.18).

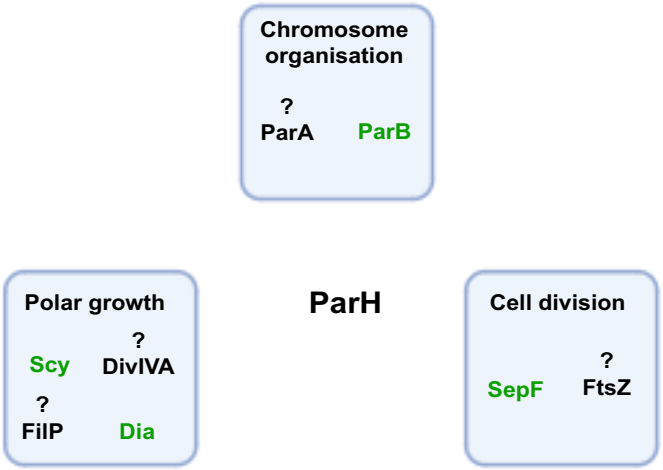

Figure 3.18 The link between ParH and partner proteins in *S. coelicolor*

This diagram provides a visual representation of the connections between ParH and its partner proteins within *S. coelicolor*. The proteins in green colour indicate positive interactions with ParH: Scy and Dia (TIPOC component), ParB (chromosome segregation), and SepF (cell division). Conversely, the black colour represent proteins for which the interactions remain to be elucidated.

- We then tested the effect of ParH mutations on these interactions. This was based on mutations that were established to affect the activity of ParA. The ParA mutant corresponding to ParH G95A, was unable to dimerise in the presence of ATP, and dimerisation is essential for ParA function. Intriguingly, the ParH G95A mutation did not affect any of the interactions, with SepF, Scy, Dia or ParB, suggesting that ParH operates differently compared to ParA, possibly not via dimerisation.
- The mutant that affected ATP hydrolysis in ParA, ParH D121A, abolished all interactions, suggesting that although it might not be via dimerisation, but ATP hydrolysis plays a role in ParA function.
- The ParH K99A mutation that affect the Walker A motif for ATP binding affect its interaction with SepF and Dia, but not with Scy and ParB suggesting that the interface between ParH and its partners are different, perhaps allowing more than one partner binding at a time.
- The ParH K94A mutation is also in the Walker A motif, and this mutant did abolish interaction with SepF, suggesting that other residues than

the K99 residue are important for the correct functioning of ParH. Unfortunately we did not test this mutant against the other partner proteins, so our conclusions are limited to the SepF-ParH interaction. Furthermore, it would be important to generate the appropriate ParA mutants to test the effect of this mutation on ParA's function.

The bacterial two hybrid assay is a powerful tool to indicate possible pairwise protein interactions. However, this assay can generate both false positive and false negative results, therefore, the bacterial two hybrid assays must be followed up by independent methods to confirm interactions. This could include *in vivo* experiments, using for example fluorescently tagged partner proteins looking for co-localisation of the proteins in question. In the next chapters we will attempt confirmation of these interactions *in vitro*, using overexpressed and purified proteins.

CHAPTER 4

4. Optimising Proteins Overexpression and Purification

4.1 Introduction

In the life cycle of *S. coelicolor* two functionally distinct modes of cell division exist, formation of the crosswall in vegetative hypha and sporulation septation in the aerial hyphae. Crosswalls separate growing hyphal filaments into multigenomic compartments. Sporulation specific cell division are formation and release of unigenomic spores (Jakimowicz and Van Wezel, 2012). However, the physiological significance of the two septa is not fully understood and both processes are governed by a tubulin-like protein, termed FtsZ. FtsZ is polymerised into Z-ring as part of early divisome (Rioseras *et al.*, 2018). The role of FtsZ in sporulation is evident during aerial hyphal septation, where FtsZ rings (Z rings) form in a ladder-like pattern to facilitate septation events. The Z ring has been described as a series of single-stranded protofilaments of FtsZ, essential for compartmentalisation of spore during active replication (Schwedock *et al.*, 1997; Grantcharova, Lustig and Fla, 2005).

In mycelial *Streptomyces*, chromosome segregation and cell division, followed by cell separation, occur exclusively during sporulation. Unlike some of the model rod-shaped bacteria, *Streptomyces* forms hyphae, which extend apically and form branches. During vegetative growth, elongated multigenomic compartments are formed that are physically not separated, chromosomes remain uncondensed, and their replication is not followed by cell division (Flärdh and Buttner, 2009). Interestingly, cell division is not essential for vegetative growth of *S. coelicolor*, but it is crucial for sporulation. Sporulation, the conversion of multigenomic aerial hyphae to spores involves synchronized, multiple septation accompanied by the condensation and segregation of tens of chromosomes into pre-spore compartments. In aerial hyphae, FtsZ forms a protofilaments of regularly spaced Z-rings along the hyphal compartment (Schwedock *et al.*, 1997; Grantcharova, Lustig and Fla, 2005).

Chromosome segregation must be synchronized with the formation of the division septum, which, in rod-shaped bacteria, separates the two daughter cells. The septation starts with the polymerization of FtsZ into a ring structure (Z-ring) that determines the division plane (Fenton and Gerdes, 2013). In *E. coli* and in *B. subtilis,* two negative regulators, the Min (MinCD) and nucleoid occlusion (SmlA and Noc) use inhibitors of FtsZ polymerization that control the timing and positioning of Z-ring formation by preventing guillotining of the unsegregated chromosomes by the division septum (Wu and Errington, 2011). However, *Streptomyces* do not have homologues of Min proteins and nucleoid occlusion proteins. Recent experiments indicated that in *S. coelicolor*, FtsZ is recruited to the septum site by SsgB as a positive control of septal position (Willemse *et al.*, 2011). Recently, in our laboratory SepF has been characterised to be an essential part of the Z-ring (Cassettari *et al*., manuscript submitted)

In *Streptomyces*, as in other rod-shaped bacteria, the ParAB proteins regulate chromosomes segregation in the sporogenic hyphal compartment (Kim *et al.*, 2000; Jakimowicz, Chater and Zakrzewska-Czerwínska, 2002). In vegetative hyphae of *S. coelicolor*, both proteins are mostly associated with the tips, while during sporulation ParA extends along the hyphae, and ParB forms an array of regularly spaced complexes (Jakimowicz, Chater and Zakrzewska-Czerwínska, 2002; Chater *et al.*, 2007). The knockout of ParA and/or ParB in *S. coelicolor* alters chromosome segregation and leads to the formation of anucleate spores (Chater *et al.*, 2007).

Previously, in the Kelemen laboratory, several novel ParA-like proteins were identified in *S. coelicolor.* One of these proteins was designated ParH and has 49% identity with *B. subtilis* Soj and 30% identity with MinD in *E. coli.* The *parH* gene is presumably co-translated with the downstream gene, which encodes a small hypothetical protein. Through bioinformatic analysis, ParH and Hyp homologues were found in numerous *Actinobacteria* (Chapter1, Figure 1.16). Interestingly, most Actinobacteria have ParH but not all of them have Hyp. ParH belongs to the family of ATPases and shows similarity to the ParA protein, which is involved in chromosome segregation during sporulation

in *Streptomyces* (Jakimowicz *et al.,* 2007). The current chapter will optimise overexpression and purification of ParH and Hyp, as well as some of the partner proteins that identified in Chapter 1 and are involved in polar growth and cell division.

4.2 Overexpression and Purification Strategies

For large-scale protein overexpression, we used plasmid pET28. Plasmid pET28 is a high copy number vector for overexpression of desired proteins in *E. coli*. It carries the kanamycin resistance gene and the T7 polymerase promoter of the gene of interest means that expression is driven by T7 polymerase. *E. coli* strain BL21 (DE3) pLysS was used as a host for overexpression because it contains the T7 polymerase gene controlled by the *LacI* repressor. This prevents RNA polymerase from transcribing the T7 polymerase gene in the absence of an inducer (IPTG), not expressing the gene of interest. In addition, the pLysS plasmid encodes the lysS gene, which encodes T7 lysozyme, which is constitutively expressed at low levels to prevent any T7 polymerase from activating gene expression prior to induction. Expression of a gene of interest can be induced by adding isopropyl β-D-1-thiogalactopyranoside (IPTG) to remove the *LacI* repressor from its operator site (Doherty *et al*., 1995; Pan and Malcolm, 2000; Schlicke and Brakmann, 2005).

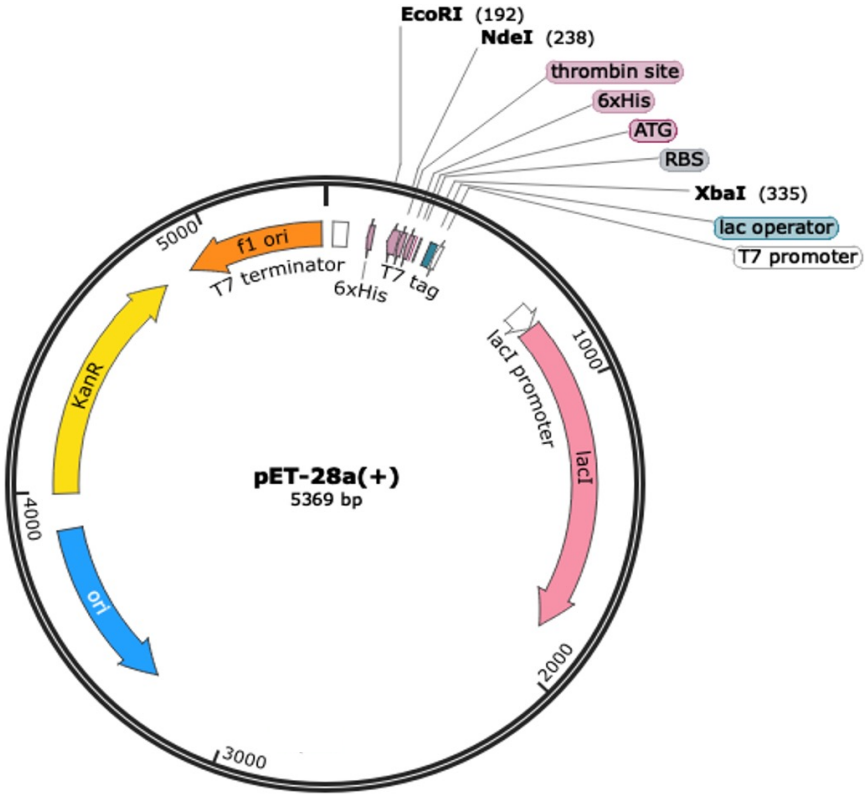

Figure 4.1 pET28a map

The pET28a vector is a high copy number plasmid for expression of N-terminally His-tagged proteins with a thrombin site, designed to overexpression and purification proteins through nickel affinity chromatography. The T7 gene polymerase controlled promoter is targeted by the LacI repressor, and this promoter can be induced by IPTG. The presence of this plasmid can be selected using kanamycin. (Created by SnapGene)

4.2.1 Expression Trial of His-ParH

For overproduction of His-ParH, *parH* gene was previously cloned into pET28a to generate pET28a-ParH. The primers '1772 *Xbal Nde*l FRW' and '1772 *Eco* UTC REV' was used to amplify parH gene from *S. coelicolor,* then digested with *NdeI* site and *EcoRI* and cloned into pET28a (Gillespie, Unpublished 2017). The approximate molecular weight of the His-ParH protein (360 amino acids) is 39.2 KDa and the pI=5.14.

In order to confirm and optimise the overproduction of His-ParH from *E.coli,* first electroporation of the *E. coli* strain BL21 (DE3) pLysS using the plasmid pET28a-ParH and was performed and the successful transformants were selected on LB agar containing both kanamycin and chloramphenicol (pLysS that does confer chloramphenicol resistance). To test that all kanamycin resistant colonies were able to efficiently overexpress His-ParH, expression trials were carried out using four different colonies were picked from the original transformation plates and re-streaked on LB agar having chloramphenicol and kanamycin then incubated overnight at 37°C. These four strains were then tested for protein overexpression in a small scale. Overnight 10 ml LB cultures containing both chloramphenicol and kanamycin were subcultured and grown for 3 hours at 37°C when 1 mM IPTG was added to each culture to induce expression of the proteins. Cultures were incubated further at 25°C overnight. The samples were collected, and the pelleted cells were re-suspended in 20 mM Tris buffer 10 mM $MgCl_2$ pH8.0 and the cells lysed by sonication five 15 second. Lysates were centrifuged and analysed both supernatant and pellet fractions using 12% SDS-PAGE.

The expression trials revealed that the ParH was expressed in the supernatant fraction for colony number 2 and 3 (Figure 4.2) therefore this were the colonies chosen for large scale native -non-denaturing- purification of His-ParH. Based on Gillespie study, the optimal condition for His-ParH expression when incubated for 20 hours after induction at 25°C. As shown in Figure 4.2, the large band with expected molecular wight of 39.2 KDa is found in the pellet fraction. However, the highest soluble amount of ParH can be seen in supernatant fraction corresponding to the colonies 2 and 3.

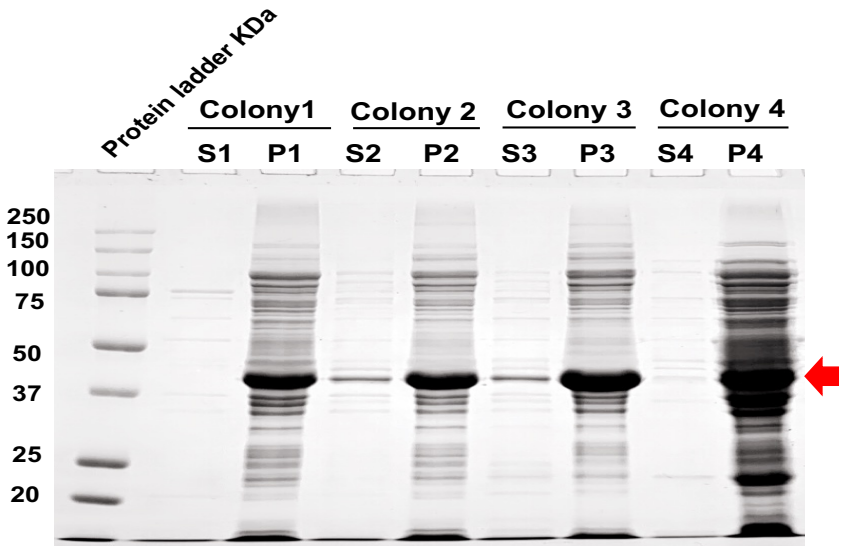

Figure 4.2 Expression trial of His-ParH

Supernatant and pellet fraction from the small-scale overexpression trials were analysed using 12% SDS-PAGE. Starting from four different colonies, after small scale protein overexpression, supernatant (S) and pellet (P) samples were analysed. The samples were loaded as follows; colony 1 (S1 & P1), colony 2 (S2 & P2), colony 3 (S3 & P3) and colony 4 (S4 & P4). All samples were collected at 25°C, 20hrs after 1mM IPTG induction. The Red arrow indicates the 39.2 KDa His-ParH, visualised by Coomassie Blue staining.

4.2.2 Large Scale Overexpression and Purification of His-ParH

After successfully confirming that His-ParH can be expressed in a soluble form, a large-scale purification was performed to produce a good quantity, purified His-ParH protein using Ni-affinity chromatography. Routinely, 800 ml of BL21 (DE3) pLysS carrying pET28a-ParH from colony 3 was grown in the conditions indicated as optimum from the expression trials. Due to the presence of His-tags on the N-terminus protein; the Nickel affinity chromatography was selected to be used as purification method. the nickel immobilised in the column is able to capture His-tagged proteins while allowing other proteins to be passed through the column. His-tagged proteins of interest are eluted by adding buffer solution containing imidazole, which competitively binds to nickel.

For His-ParH purification, cultures were collected and resuspended into native buffer A with low concentration of imidazole to block binding of proteins with low affinity to the Nickel columns (50mM Tris 10mM $MgCl_2$ 300 mM NaCl 10mM imidazole). Cells were lysed using constant system cell disruptor twice and lysates were sonicated to break up the dense DNA in the lysate then centrifuged at 20000 rev/min to generate a clear supernatant fraction. The supernatant was also filtered through a 0.45 µm filter before being loaded onto the nickel column for purification.

After loading the sample onto the Ni-NTA column, multiple washes were performed with native buffer A (10 mM imidazole for wash1) and native buffer B (20 mM imidazole for wash2) to elute any non-specific binding. Native Buffer C (300 mM imidazole) was used to elute His-tagged proteins of interest. In the case of gravity flow columns, final elution buffer (native buffer D) is used for final elution, containing 500 mM imidazole to remove any proteins from the column.

In order to determine whether His-ParH protein was successfully purified, fractions were analysed through 12% SDS-PAGE gel. As can be seen from figure below, His-ParH was purified successfully and that the protein bands in the elution fractions correspond to the expected size of the His-tagged proteins (Figure 4.3).

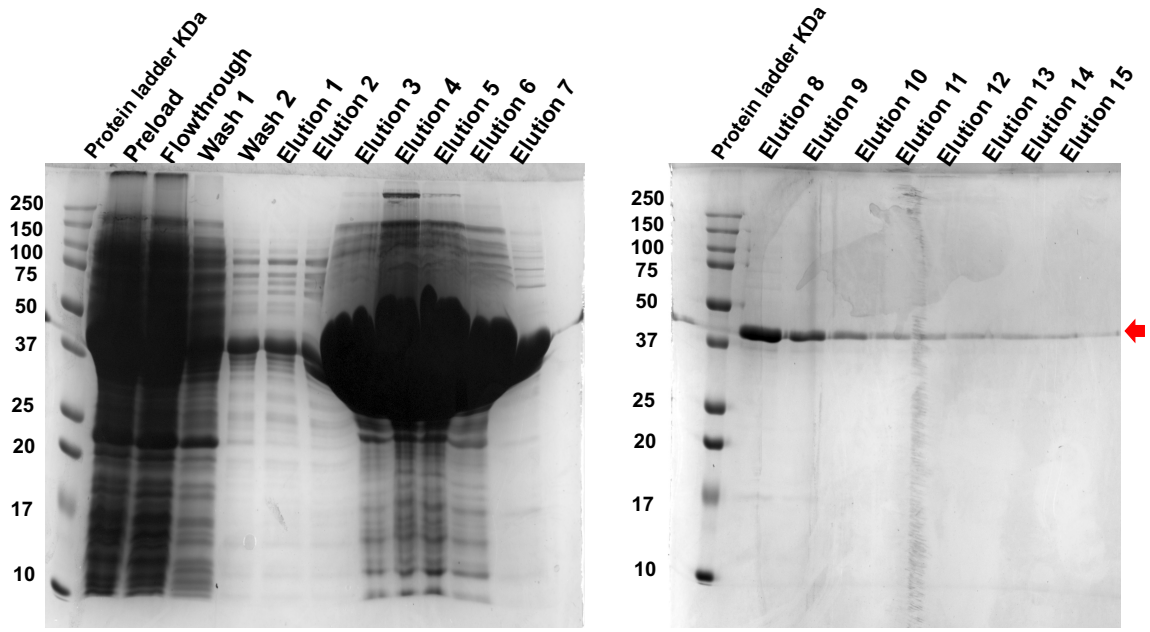

Figure 4.3 Large scale His-ParH purification using native conditions

Purification of His-ParH from BL21 pLysS after 20 hrs induction with 1 mM IPTG at 25°C. Native purification using Ni-NTA gravity flow column. Samples analysed include the preload, flow through, two wash fractions, wash1 and wash2,followed by the elution fractions. 5 µl standard was loaded into the first lane. Molecular weight markers shown in KDa. All samples were analysed using 12% SDS PAGE and visualised by Coomassie staining. The Red arrow indicates the 39.2 KDa His-ParH protein band.

4.2.3 Expression Trial of His-Hyp

After successful purification of His-ParH, we proceeded to purify the His-Hyp protein using nickel affinity chromatography. The *hyp* gene was previously cloned into pET28a to generate pET28a-Hyp. The *hyp* gene was amplified from *S. coelicolor* using primers 1771-*XbaI*-*NdeI*-FRW and 1771-*Eco*-UTC-REV, then digested with *NdeI* and *EcoRI* and cloned into pET28a. Forwarded primer adds an *NdeI* site that inserts the hyp ATG start codon into the restriction site and allows in-frame translation of Hyp adjacent to the His tag. The molecular weight of the expressing His-Hyp protein is approximately 21.4 KDa with pI= 7.2 (Gillespie, Unpublished 2017).

As with the purification of His-ParH, we aimed to determine the optimal conditions for the production of His-Hyp in *E. coli*. We used the same

expression trial used to determine optimal conditions for His-ParH production. 12% SDS-PAGE were used to analyse pellet and supernatant fractions from samples originated from 5 random transformant colonies . Here the cells were grown at 25°C after induction by IPTG as previously it was shown that to get soluble Hyp, cells needed to be growth at lower temperature (Gillespie, Unpublished 2017). Optimal expression of His-Hyp was observed after induction for 20 hours at 25°C, and under these we detected a 21.4 KDa protein mainly in the pellet fractions. A small amount of His-Hyp was also seen in the supernatant fraction collected under the same conditions. We decided to use colony 2 for large scale His-Hyp protein purification (Figure 4.4).

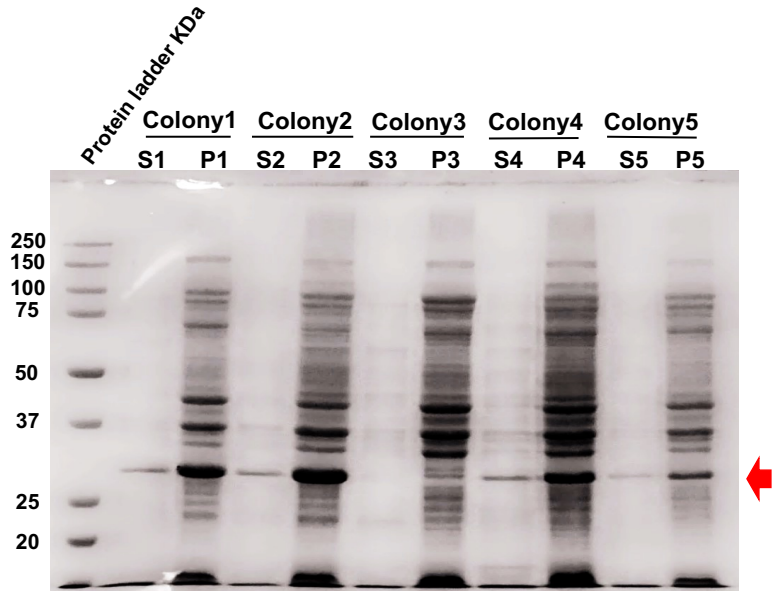

Figure 4.4 Expression trial of His-Hyp

Supernatant and pellet fraction from the from the small scale overexpression trials were analysed using 12% SDS-PAGE. The samples were loaded as follows; colony 1 (S1 & P1), colony 2 (S2 & P2), colony 3 (S3 & P3), colony 4 (S4 & P4) and colony 5 (S5 & P5). All samples were collected at 25°C, 20hrs after 1mM IPTG induction. The red arrow indicates the 21.4 KDa protein band of His-Hyp. The proteins were visualised by Coomassie Blue staining.

Interestingly Hyp was detected not exactly at its molecular weight of 21.4 KDa, but somewhat higher. This is consistent with previous Hyp purifications,

and currently we do not know what causes the slightly aberrant mobility of Hyp in the SDS-PAGE gels (more details in the summary section) (Figure 4.4).

4.2.4 Large Scale Expression and Purification of Hyp

Purification of His-Hyp was performed in the same way as the purification of His-ParH after expression using the conditions determined in the expression trials. Production of His-Hyp was carried out using 800 ml of cell cultures grown and induced as in the small scale trials. The collected cells were resuspended in the Tris loading buffer with low imidazole concentration (50mM Tris 10mM $MgCl_2$ 300 mM NaCl 10mM imidazole) and purified as described for His-ParH, using nickel column chromatography. His-Hyp was eluted with increased imidazole concentration of 300 mM. Fractions were collected and analysed on 12% SDS-PAGE.

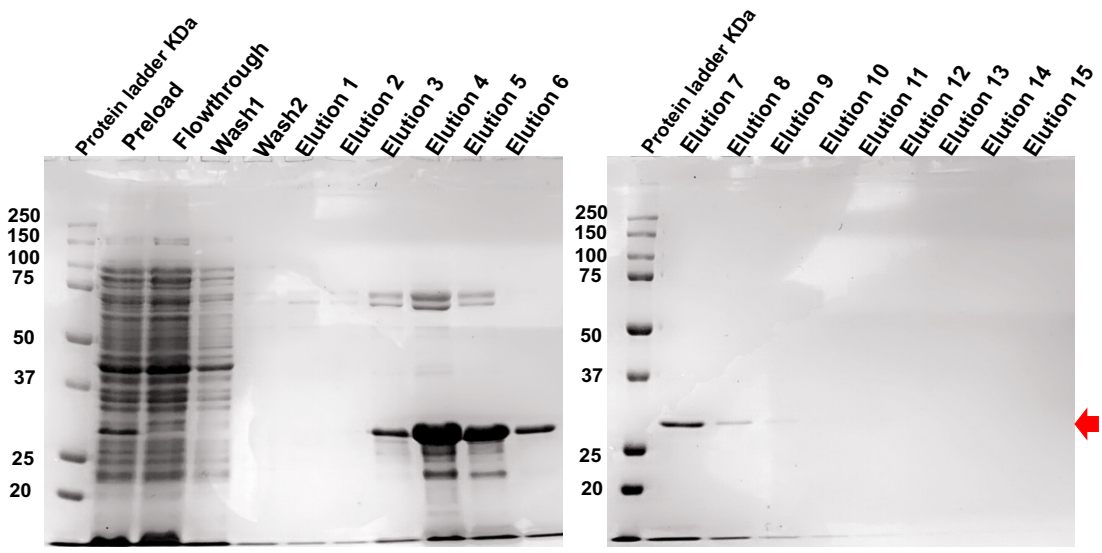

Figure 4.5 Large scale His-Hyp purification using native conditions

Purification of His-Hyp from BL21 pLysS carrying pET28-Hyp after 20 hrs induction with 1 mM IPTG at 25°C. Native purification using Ni-NTA gravity flow column was used Samples analysed include the preload, flow through, wash1 and wash2 followed by the elution fractions. Molecular weight markers shown in KDa. All samples were analysed using 12% SDS PAGE and visualised by Coomassie staining. The Red arrow indicates the 21.4 KDa His-Hyp.

4.2.5 Expression Trial of SepF, SepF F71A, FtsZ, Scy, and DivIVA proteins

Based on the bacterial two hybrid assays, which raised the possibility of interactions between ParH and SepF, Scy and Dia, we decided to purify these proteins together with some of the proteins that did not examine their interactions with ParH, namely FtsZ. We next wished to purify SepF, the mutant SepF F71A, FtsZ, Scy, and DivIVA in order to perform further in *vitro* investigation in Chapter 5. Appropriate pET28 plasmids, pET28-SepF, pET28-SepF F71A, pET28-FtsZ, pET28-Scy, pET28-DivIVA were available in the Kelemen laboratory (L Clarks, M Gillespie, A P Lau, Unpublished). After transformation of these plasmids into BL21 (DE3) pLysS, we picked several (3-5) independent colonies. The optimal conditions for production of these proteins were investigated using the same protocol employed to determine optimal production of His-ParH. In order to confirm overexpression of these proteins prior to embark on a large scale purification, expression trials were carried out from samples generated from 4-5 independent transformant colonies. The fractions, pellet and supernatant from expression trials were analysed using 12% SDS-PAGE (Figure 4.6 A &B, Figure 4.7 A&B, and Figure 4.8).

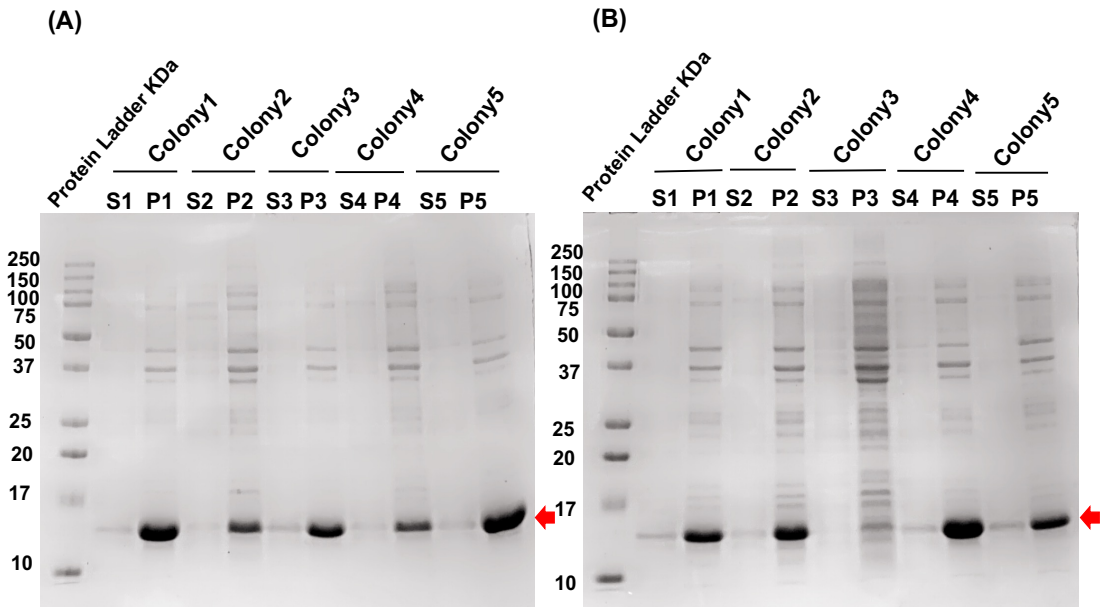

Figure 4.6 Expression trial of His-SepF and His-SepF F71A

(**A** and **B**) Supernatant and pellet fraction from samples overexpressing His-SepF (A) and His-SepF F71A (B) analysed using 12% SDS-PAGE. The samples were loaded as follows: colony 1 (S1 & P2), colony 2 (S2 & P2), colony 3 (S3 & P3), colony 4 (S4 & P4) and colony 5 (S5 & P5). All samples were collected at 25°C, 20hrs after 1mM IPTG induction. The Red arrow indicates the 13.0 KDa protein band for both SepF and SepF F71A. The proteins were visualised by Coomassie Blue staining.

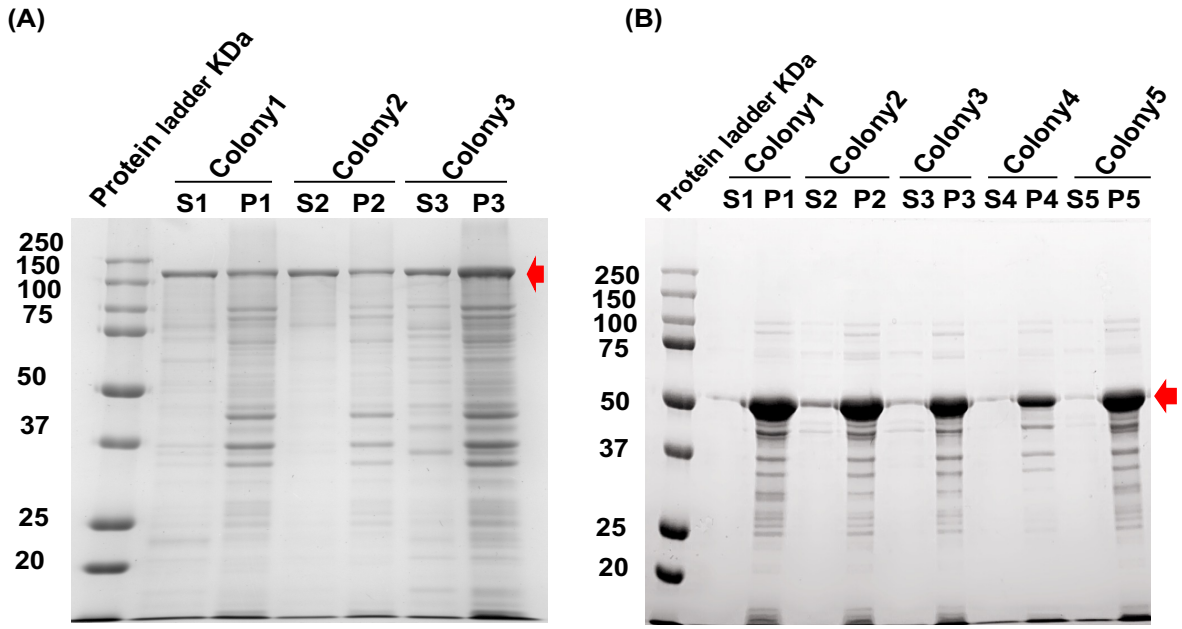

Figure 4.7 Expression trial of His-Scy and His-FtsZ

(A) Supernatant and pellet fractions from samples originating from 3 independent colonies expressing His- Scy were analysed using 12% SDS-PAGE. The samples were analysed as follows; colony 1 (S1 & P1). colony 2 (S2 & P2), and colony 3 (S3 & P3). All samples were collected at 25°C, 20hrs after 1mM IPTG induction. The red arrow indicates the 148.5 KDa His-Scy protein. The proteins visualised by Coomassie Blue staining.

(B) Supernatant and pellet fractions from samples originating from 5 independent colonies expressing His-FtsZ were analysed using 12% SDS-PAGE. The samples were analysed as follows colony 1 (S1 & P1), colony 2 (S2 & P2), colony 3 (S3 & P3), colony 4 (S4 & P4) and colony 5 (S5 & P5). All samples were collected at 25°C, 20hrs after 1mM IPTG induction. The red arrow indicates the 43.3 KDa His-FtsZ protein. The protein visualised by Coomassie Blue staining.

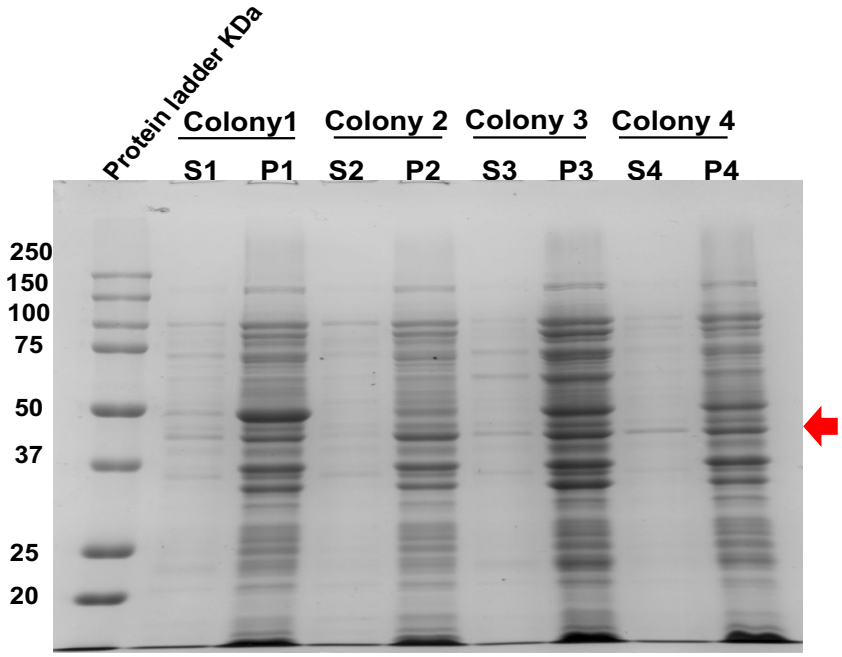

Figure 4.8 Expression trial of His-DivIVA

Supernatant and pellet fraction from samples originating from 4 independent colonies expressing His-DivIVA were analysed using 12% SDS-PAGE. The samples were analysed as follows; colony 1 (S1 & P1), colony 2 (S2 & P2), colony 3 (S3 & P3), and colony 4 (S4 & P4). All samples were collected at 25°C, 20hrs after 1mM IPTG induction. The red arrow indicates 43.3 KDa His-DivIVA protein, visualised by Coomassie Blue staining.

From the expression trials (Figure 4.6 A&B, Figure 4.7 A&B, and Figure 4.8) we found good overexpression for SepF, the mutant SepF F71A, Scy and FtsZ, but the overexpression was weak for DivIVA. For all the different overexpression samples, most proteins were in the pellet fractions, but there was reasonable amount also in the supernatants, so we decided to perform large scale overexpression and purification experiments for all these proteins

4.2.6 Large scale purification of SepF, SepF F71A, FtsZ, Scy, and DivIVA proteins

Production of SepF, SepF F71A, FtsZ, Scy, and DivIVA proteins, in order to achieve large scale purification, were carried out by generating 800 ml LB cultures using the same conditions as in the expression trials. All cells were resuspended in the Tris buffer with low concentration of imidazole (50mM Tris 10mM $MgCl_2$ 300 mM NaCl 10mM imidazole) and purified using nickel column chromatography. The His-tagged proteins were eluted with a step increase in imidazole concentration to 300 mM. Fractions were collected and analysed using 12% SDS-PAGE (Figure 4.9, Figure 4.10, Figure 4.11, Figure 4.12, and Figure 4.13). Although all washing fractions (wash 1 and wash 2) were performed, we did not load them into gels.

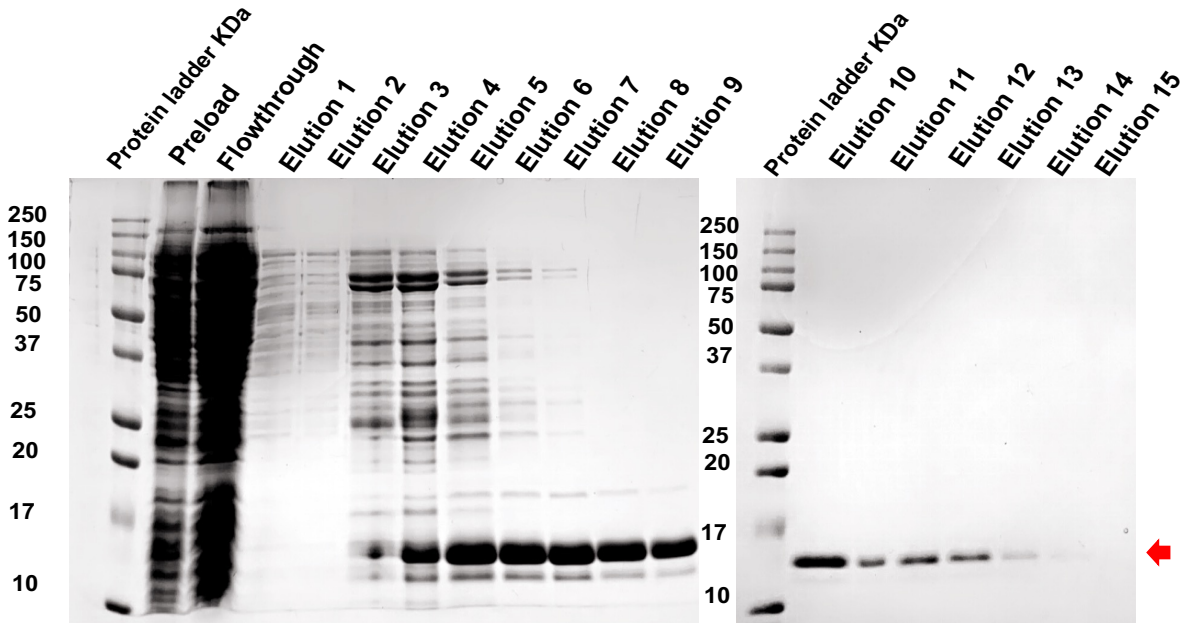

Figure 4.9 Large scale His-SepF purification using native conditions

Purification of His-SepF from BL21 pLysS carrying pET28-SepF after 20 hrs induction with 1 mM IPTG at 25°C. Native purification using Ni-NTA gravity flow column was used. Samples analysed included the preload, flow through, wash1 and wash2 followed by the elution fractions. Molecular weight markers shown in KDa. All samples were analysed using 12% SDS PAGE and visualised by Coomassie staining. The Red arrow indicates the 13.0 KDa His-SepF.

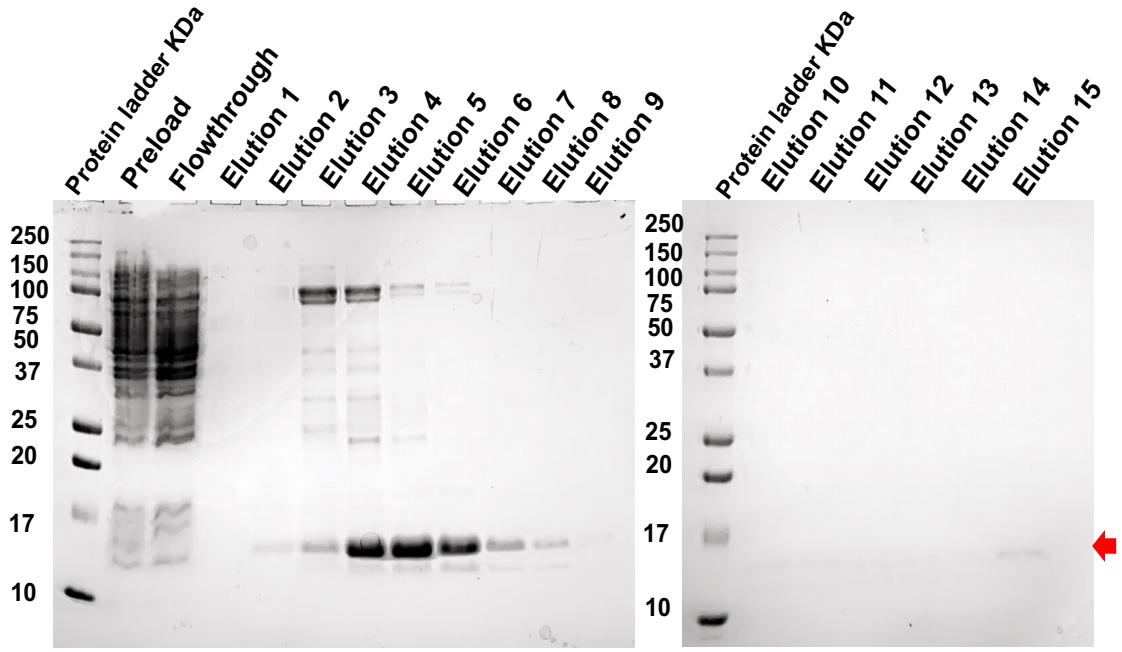

Figure 4.10 Large scale His-SepF F71A purification using native conditions

Purification of His-SepF F71A from BL21 pLysS carrying pET28-SepF F71A after 20 hrs induction with 1 mM IPTG at 25°C. Native purification using Ni-NTA gravity flow column was used. Samples analysed included the preload, flow through, wash1 and wash2 followed by the elution fractions. Molecular weight markers shown in KDa. All samples were analysed using 12% SDS PAGE and visualised by Coomassie staining. The Red arrow indicates the 13.0 KDa His-SepF F71A.

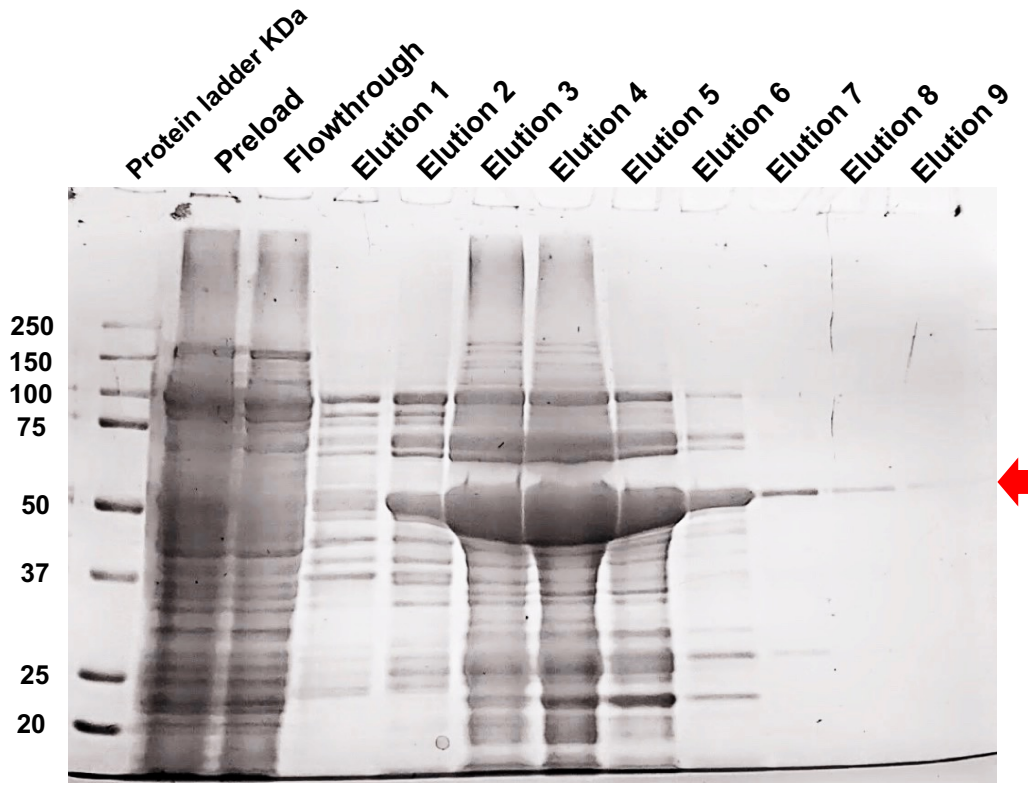

Figure 4.11 Large scale His-FtsZ purification using native conditions

Purification of His-FtsZ from BL21 pLysS carrying pET28-FtsZ after 20 hrs induction with 1 mM IPTG at 25°C. Native purification using Ni-NTA gravity flow column was used. Samples analysed included the preload, flow through, wash1 and wash2 followed by the elution fractions. Molecular weight markers shown in KDa. All samples were analysed using 12% SDS PAGE and visualised by Coomassie staining. The Red arrow indicates the 43.3 KDa His-FtsZ.

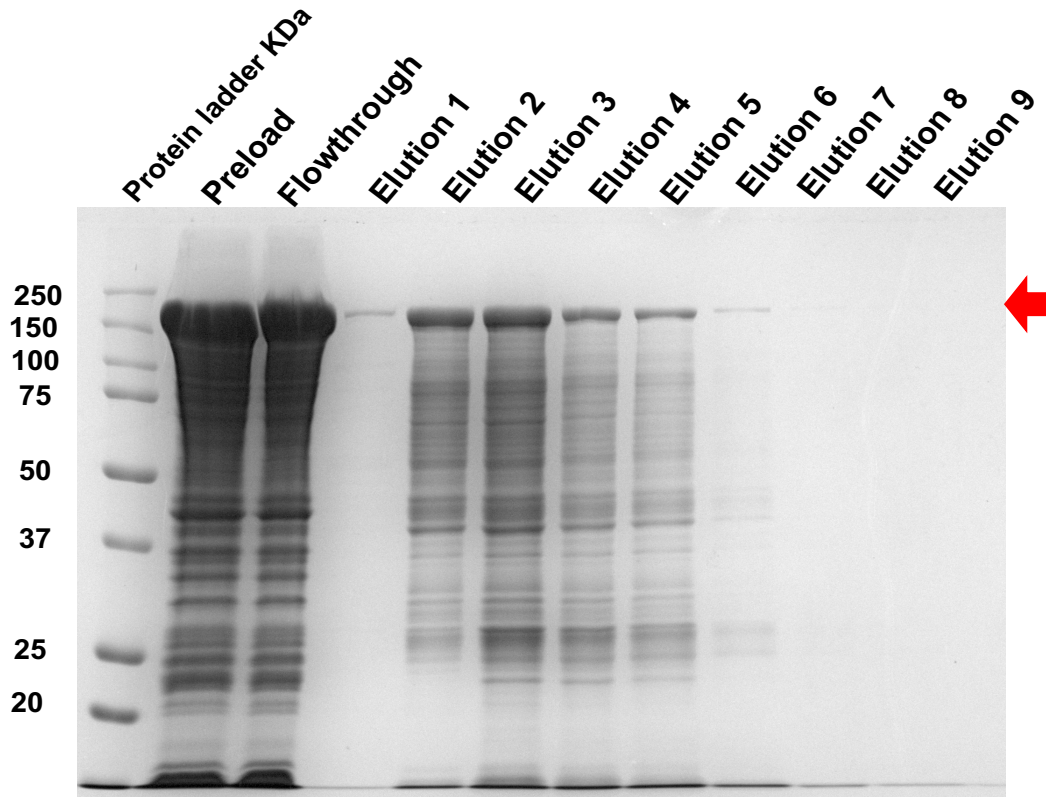

Figure 4.12 Large scale His-Scy purification using native conditions

Purification of His-Sc from BL21 pLysS carrying pET28-Scy after 20 hrs induction with 1 mM IPTG at 25°C. Native purification using Ni-NTA gravity flow column was used. Samples analysed included the preload, flow through, wash1 and wash2 followed by the elution fractions. Molecular weight markers shown in KDa. All samples were analysed using 12% SDS PAGE and visualised by Coomassie staining. The Red arrow indicates the 148.6 KDa His-Scy.

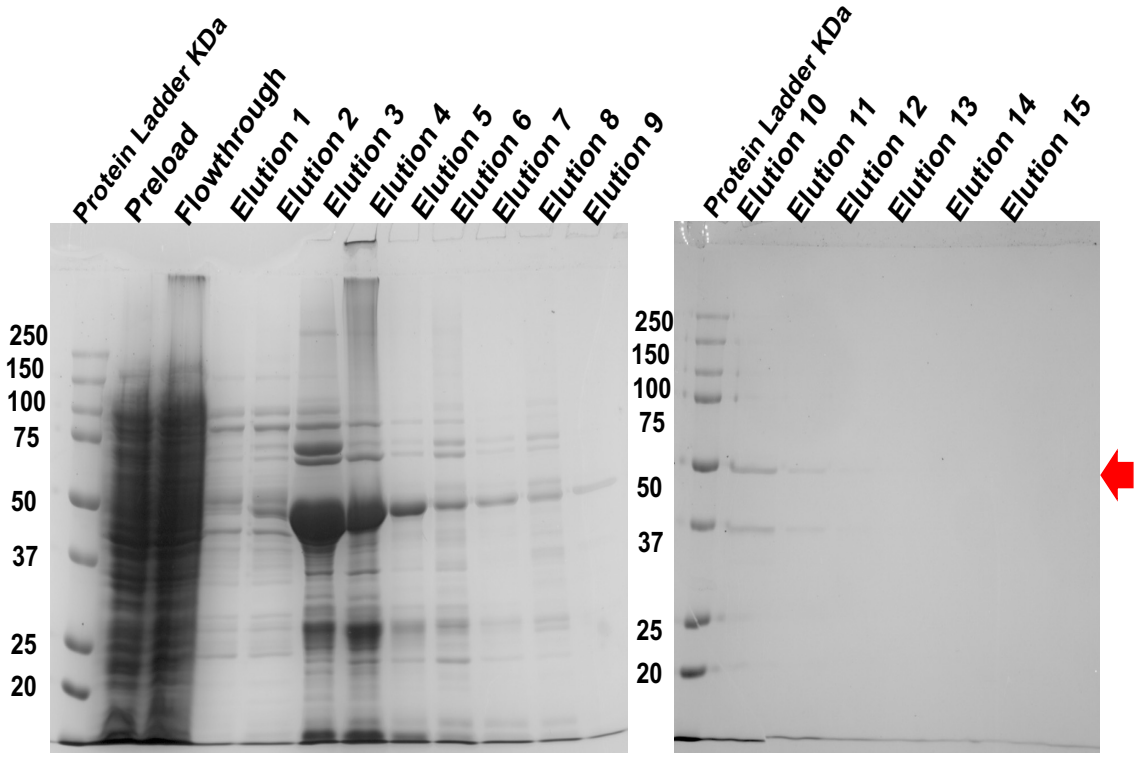

Figure 4.13 Large scale His-DivIVA purification using native conditions

Purification of His-DivIVA from BL21 pLysS carrying pET28-DivIVA after 20 hrs induction with 1 mM IPTG at 25°C. Native purification using Ni-NTA gravity flow column was used. Samples analysed included the preload, flow through, wash1 and wash2 followed by the elution fractions. Molecular weight markers shown in KDa. All samples were analysed using 12% SDS PAGE and visualised by Coomassie staining. The Red arrow indicates the 43.3 KDa His-DivIVA.

We have successfully generated His-tagged proteins, but the affinity chromatography did not generate fully clean protein preparations. In the case of ParH and SepF we generated fractions that were sufficiently clean for further biochemical analysis in Chapter 5.

4.3 Summary

In this Chapter we carried out large scale protein purifications for several proteins, including ParH, Hyp, proteins of the cell division machinery, SepF (SepFTR, SepF F71A and FtsZ) and proteins of polar growth, Scy and DivIVA. We have demonstrated that we could purify reasonable quantity of His-tagged proteins for all, using native purification conditions. This is very important, as correct protein folding can be expected from proteins that were purified under native conditions, whilst non-denaturing purification can generate proteins that are not correctly folded.

The observation that Hyp was detected at a molecular weight slightly higher than its expected size of 21.4 kDa on SDS-PAGE gels raises intriguing questions regarding its migration behavior (Figure 4.4). This deviation from the anticipated size could be attributed to a range of factors inherent to SDS-PAGE analysis. Notably, post-translational modifications (PTMs) are a prime consideration, as they can lead to shifts in protein mobility due to altered charge or size. Proteins with non-canonical folds or conformations might also exhibit anomalous migration patterns. Moreover, the presence of protein aggregates or multimers can influence migration behavior. The interaction of proteins with SDS micelles and variations in electrophoretic mobility might further contribute to the observed discrepancy. Another plausible explanation could be variations in the net charge of Hyp arising from modifications or structural features, impacting its migration rate. Additionally, the composition of the gel or gel artifacts could play a role. To comprehensively decipher the underlying cause for this phenomenon, further investigations are warranted. Techniques such as mass spectrometry could elucidate potential PTMs, while diverse SDS-PAGE conditions and careful analysis of gel integrity could shed light on the reasons for the unusual migration pattern.

Although we managed to purify all of our proteins using native conditions, we also found that our overexpression conditions did generate a lot of proteins in the pellet fractions, which we did not use for purification purposes. Further experiments could be carried out to increase the proportion of proteins in the soluble fraction compared to that in the insoluble, pellet

fraction. This could be achieved by lowering the IPTG concentration used or lowering the temperature at which the cells were grown after the induction, to slow down the overexpression rate promoting the production of correctly folded, soluble proteins.

This chapter generated an excellent protein resource for further biochemical studies in the Kelemen laboratory. In this thesis, we will use the preparation of ParH, Hyp and SepF in Chapter 5.

CHAPTER 5

5. Analysis of Protein – Protein Interactions Using Native PAGE Gel

5.1 Introduction

In chapter 3, we investigated protein-protein interaction *in vivo* using bacterial two hybrid assay in the heterologous host *E. coli*. Interestingly we have identified a positive interaction between His-ParH and the cell division protein SepF (Chapter 3, Figure 3.3). Then we tested interaction between His-ParH and two SepF mutations, showing that SepF F71A is important for their interaction, the phenylalanine at position 71 of SepF is involved in the interaction. Interaction between SepF and selected of ParH mutants was also investigated using bacterial two hybrid assay (Chapter 3, Figure 3.7, and Figure 3.8). Mutations in residues that are involved in ATP binding and ATP hydrolysis affected the interaction between ParH and SepF suggesting that ATP binding of ParH is necessary for the protein-protein interaction. In addition, the bacterial two hybrid assay confirmed the positive interaction between ParH and the coiled-coil protein Dia (Chapter 3, Figure 3.9).

ParA/MinD family proteins are dimerised in the presence of ATP, allowing them to bind to surfaces or generate binding sites for their partners (Leonard TA, 2005; Hu Z, *et al*. 2002). According to structural and biochemical analysis of Soj (ParA) in *B. subtilis*, ATP facilitates DNA binding by dimerising Soj, which activates its interaction with DnaA. Soj has a monomeric state in the presence of ADP, which inhibits DNA replication initiation by inhibiting DnaA (Lutkenhaus, 2012). The *Streptomyces* ParA protein undergoes ATP-dependent dimerisation, which can further assemble into filaments in the presence of ATP. When ParA does not bind to ATP, the protein disassembles into the monomeric state. During cell division, chromosome segregation is organised by this regulatory mechanism; the ParA spreads over the nucleoid and pulls the ParB to bind to DNA (Lutkenhaus, 2012). Cell division occurs when ATP is released, causing the filaments to release, resulting in the pulling of the DNA. This pattern regulates the positioning of the Z ring and on the nucleoid leading to chromosome segregation (Lutkenhaus, 2012).

What the bacterial two hybrid screening showed in the previous chapter (Chapter 3), it is essential that partner proteins of ParH interact to regulate their function. In various organisms, there are examples where the interactions between partner proteins play a critical role in their function. In *E. coli,* the genes for the MinD and MinE proteins are located in the *minCDE* operon. The interaction of MinD with MinE affects the oligomeric state of MinD through regulating its ATPase activity (Hu and Lutkenhaus, 2001). By forming dimers in the presence of ATP, MinD can interact with MinE. A subsequent interaction between MinD and MinE triggers ATP hydrolysis, which produces MinD monomers (Lackner, Raskin and De Boer, 2003). As a monomer, MinD cannot interact with MinE. It is the interaction between MinD and MinE that regulates the nucleotide binding of MinD that determines the pole-to-pole oscillations of MinD localisation (Lutkenhaus, 2012).

Moreover, in *B. subtilis*, MinJ acts as molecular bridge which often participates in the interaction between MinD and DivIVA (Jemth P, Gianni S. 2007). Research shows DivIVA localises at the cell poles during cell division, and it is responsible for the polar localisation of MinC/MinD, the division inhibitor. Hence, this localisation prevents the formation of Z-ring at the poles (Edwards DH, Errington J ,1997).

In the current chapter, we will analyse ParH and its polymerisation properties using native PAGE, followed by testing the effect of the protein–protein interaction on ParH polymerisation in *vitro.* We will also investigate in *vitro* protein-DNA interaction using Electrophoretic Mobility Shift Assay (EMSA).

5.2 Results

5.2.1 Protein Dialysis

Initially, the purified proteins (Chapter 4) were dialysed into a Tris-based buffer in order to remove the imidazole salts from the preparations. A method for maintaining protein solubility during dialysis involve adding charged L-amino acids, such as arginine (Gillespie, Unpublished 2017) was used previously for the purification of Hyp, because Hyp showed precipitation after dialysis without arginine in the buffer. When we assessed interactions between ParH and Hyp we dialysed both proteins using a Tris buffer that contains arginine to maintain the His-tagged protein in soluble form (50 mM Tris, 100 mM KCl, 100 mM Arginine pH 8.0). However, when assessing ParH on its own and in combination with other proteins, we conducted the dialysis without arginine, in buffer. Initially, dialysed preparations of ParH were kept on ice in the cold room. However, later we found that incubation of ParH samples promoted polymerisation, and from then, all freshly dialysed proteins were aliquoted, quickly frozen using liquid nitrogen and kept at -20^{o}C.

5.2.2 Analysis of ParH interactions using Native – PAGE

A key feature of ParA proteins is their ability to form dimers in the presence of ATP. Switching between different states, monomeric and dimeric states, controls the activity of ParA that controls cell division and chromosome segregation. Previously in the Kelemen lab analytical gel filtration revealed that unlike the dimer formation of ParA, ParH has multiple oligomeric states (Gillespie, Unpublished 2017).

We have confirmed this using native PAGE, where His-ParH appeared as multiple bands in a ladder-like formation with at least 10 bands perceptible, and these bands were also distinguished by their regular spacing on the gel (Figure 5.1).

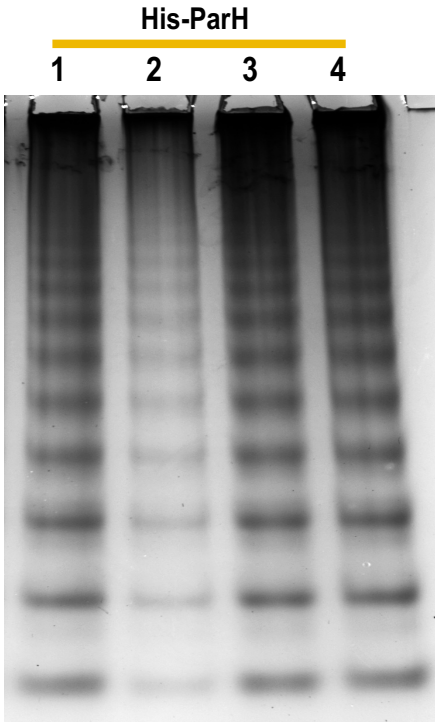

Figure 5.1 Native-PAGE of His-ParH

His-ParH were analysed using 6% native-PAGE. All His-ParH (Lanes 1, 2, 3, and 4) produced multiple bands in a ladder-like formation. All lanes had the same amount of ParH (700 pmol). Dialysed samples were kept into the cold room for days before running the gel. Gel was stained by silver staining.

ParH oligomers are proposed to be built from the monomer subunit and can also be reformed from the monomeric state of ParH (Gillespie, Unpublished 2017). We found that polymerisation progressed to ParH forming longer polymers when freshly dialysed samples were kept on ice for days without any additional co-factor (Figure 5.2).

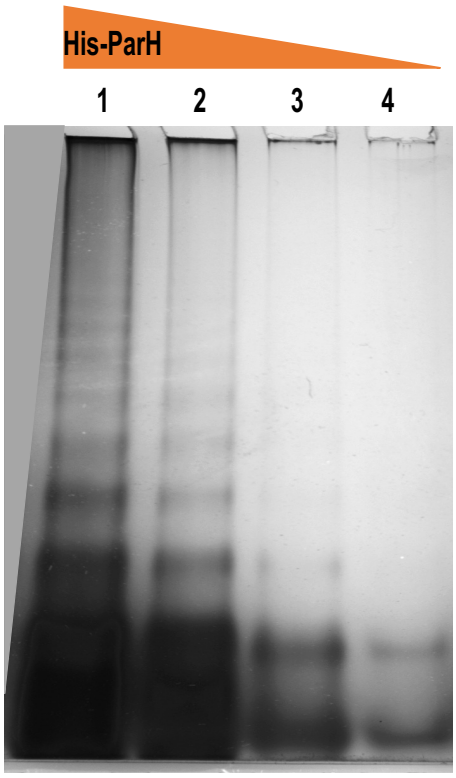

Figure 5.2 Native-PAGE of freshly dialysed His-ParH

The freshly dialysed His-ParH were analysed using 6% native-PAGE. All His-ParH Lane1 (700 pmol), Lane 2 (280 pmol), Lane 3 (70 pmol), and Lane4 (28 pmol) produced multiple bands in a ladder-like formation. All samples were dialysed and freshly loaded into the gel. Gel was stained by silver staining.

To test different conditions affecting ParH polymerisation, it was important to standardise the oligomer state of the starting preparations. Hence, we generated a fresh large His-ParH preparation that was dialysed and aliquots were quick frozen and kept at -20^{o}C.

5.2.2.1 ATP has an effect on the oligomerisation of His-ParH

For further investigation to study ParH behaviour in presence of ATP at different conditions, and interaction with His-Hyp, His-Dia, and His-SepFTR, we utilised in *vitro* Native-PAGE gel method. Freshly dialysed His-ParH protein (280 pmol) was incubated in the absence and in the presence of 1mM ATP and 20 mM $MgCl_2$ at 30° C for 20 minutes in a Tris buffer (50 mM Tris, 150 mM

KCl, pH 8.0). We used different amount of His-ParH (28-280 pmol) to test whether polymerisation was dependent on ParH concentration. After incubation the samples were analysed through 6% native-PAGE and run for 2 hours at 100 V. The gel was then silver stained to observe the ParH bands (Figure 5.3).

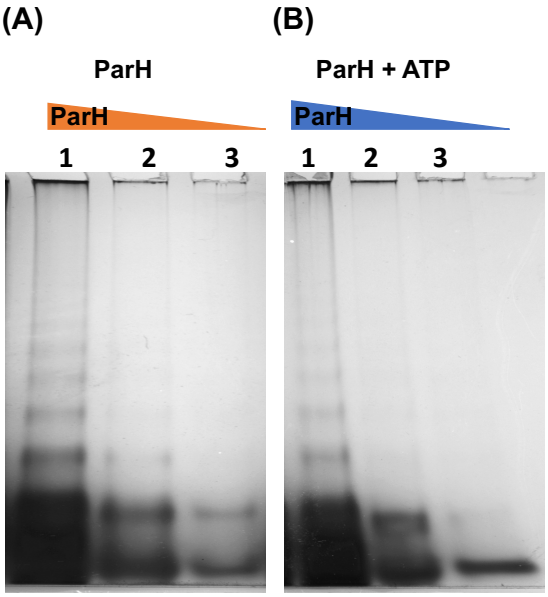

(C)

	Figure (A)			Figure (B)		
	1	2	3	1	2	3
ATP Mg^{+2}	-	-	-	2 µl	2 µl	2 µl
ParH	2 µl Conc	5 µl 10X Dil	2 µl 10X Dil	2 µl Conc	5 µl 10X Dil	2 µl 10X Dil

Figure 5.3 Native-PAGE of His-ParH with ATP

His-ParH (280 pmol) was incubated with and without 1 mM ATP before analysis using 6% native -PAGE. **(A)** His-ParH 280 pmol (Lane1), 70 pmol (Lane 2), and 28 pmol (Lane 3) formed multiple bands that disappeared gradually as ParH concentration decreased. **(B)** When ParH were incubated with constant amounts of 1mM ATP and 20mM $MgCl_2$ (280 pmol, Lane 1) , (70 pmol, Lane 2), and (28 pmol, Lane 3), it is notable the higher bands tend to disappear. The gel was visualised by silver staining for observing proteins. **(C)** the volume of proteins and ATP.

The native result shows that ParH forms multiple regular spaced bands (Figure 5.3 A) indicating that ParH can polymerise into different oligomer forms. The oligomerisation was more clear at samples with higher ParH concentration. Previous study tested the effect of ATP on ParH polymerisation (Gillespie, Unpublished 2017), expecting that like ParA , ParH might form dimers in the presence of ATP, but ParH did not dimerise in the presence of ATP. Here we investigated the possibility that ATP affected ParH

oligomerisation. Native-PAGE revealed that at any given ParH concentration, in the presence of ATP there were less higher oligomers observable (Figure 5.3 B). This suggests that ATP has the ability to influence His-ParH oligomerisation by promoting the depolymerisation of ParH. This is very different from the ATP dependent dimerisation of ParA and suggests that ParH operates differently from ParA.

5.2.2.2 ParH shows a DNA binding activity *in vitro*

To further understand the significance of the role ParH has in chromosome organisation, we investigated the ability of ParH to interact with DNA using native-PAGE. Previous studies have illustrated that Soj, the ParA homologue in *B. subtilis*, binds to DNA non-specifically in the presence of ATP. Dimerisation of Soj (ParA) plays an essential role in regulating DnaA by forming nucleoprotein complex with DNA (Hester and Lutkenhaus,2007). Freshly dialysed His-ParH proteins were incubated with DNA in absence and presence 1 mM ATP and 20 mM $MgCl_2$ for 20 minutes at 30°C in a Tris buffer (50 mM Tris, 150 mM KCl, pH 8.0). After incubation the samples were analysed using 6% native-PAGE and run for around 2 hours at 100 V.

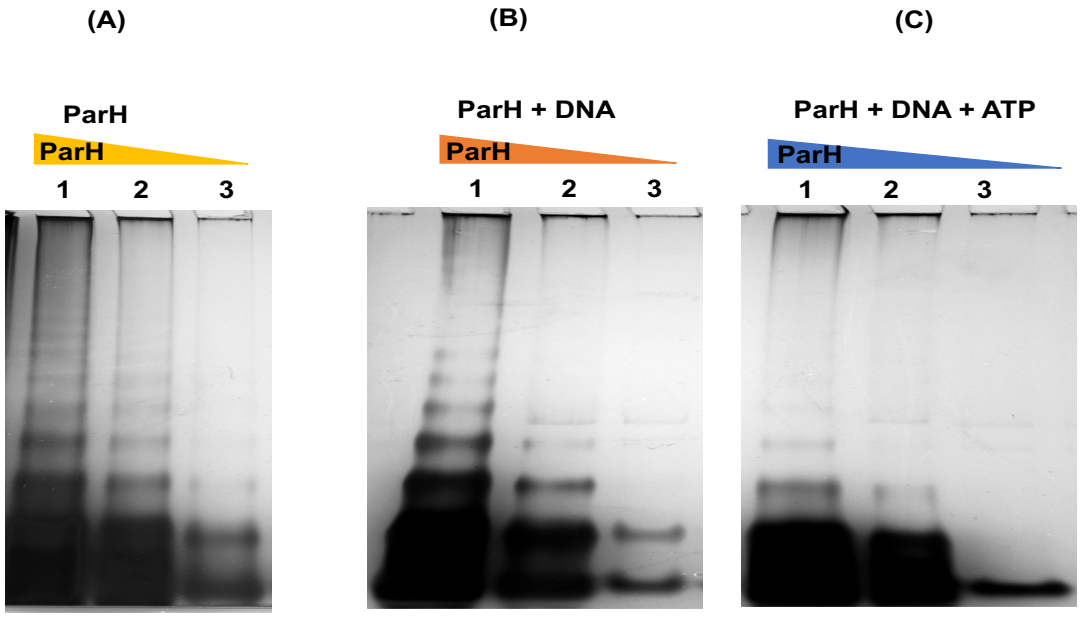

(D)

	1	2	3
Buffer	14µl	17µl	14µl
ATP Mg^{+2}	-	-	-
ParH	5 µl Conc	2 µl Conc	5 µl Dil
DNA	-	-	-

1	2	3
14µl	17µl	14µl
-	-	-
5 µl Conc	2 µl Conc	5 µl Dil
1 µl	1 µl	1 µl

1	2	3
14 µl	17µl	14µl
2 µl	2 µl	2 µl
5 µl Conc	2 µl Conc	5 µl Dil
1 µl	1 µl	1 µl

Figure 5.4 6% Native- PAGE of ParH with DNA in presence of ATP

His-ParH and DNA were incubated both separately and together in presence and absence of ATP before analysing samples by 6% native-PAGE. **(A)** ParH oligomerisation used as control. **(B)** ParH proteins were incubated with DNA as follows 700 pmol, 280 pmol, and 70 pmol. **(C)** Decreasing amounts of His-ParH proteins were incubated with DNA in presence of 1 mM ATP and 20 mM $MgCl_2$. **(D)** Table presenting the amounts of ParH and DNA. Reactions incubated at 30˚C for 20 minutes before loading into gel. The gel ran for 2 hours low voltage at 100V. Native-PAGE gel was visualised by silver staining.

From the data in Figure (5.4) above, it is apparent that the higher level of His-ParH oligomerisation has been influenced by DNA when compared to the control lanes Figure (5.4 A). In the presence of DNA, there were slightly less higher oligomers and this depolymerisation was further promoted in the presence of ATP. When comparing lanes with the same amount of ParH, it is

clear that the ATP-dependent depolymerisation is promoted in the presence of DNA (Lane 3 in 5.4 C and Lane 2 in 5.3 B).

5.2.2.3 Interaction between His-ParH and His-Hyp

The gene encoding ParH is located within a gene operon that contains another gene encoding a small hypothetical protein called Hyp (Chapter 1, Figure 1.15). The gene organisation suggests that ParH and Hyp are co-translated and hence the expectation is that their functions are linked. Previously in the Kelemen lab, the structure of Hyp has been solved and indicated that Hyp belonged to the ribbon-helix-helix type DNA binding proteins (Gillespie, Unpublished 2017).

Initially, to test the interaction between ParH and Hyp using native PAGE, we used proteins (ParH and Hyp) that were dialysed into a Tris buffer containing arginine (50 mM Tris, 100 mM KCl, 100 mM Arg pH 8.0), as Hyp needed the presence of arginine to stay soluble. Historically this experiment was carried out before we established that His-ParH was polymerising when stored on ice. The preparations used in these experiments were stored on ice after dialysis. His-ParH protein was incubated in the absence and in the presence of His-Hyp protein and in the absence and presence of ATP using a Tris buffer (50 mM Tris, 100 mM KCl, 100 mM Arg pH 8.0) for 20 minutes at 30°C. After incubation all samples were analysed using 6% native-PAGE and run for 2 hours at low voltage 100 V. Then the gel was stained by silver staining (Figure 5.5).

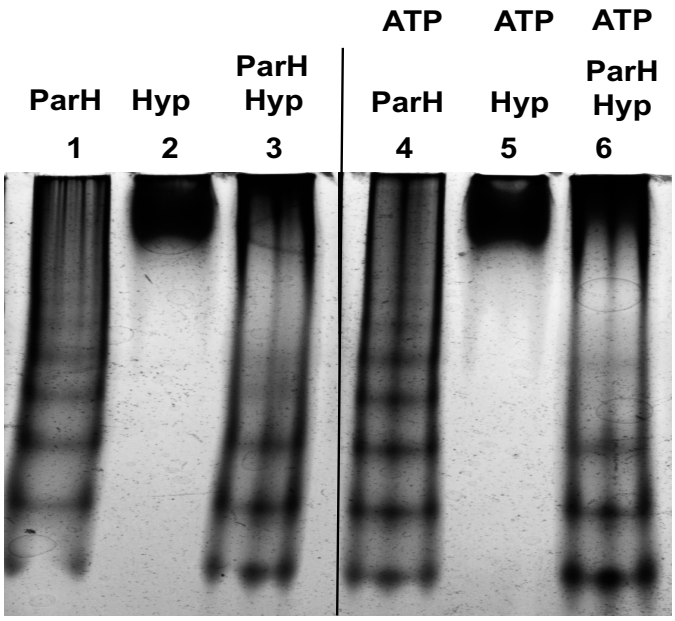

Figure 5.5 Native-PAGE of His-ParH and His-Hyp

His-ParH and His-Hyp were incubated at 30° C for 20 minutes both separately and together before analysis using 6% native-PAGE. His-ParH (Lane 1). His-Hyp (Lane 2). His-ParH and His-Hyp were mixed in (Lane 3). In lanes 4, 5, and 6 proteins were incubated with the addition of 1mM ATP and 20 mM $MgCl_2$. When the proteins were mixed either in presence of ATP or absent some of the higher His-ParH bands disappeared. Samples were analysed using 6 % native-PAGE and run for 2 hours 100 V. The gel was visualised by sliver staining.

According to Gillespie's data (2017), His-Hyp formed a single band, which is consistent with analytical gel filtration data that revealed that Hyp is tetrameric. A distinctive feature of the His-ParH form oligomerisation products that are regularly increasing in size. In this experiment, when the His-ParH and His-Hyp were incubated together, the top bands of His-ParH disappeared and the His-Hyp band changed as well. In their place is a band at the very top of the gel and a short smear underneath. It is likely that higher order assemblies are formed as a result of the interaction of both proteins. A noteworthy observation is the fact that the three lower His-ParH bands did not change, suggesting that the interaction may involve Hyp and the highest ParH oligomers. There is also an interesting observation that ATP does not seem to alter the ParH-Hyp interaction. Perhaps ATP is not required for interaction between ParH and Hyp. It is also worth noting that the absence of ATP did not

prevent the formation of many oligomers by His-ParH and did not promote depolymerisation of ParH, suggesting that Hyp might bind to the higher oligomer forms and prevent depolymerisation of ParH.

Then, we aimed to examine the interaction between His-ParH and His-Hyp, which were freshly dialysed into a Tris buffer not containing arginine using the native-PAGE method. Different concentrations of ParH and a set amount of Hyp proteins were incubated both independently and together in a Tris buffer (50 mM Tris, 150 mM KCl, pH 8.0) for 20 minutes at 30° C. After incubation all samples were analysed using 6% native-PAGE and run for 2 hours at low voltage 100 V. The gel was then silver stained (Figure 5.6)

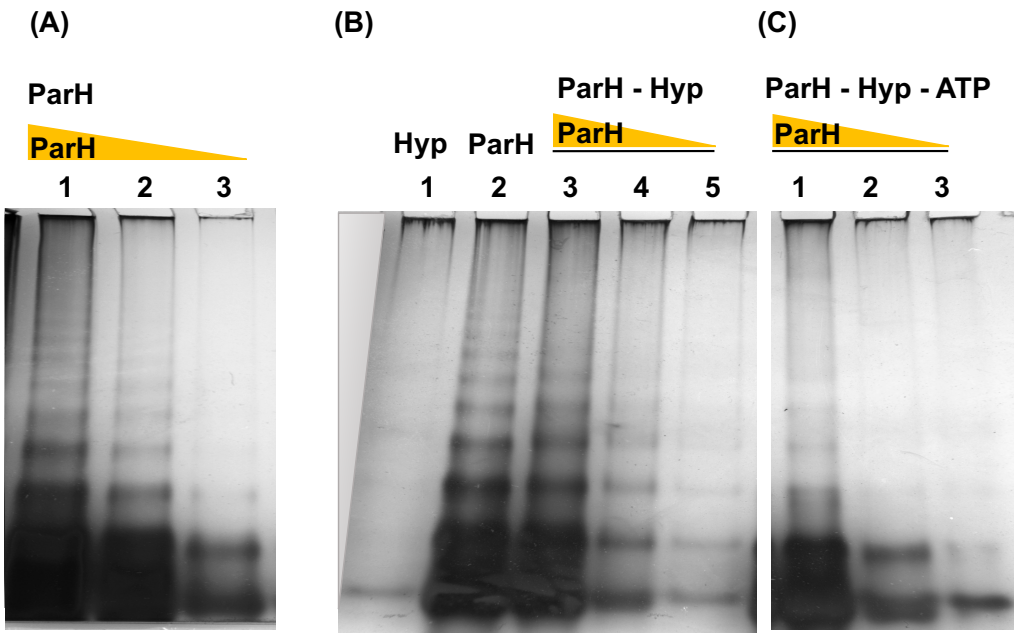

(D)

	1	2	3
ATP Mg^{+2}	-	-	-
ParH	2 µl Conc	5 µl Dil	2 µl Dil
Hyp	-	-	-

1	2	3	4	5
-	-	-	-	-
-	2 µl Conc	2 µl Conc	5 µl Dil	2 µl Dil
5 µl	-	5 µl	5 µl	5 µl

1	2	3
2 µl	2 µl	2 µl
2 µl Conc	5 µl Dil	2 µl Dil
5 µl	5 µl	5 µl

Figure 5.6 Native-PAGE of His-ParH and His-Hyp

His-ParH and His-Hyp were incubated at 30 C for 20 minutes both separately and together before analysis using 6% native-PAGE. **(A)** His-ParH (280 pmol, 70 pmol, 28 pmol) oligomerisation used as control. **(B)** His-Hyp 20 pmol (lane 1). His-ParH 280 pmol (lane 2). Then His-ParH incubated with constant amount of His-Hyp (20 pmol) in (lanes 3,4,5). **(C)** Proteins His-ParH and His-Hyp were incubated in the presence of 1 mM ATP and 20 mM $MgCl_2$ (Lanes 1,2,3). Samples were analysed using 6 % native-PAGE and run for 2 hours 100 V. The gel was visualised by silver staining. **(D)** Table showing the concentrations of ParH and Hyp in the reaction.

Unfortunately, we could not fully repeat the previous observation, where Hyp was interacting with the higher oligomer forms. This might have been because the Hyp preparation used here was not concentrated enough. To establish the link between ParH and Hyp, these experiments need to be repeated with a better Hyp preparation.

5.2.2.4 Oligomerisation of ParH and Coiled-coil protein Dia

Previous studies have been studying the interaction between polar growth and cell division proteins. Preliminary data from Kelemen laboratory established that the Dia coiled coil protein (SCO5569) was involved in the controlling the hyphal width and affected the distance between the sporulation septa. In the previous chapter (Chapter 3), we established an interaction between ParH and Dia in *vivo* using a bacterial two hybrid system (Chapter 3, Figure 3.11). For further examination, in the current chapter, we aimed to investigate the interaction between ParH and coiled-coil protein Dia in *vitro* using native-PAGE. To achieve this, reactions were carried out in which His-Dia (135 pmol) and His-ParH (280 pmol, 70 pmol and 28 pmol) were incubated separately and then together. Incubations were performed for 20 minutes at 30˚C in a Tris buffer (50 mM Tris, 150 mM KCl, pH 8.0). As part of our investigation into whether ATP affected the polymerisation state of these proteins, samples were also incubated with ATP. After incubation, the samples were analysed using 6% native-PAGE and run for 2 hours at low voltage 100 V. The gel was then visualised by silver staining (Figure 5.7).

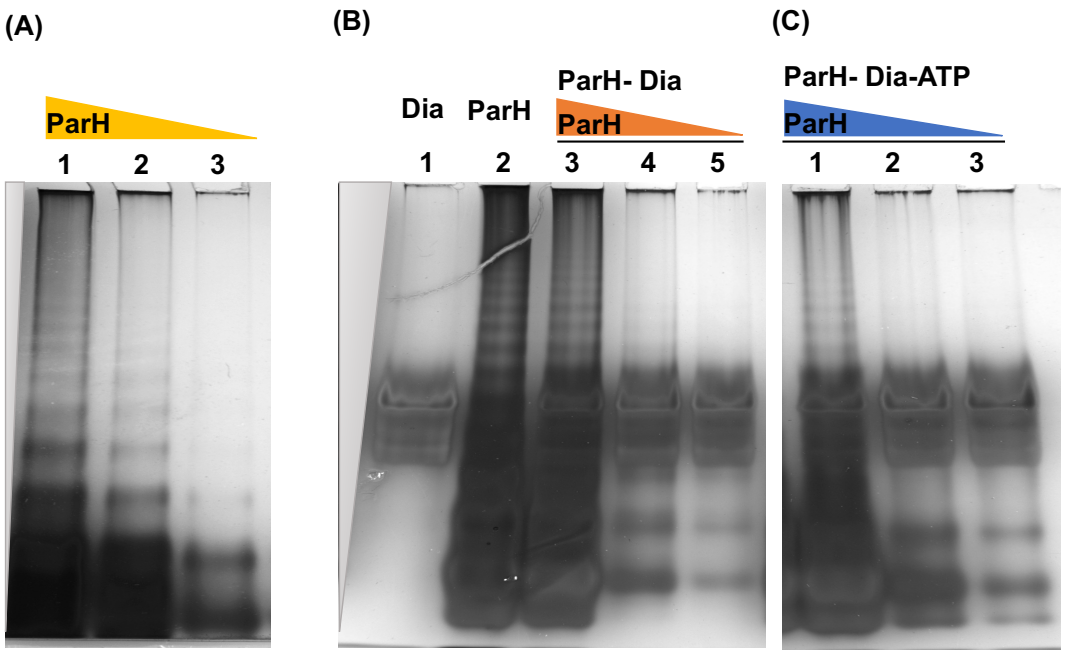

(D)

	1	2	3
ATP Mg^{+2}	-	-	-
ParH	2 µl Conc	5 µl Dil	2 µl Dil
Dia	-	-	-

1	2	3	4	5
-	-	-	-	-
-	2 µl Conc	2 µl Conc	5 µl Dil	2 µl Dil
5 µl	-	5 µl	5 µl	5 µl

1	2	3
2 µl	2 µl	2 µl
2 µl Conc	5 µl Dil	2 µl Dil
5 µl	5 µl	5 µl

Total Volume: 20 µl

Figure 5.7 Native-PAGE of His-ParH and His-Dia

A native-PAGE gel was performed to test the His-ParH and His-Dia interaction. ParH and Dia proteins were incubated both at 30° C for 20 minutes before analysing the samples using 6% native-PAGE. **(A)** His-ParH (280 pmol, 70 pmol, 28 pmol) native was performed as control. **(B)** His-Dia 135 pmol (Lane 1) formed three bands. His-ParH 280 pmol (Lane 2). His-ParH 280 pmol (Lane 3), 70 pmol (Lane 5), and 28 pmol (Lane 5) were mixed with constant amount of His-Dia 135 pmol. **(C)** His-ParH proteins were incubated with fixed amount of His-Dia in presence of 1 mM ATP and 20 mM $MgCl_2$ (Lanes 1, 2, and 3). **(D)** Table showing the concentrations of ParH and Hyp in the reaction. For observing proteins, the gel was visualised by sliver staining.

On the basis of the native form, the His-Dia apparently has three to four bands, while ParH appears as multiple bands in regular space. The bacterial two hybrid assays revealed a positive interaction between His-ParH and His-Dia in *vivo* (Chapter 3, Figure 3.11). Here native-PAGE suggests that the

presence of Dia might have inhibited His-ParH depolymerisation in the presence of ATP in *vitro*. Comparing lanes 2 and 3 in Figure (5.3 A & B) with lanes 2 and 3 in Figure (5.7 C), the presence of Dia inhibited ParH depolymerisation.

5.2.2.5 Interaction of ParH and the cell division protein SepF

In chapter 3, we had already observed His-ParH and His-SepF interaction in *vivo* through a bacterial two hybrid assay in heterologous host *E. coli* (Chapter 3, Figure 3.3). To better understand this interaction, we examined this interaction in *vitro* through native-PAGE. To achieve this, reactions were conducted in which His-SepF (45 pmol) and His-ParH (70 pmol), (28 pmol) and (14 pmol) were incubated separately and then together in His-ParH (70 pmol), (28 pmol), and (14 pmol) in which the amount of His-SepF (45 pmol) remained constant. The incubations were carried out for 20 minutes at 30˚C in a Tris buffer (50 mM Tris, 150 mM KCl, pH 8.0). To investigate whether ATP had an effect on the polymerisation state of these proteins, we also incubated samples in the presence of 1 mM ATP. In the presence of ATP, His-SepF was incubated with His-ParH in (70 pmol), (28 pmol), and (14 pmol) in which His-SepF had a fixed amount (45 pmol). After incubation the samples were then analysed using 6% native-PAGE and run for 2 hours at low voltage 100 V. The gel was then visualised by silver staining (Figure 5.8).

(A)

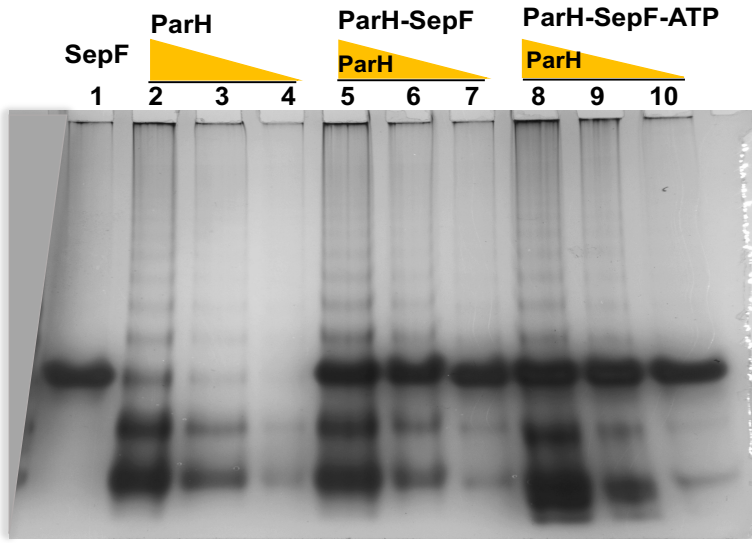

(B)

ParH	5 µl Dil	2 µl Dil	1 µl Dil
SepF	3 µl	3 µl	3 µl

Total Volume 20 µl

Figure 5.8 Native-PAGE of His-ParH and His-SepF

(A) His-ParH and His-SepF were incubated both separately and together in presence and absence 1 mM ATP and 20 mM $MgCl_2$ at 30° C for 20 minutes before analysis using 6% native-PAGE. His-SepFTR (45 pmol) (Lane 1) ran as a single band. His-ParH 70 pmol (Lane 2), 28 pmol (Lane 3), 14 pmol (Lane 4). His-ParH proteins were incubated with fixed amount of His-SepF (45 pmol) in the absence of 1 mM ATP and 20 mM $MgCl_2$ (Lanes 5 to 7). His-ParH proteins were incubated with fixed amount of His-SepFTR 45 pmol in presence of 1 mM ATP and 20 mM $MgCl_2$ (Lanes 8 to 10). For observing proteins, the gel was visualised by sliver staining. **(B)** table represents ParH and SepF amount in this reaction.

According to this gel (Figure 5.8), His-SepF consists of only one band. Although the bacterial two hybrid assay confirmed the positive interaction between His-ParH and His-SepF in the previous chapter (Chapter 4), we could only detect subtle differences that needed further confirmation. Perhaps in the presence of SepF, there was slightly more higher order polymer forms of ParH (Figure 5.8).

To test whether these subtle differences were meaningful we decided to investigate these interactions by increasing the incubation period. In order to achieve this, reactions were carried out in which His-SepF (45 pmol) and decreasing concentrations of His-ParH (70 pmol), (28 pmol) and (14 pmol). The proteins were incubated overnight separately and then together in His-ParH (70 pmol), (28 pmol), and (14 pmol) in which the amount of His-SepF

(45 pmol) remained constant. Furthermore, we investigated whether 1 mM ATP affected the polymerisation state of these proteins as well. In the presence of ATP, His-SepF was incubated with His-ParH in (70 pmol), (28 pmol), and (14 pmol) in which His-SepF had a fixed amount (45 pmol). The incubations were carried out overnight at room temperature in a Tris buffer (50 mM Tris, 150 mM KCl, pH 8.0). After incubation the samples were then analysed using 6% native-PAGE and run for 2 hours at low voltage 100 V. For observing proteins then the gel was visualised by silver staining (Figure 5.9).

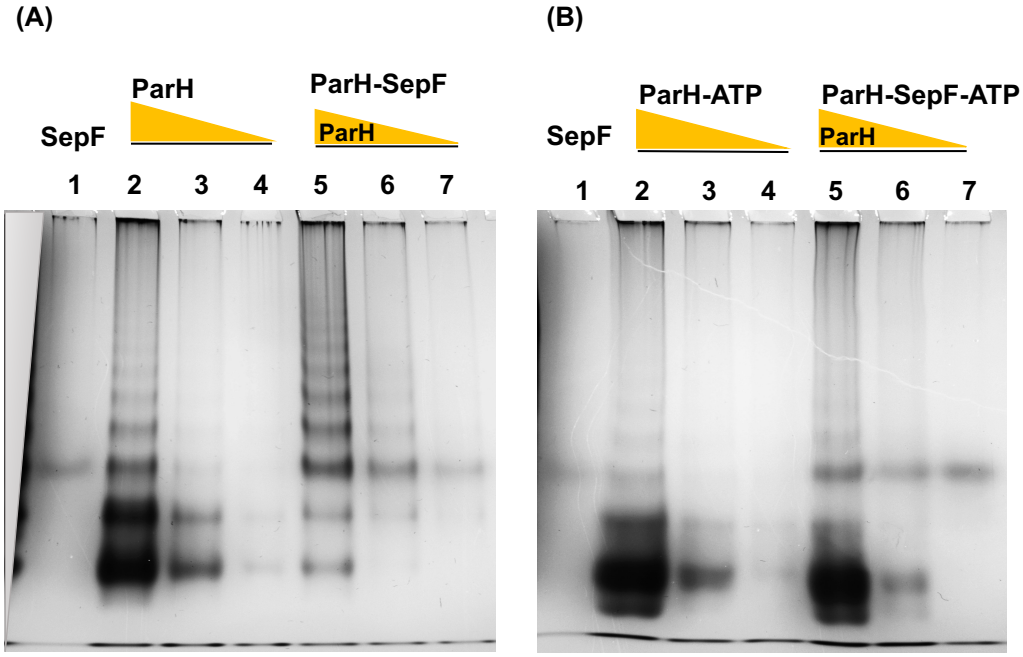

Figure 5.9 FigureNative-PAGE of ParH and SepF

A native-PAGE gel was performed to test the effect of ATP on ParH and SepF. His-ParH and His-SepF were incubated both separately and together in presence and absence ATP and $MgCl_2$ at room temperature overnight before analysis using 6% native-PAGE.

(**A**) In absence of ATP, His-SepF 45 pmol (lane 1) ran as a single band. His-ParH (70 pmol, Lane 2), (28 pmol, Lane 3), and (14 pmol, Lane 4). Increasing volume of His-ParH proteins were incubated with fixed amount of His-SepF (Lanes 5 to 7).

(**B**) In presence of 1 mM ATP and 20 mM $MgCl_2$, His-SepF 45 pmol (lane 1) ran as a single band. His-ParH (70 pmol, Lane 2), (28 pmol, Lane 3), and (14 pmol, Lane 4). Increasing amount of His-ParH proteins were incubated with fixed amount of His-SepF (45 pmol) in presence of 1 mM ATP and 20 mM $MgCl_2$ (Lanes 5 to 7). For observing proteins, the gel visualised by sliver staining.

Interestingly, after incubation overnight, ParH readily polymerised to higher order assemblies in the presence of SepF, suggesting that SepF promotes ParH polymerisation (Figure 5.9). ATP promotes de-polymerisation of ParH, which was independent on the presence or absence of SepF.

5.2.3 Investigating ParH-DNA binding activity using Electrophoretic Mobility Shift Assay

Due to the observation of ParH-DNA interaction through native-PAGE in previous section (Figure 5.4), we aimed to conduct further confirmatory experiment to study the potential that ParH could be a DNA binding protein. In order to achieve this an Electrophoretic mobility shift assay (EMSA) was performed using purified ParH protein and two PCR fragment containing either a DNA fragment carrying the *parH gene* or a random DNA fragment (*dia*) from *S. coelicolor*. To generate PCR DNA, the *parH* gene from the *S. coelicolor* chromosomal DNA was amplified using the primers 'ParH P EgFp *BamHI* FRW' and 'ParH SQcrsp REV', and the *dia* gene from the *S. coelicolor* chromosomal DNA was amplified using the primers. An increasing concentration of ParH was incubated with a fixed amount of each DNA for 20 minutes at room temperature in a Tris buffer (50 mM Tris, 150 mM KCl, pH 8.0). Then, all samples were analysed on a 1% agarose gel made with TAE buffer without the addition of ethidium bromide. After running the gel at 50 V for 2 hours, it was incubated for 1 hour in TAE buffer containing 2 μg/ml ethidium bromide in order to stain the DNA (Figure 5.10).

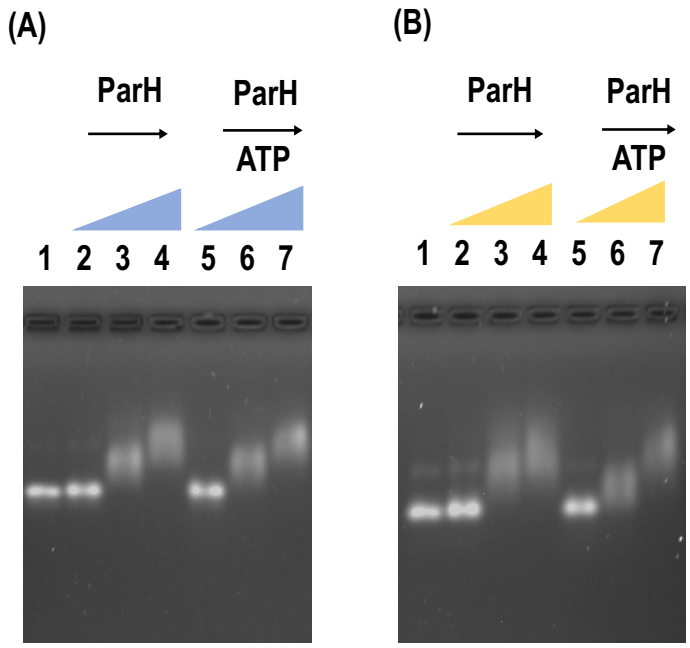

Figure 5.10 Electrophoretic mobility shift assay of ParH and DNA

An electrophoretic mobility shift assay was performed in two PCR fragment DNA from *S. coelicolor* using purified ParH protein. **(A)** PCR fragment *dia*, **(B)** PCR fragment *parH*. Both reactions were incubated at 30°C for 20 minutes. Lane 1 for both reactions A and B only DNA as control and with increasing amounts (lanes 2-7) and added 1 mM ATP and 20 mM $MgCl_2$ for both reaction (lanes 5-7). The amount of ParH protein increased as follows: 140 pmol (Lanes 2 & 5), 700 pmol (Lanes 3 & 6), and 1400 pmol (Lanes 4 & 7) 1400 pmol. Samples were analysed on 1% agarose gel made with TAE buffer without the addition of ethidium bromide. Subsequently, the gel was incubated for 1 hour in TAE buffer involving 2 μg/ml ethidium bromide for the DNA staining.

Observable evidence from this experiment shows that ParH is a DNA binding protein. There is a clear shift in the positions of both DNA fragments, *parH* and *dia*, in the agarose gel after incubation with the His-ParH protein in comparison to the control lane. Interestingly the shift gets higher when the concentration of ParH protein increases with fixed amount of DNA. This suggests that ParH-DNA binding activity appears to be non-specific. Otherwise, the shift would be at a specific position and then not shifted further. The fact that both DNAs generated a shift also suggests that ParH non-specifically binds to any DNA fragment. It is discernible that there were no

differences in the result, either in the presence or absence of ATP and $MgCl_2$, suggesting that they might be not necessary for this interaction.

The most striking observation that emerged from the data was that native-PAGE and EMSA revealed that ATP and $MgCl_2$ were not necessary for ParH-DNA binding activity, but ParH depolymerisation was promoted by ATP and the presence of DNA (Figure 5.4 B and C). We cannot say whether the different oligomers have different affinity to DNA and further investigations are needed to establish the interaction between ParH and DNA.

Next, we aimed to investigate whether the ParH partner protein identified by lab colleagues, Dia could affect the DNA binding activity of His-ParH. To examine this, reactions were set up to indicate a gel shift using the *dia* PCR fragment in the presence of increasing amounts of purified His-Dia as a control, increasing amounts of purified His-ParH, and increasing amounts of purified His-ParH and His-Dia together. The reactions were carried out in the presence of 1 mM ATP and 20 mM $MgCl_2$ and incubated for 20 minutes at room temperature in a Tris buffer (50 mM Tris, 150 mM KCl, pH 8.0). All samples were analysed on 1% agarose gel without the addition of ethidium bromide (native gel) (Figure 5.11).

(A)

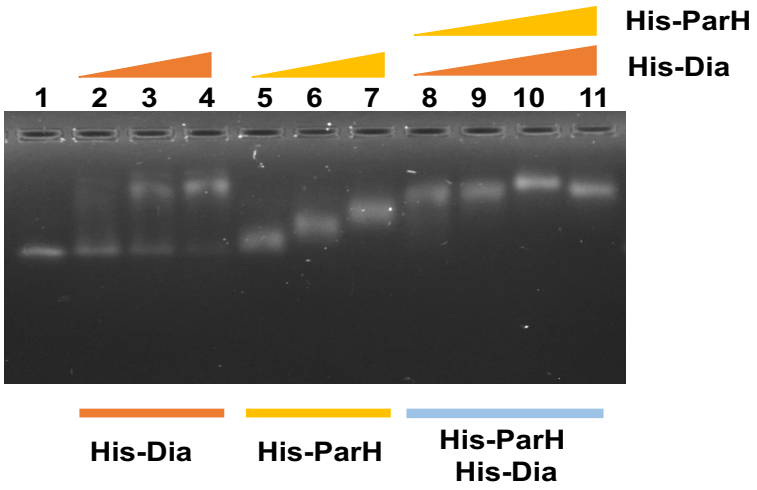

(B)

	1	2	3	4	5	6	7	8	9	10	11
ParH	-	-	-	-	3 µl	5 µl	10 µl	3µl	5 µl	5 µl	10 µl
Dia	-	3 µl	5 µl	10 µl	-	-	-	3 µl	5 µl	10 µl	5 µl
DNA	1µl	1µl	1µl	1µl	1µl	1µl	1µl	1µl	1µl	1µl	1µl

Figure 5.11 Electrophoretic mobility shift assay of His-Dia, His-ParH and DNA

An electrophoretic mobility shift assay was performed in which PCR fragment DNA (*dia*) was incubated for 20 minutes at room temperature both in the absence (Lane 1) with increasing amounts of His-Dia in lanes (2,3,4) and His-ParH in lanes (5,6,7) protein in a Tris buffer (50 mM Tris, 150 mM KCl, pH 8.0) with the addition of 1 mM ATP and 20 mM $MgCl_2$. The amount of protein was increased as follows: His-Dia 81 pmol (Lane 2), 135 pmol (Lane 3), and 270 pmol (Lane 4). His-ParH amount was increased as follows: 420 pmol (Lane 5), 700 pmol (Lane 6) and 1400 pmol (Lane 7). The DNA was also incubated with increasing amounts of His-Dia and His-ParH in lanes (8 to 11). All samples were analysed on 1 % agarose gel made with TAE buffer without the addition of ethidium bromide. The gel was subsequently incubated for 1 hour in TAE buffer involving 2 µg/ml ethidium bromide for the DNA staining.

Surprisingly, in the Figure (5.11) above, an electrophoretic mobility shift assay revealed that His-Dia can also bind DNA since it shows a clear DNA shift in the presence of this protein. Then, this experiment indicated that Dia, a partner protein of ParH did affect the ParH-DNA interaction. The addition of His-Dia to the His-ParH-DNA reaction showed an increase in the observable shift (for example Lanes 2,5 and 8 in Figure 5.11). It is possible that the ParH-Dia interaction forms a larger nucleoprotein complex on the DNA due to the

ParH-Dia interaction, causing a large shift when compared to a complex composed solely of His-ParH protein. However, unlike the ParH-DNA interaction that is non-specific, the Dia-DNA interaction might be specific, because the position of the shift did not change when more Dia was added to the sample. Further investigations are needed to establish how Dia binds to DNA and how the presence of ParH affects this interaction.

5.2.3.1 Electrophoretic Mobility Shift Assay reveals that the coiled-coil protein Dia is a DNA binding protein

In previous observation (Figure 5.11), it is evident from the experiment that Dia is a DNA binding protein. There was a clear shift in the DNA fragment in the gel after incubation with His-Dia protein compared to the control lane. Because of this observation, we decided to perform a further experiment to test the ability of His-Dia to shift different DNA fragments, other than the *dia* gene itself. To achieve this, an electrophoretic mobility shift assay (EMSA) was performed using purified His-Dia protein and different DNA fragments generated by PCR. The *dia* gene from *S. coelicolor* chromosomal DNA was amplified using the primers, the *parH* gene from *S. coelicolor* chromosomal DNA was amplified using the primers 'ParH P EgFp *BamHI* FRW' and 'ParH SQcrsp REV', and the *sepFmcherry* gene from *S. coelicolor* plasmid was amplified using the primers 'SepF2 XbaI BgI FRW' and 'mCherry REV'. All these DNA fragments were used in the lab by other students and here they represented a variety of DNA fragments to test whether Dia was a non-specific DNA binding protein. Increasing concentrations of His-Dia was incubated with a fixed amount of DNA fragments PCR (*dia*, *parH*, *sepFmCherry*). The reactions were incubated with the addition of 1 mM ATP and 20 mM $MgCl_2$ in a Tris buffer (50 mM Tris, 150 mM KCl, pH 8.0) for 20 minutes at room temperature (Figure 5.12).

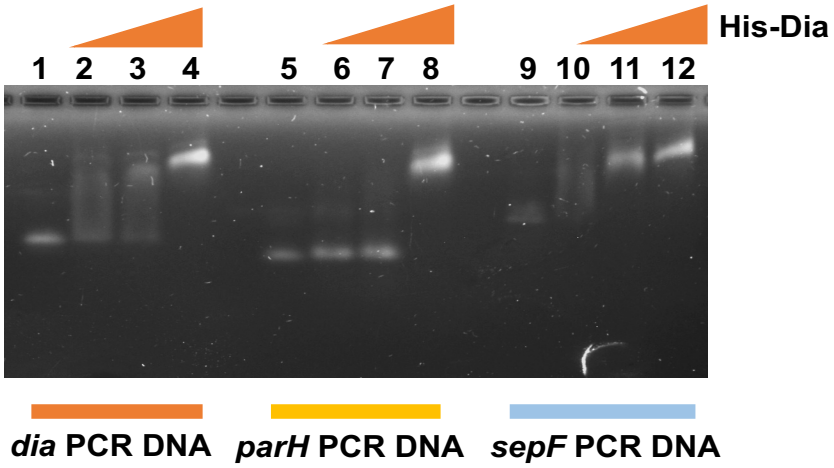

Figure 5.12 Electrophoretic mobility shift assay of His-Dia and DNA

An electrophoretic mobility shift assay was performed in which PCR fragments DNA (*dia*, *parH*, and *sepF*) were incubated separately for 20 minutes at room temperature both in the absence (lane 1) and with increasing amounts of His-Dia protein as follows 81 pmol, 135 pmol, 270 pmol (lanes 2,3,4 – 6,7,8 - 10,11,12) in a Tris buffer (50 mM Tris, 150 mM KCl, pH 8.0) with the addition of 1 mM ATP and 20 mM $MgCl_2$.

A PCR fragment containing the *dia* gene from *S. coelicolor* was incubated with increasing amount of protein as follows: His-Dia 81 pmol, 135 pmol, 270 pmol (Lanes 2,3, and 4). A PCR fragment containing the *parH* gene from *S. coelicolor* was incubated with increasing amount of protein as follows: His-Dia 81 pmol, 135 pmol, 270 pmol (Lanes 6, 7, and 8). A PCR fragment containing the *parH* gene from *S. coelicolor* was incubated with increasing amount of protein as follows: His-Dia 81 pmol, 135 pmol, 270 pmol (Lanes 10, 11, and 12). Lanes 1, 5, and 9 used as control for DNA. All samples were analysed on 1 % agarose gel made with TAE buffer without the addition of ethidium bromide. The gel was subsequently incubated for 1 hour in TAE buffer involving 2 μg/ml ethidium bromide for DNA staining.

All DNA fragments were shifted in the presence of His-Dia. As with two of the DNA fragments only the highest concentration of Dia generated a shift, and with the third DNA the shifts in the last two lanes are very similar (Figure 5.12), it is not possible to establish whether increasing amount of Dia generates a complex with slower mobility. The fact that there was a shift with three different DNA fragments suggest that the DNA binding was not sequence specific. However, the possibility of a well-defined shift suggests that Dia might bind to these DNA fragments with a specific stoichiometry, for example by binding to the DNA ends. Stoichiometry refers to the specific ratio of Dia

protein to DNA molecule in a binding complex. In the other words, Dia protein might bind to the ends of the DNA fragments in a defined and specific ratio, possibly utilizing a binding domain that recognizes the unique properties of DNA ends (a 5' end and a 3' end). This is an exciting possibility and further EMSA experiments using different DNA fragments, will have to address where within the DNA fragment Dia binds.

5.2.4 Possible Phosphorylation of His-ParH

Although the main observation in the presence of ATP was ParH de-polymerisation (Figure 5.3), intriguingly we also observed a new band, just below the monomeric ParH (marked by red arrow, Figure 5.13), might suggest that ATP has additional functions. Initial observations suggest that there may be a link between the bands that appeared below the monomeric ParH and the presence of ATP.

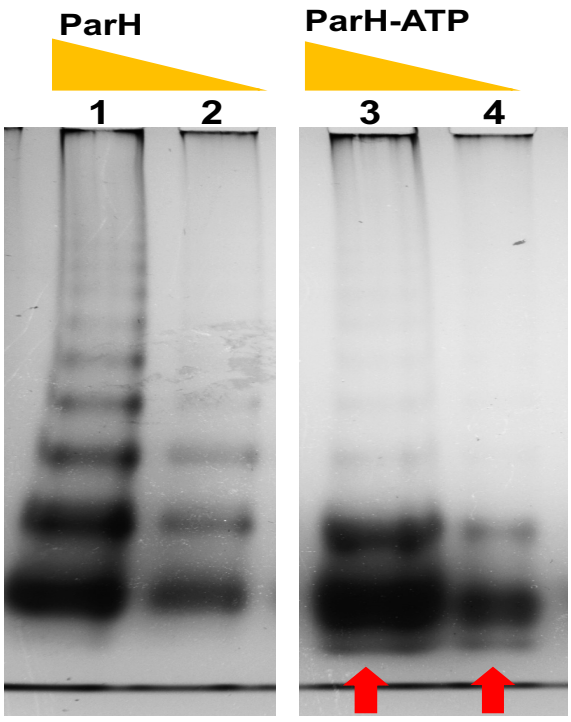

Figure 5.13 His-ParH Native PAGE gel

Lane (1) and Lane (2) represents His-ParH oligomers while Lane (3) and Lane (4) His-ParH in presence of 1mM ATP. The red arrow represents the small bands just below the monomeric ParH.

From the data in Figures 5.7, 5.8, and 5.13, it is apparent that there is a link between the presence of ATP and the appearance of a band just below the monomeric ParH. We decided to examine the protein phosphorylation profile of this additional band by excising it and analysing it (Gerhard Salbach, John Innes Centre).

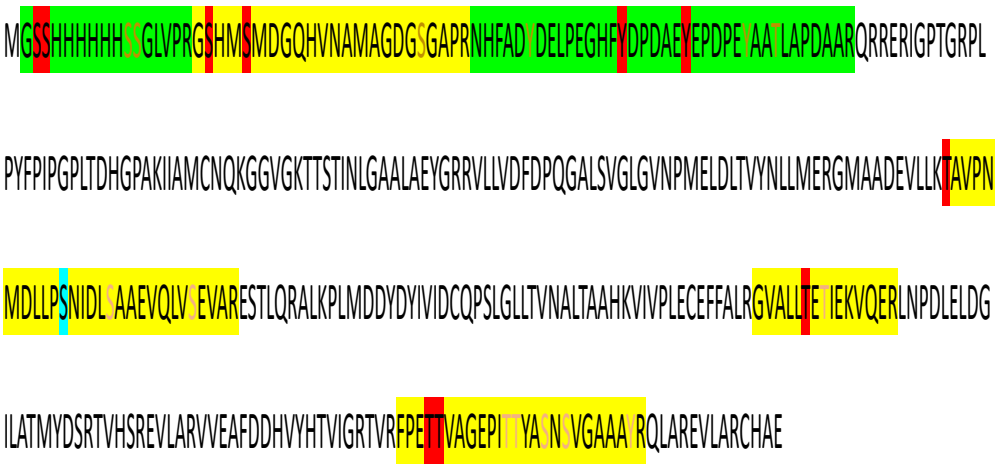

Figure 5.14 Possible phosphorylation of His-ParH

Mass spectrophotometry was performed for analysis of putative phosphorylation sites of His-ParH, using the band below the monomeric form of ParH. The coloured green or yellow stretches show 6 tryptic peptides with potential phosphorylation sites on S/T/Y (red colour). Non-coloured stretches were also covered with identified peptides but do not contain phosphorylated residues.

The data reported here (Figure 5.14) appear to support the assumption that ParH might be phosphorylated in the presence of ATP. As there were several phosphorylated residues found in our preparation, it was important to compare the phosphorylation profile of the band with the lowered mobility with the monomeric ParH. However, we have not been able to complete this, due to lack of time. It will be necessary to carry out further tests to establish whether ParH can auto phosphorylate itself in the presence of ATP.

Given the current preliminary findings, there remains a lack of comprehensive understanding regarding this aspect. Consequently, it becomes imperative to delve into further investigations in order to conclusively ascertain whether ParH undergoes self-phosphorylation or is potentially phosphorylated through ATP. Additional research is needed to shed more light on this matter and establish a clearer perspective.

5.3 Summary

This chapter has demonstrated the investigation of the interactions of His-ParH with partners *in vitro* using the native-PAGE method. First of all, we examined that whether ParH oligomerisation was affected in the presence of ATP. Using native-PAGE we were able to illustrate that ParH assemblies into multiple oligomers. Surprisingly, ATP had an effect on His-ParH oligomerisation through boosting its depolymerisation (Figure 5.3 B). These data are very different from other observations ParA-like proteins, where polymerisation of ParA is promoted by the presence of ATP. In addition, our data revealed that ParH oligomerised in ATP independent manner.

The positive interaction of ParH and Hyp was observed in *vitro* through native-PAGE (Figure 5.5). This interaction occurred only between the higher order oligomerisation of ParH and Hyp. Interaction of ParH and Hyp was independent of ATP, suggesting that the ATP-dependent depolymerisation of ParH might be inhibited in the presence of Hyp.

We then turned to observe interaction between ParH and coiled coil protein Dia (Figure 5.7), ParH and cell division protein SepF (Figure 5.8). We observed positive interaction for both proteins in *vivo* using the bacterial two-hybrid assay (Chapter 3, Figure 3.3, and Figure 3.11). Here, SepF was convincingly promoting ParH polymerisation when the partner proteins were incubated overnight (Figure 5.9). Dia on the other hand, similarly to Hyp, might prevent the depolymerisation of ParH.

Previous studies revealed that the binding of Soj (ParA) to DNA required the presence of ATP to stimulate Soj dimerisation (Graham, 2011). However, our finding through the EMSA technique showed that ParH had affinity for DNA binding which did not require the presence of ATP in the conditions we tested (Figure 5.10 A and B). This suggests that ATP is not essential for the interaction of ParH with DNA. We also confirmed that ParH is a non-specific DNA binding protein.

All the above suggests a complex interplay of proteins promoting either polymerisation of ParH, or the ATP dependent depolymerisation of ParH. We found that the effect of SepF on ParH polymerisation was only clearly observed when incubated overnight. Hence some of the other interaction partners, DNA, Dia or Hyp should be tested again using longer incubation times.

S. coelicolor is one of the bacteria encoding the largest number of eukaryotic type kinases. Most distinct Ser/Thr/Tyr phosphorylation events were detected during the presporulation and sporulation stages (80%) (Manteca *et al.*, 2011). The discovery of a kinase domain in ParH, a ParA-like protein involved in chromosome organisation in *S. coelicolor*, adds complexity to its function. This kinase domain suggests potential roles in phosphorylation, which could impact DNA binding, protein interactions, and cellular dynamics related to chromosome organization. This raises intriguing questions about the mechanism of action of ParH in chromosome organization. Does the kinase domain play a role in modulating ParH interaction with DNA, possibly affecting chromosomal compaction or segregation? Could it be involved in mediating protein-protein interactions, influencing the formation of higher-order assemblies or complexes involved in chromosome organization? Additionally, the source of phosphate for the phosphorylation, whether it's through autophosphorylation or ATP, could have implications for ParH regulatory mechanisms.

To conclude, it's important to acknowledge that there remains a potential scenario where ParH could undergo autophosphorylation when ATP is present.

5.4 Acknowledgment

Protein phosphorylation profile were done by Gerhard Salbach, John Innes Centre, Norwich.

CHAPTER 6

6. Identifying Gene Expression Profile in the *parH* mutant

6.1 Introduction

During chromosome segregation prior to sporulation in *S. coelicolor,* the ParA protein encoded in the *parAB* operon is involved in the regulation of segregation machinery, during which helical filaments of ParA are formed along the length of aerial hyphae in an ATP dependent manner. This contributes to the mechanism to precisely distribute and segregate several dozens of chromosomes, each of which end up in the pre-spore compartments. Elimination of ParA resulted in mis-segregated chromosomes leading to uneven pre-sporulation compartments and being anucleate (Jakimowicz et al., 2007). This also suggests that chromosome segregation affected septum placement. Given that ParH is a ParA-like protein, ParH protein should share similar biochemical properties with ParA proteins (Gillespie, Unpublished 2017).

Furthermore, the recent study in Kelemen lab represented the macroscopic phenotype of *parH* and *hyp* mutants (Gillespie, unpublished 2017). This study revealed that *parH* mutant had a delayed development phenotype compared to the wild type (Figure 6.1).

Figure 6.1 Phenotype of a *parH* null mutant

The wild type M145 and the *parH* mutant were inoculated onto SFM medium. The plates were incubated at 30°C for 5 days. The *parH* mutant is developmentally delayed compared to the wild type, it is delayed in sporulation and is unable to produce the grey pigment related to spore maturation. Taken and modified from Gillespie Unpublished, 2017.

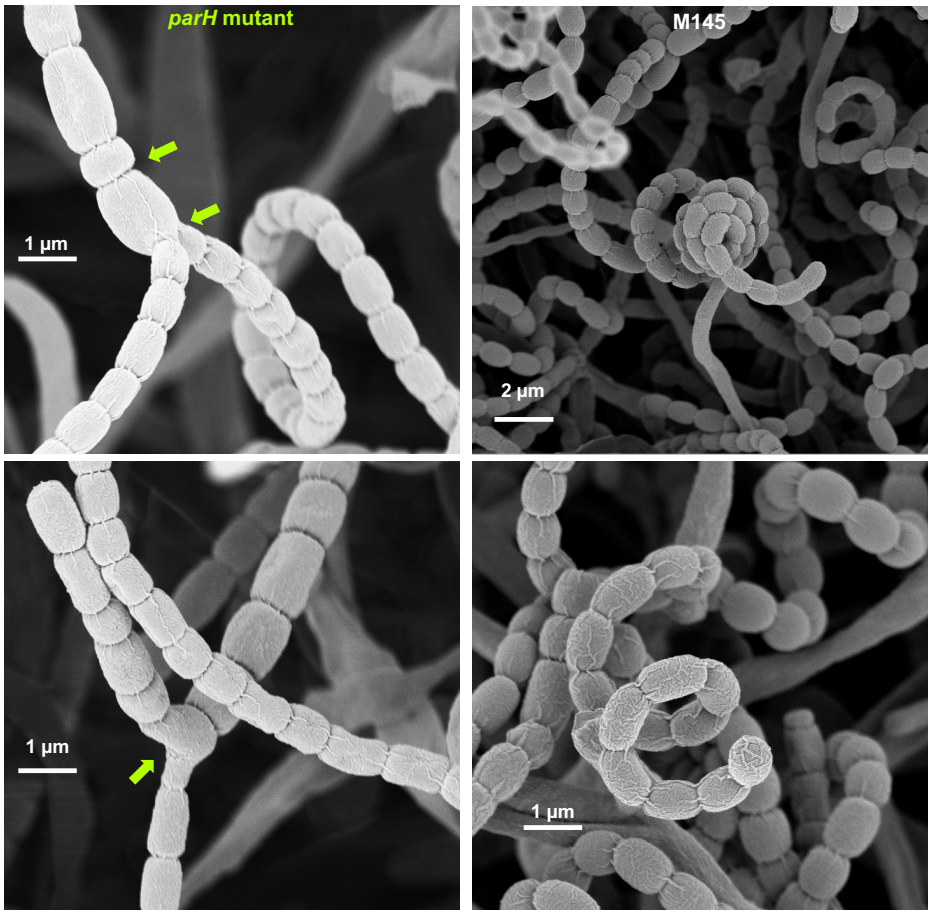

Figure 6.2 Microscopic characterisation of *parH* mutant morphology

Both strains, wild type M145 and the *parH* mutant were grown on SFM medium for 5 days. The arrows indicated uneven spores of *parH* mutant (left).The plates were incubated at 30˚C. Images were taken by Zeiss Gemini 300 scanning electron microscope.

Using scanning electron microscopy, we observed changes in spore development in the *parH* mutant when compared to the wild type M145. Instead of evenly placed septa flanking well segregated chromosomes in the wild type M145, we observe irregular septum placement along hyphal length in the *parH* mutant (Figure 6.2). Moreover, unevenness of spores size in the *parH* mutant suggests that the amount of DNA in each compartment is different, similarly to the *parH* mutant. Unlike in the wild type, where spore chains are unbranched, in the *parH* mutant it was easy to find spore chains that branched (Figure 6.2). As mentioned earlier (Chapter 1), it is only the

vegetative mycelium that undergoes branching and does not occur in aerial hyphae. It is possible that this observation is caused by the interaction between ParH and TIPOC, which can potentially influence TIPOC's actions. Using the bacterial two hybrid assays we demonstrated interaction between ParH and Scy (Chapter 3, Figure 3.11), which is consistent with this.

The knockout phenotype of the *parH* mutant suggests that gene expression profile of this mutant is likely to be different from that of the wild type strain. Apart from its involvement in partitioning, ParH may have indirect effects on gene expression. Regulatory proteins like ParH can interact with other cellular components, including transcription factors or signaling molecules, which might influence gene expression patterns. Additionally, disruption of partitioning processes could potentially lead to alterations in chromosome organisation, affecting the accessibility of certain genes to the transcription machinery and thereby influencing gene expression. Thus the aim of this chapter is identifying the gene expression profile of the wild type M145 and *parH* mutant to investigate the different expression patterns in these two strains.

6.2 Results

6.2.1 ParH knockout affects sporulation

In order to prepare samples for RNA preparations, we grew the wild type and the *parH* mutant strains on SFM medium covered with cellophane, in order to facilitate the collection of all cells at distinct developmental time points. To monitor morphological differentiation, the *parH* mutant strain and wild type strain were plated on cellophaned SFM medium at a density of approximately 10^6 spores/plate each. The plates were incubated at 30°C and the growth was observed over a 96-hour period (Figure 6.3 A, B, and C). In the wild-type, M145, 24 hours of growth generated a matt layer of growth representing vegetative growth, with aerial growth appearing at 40 hours producing a whitish fluffy surface. Observable grey pigment production, indicating

sporulation, started at 48 hours and developed fully at 72 hours in the wild type strain (Figure 6.3 A).

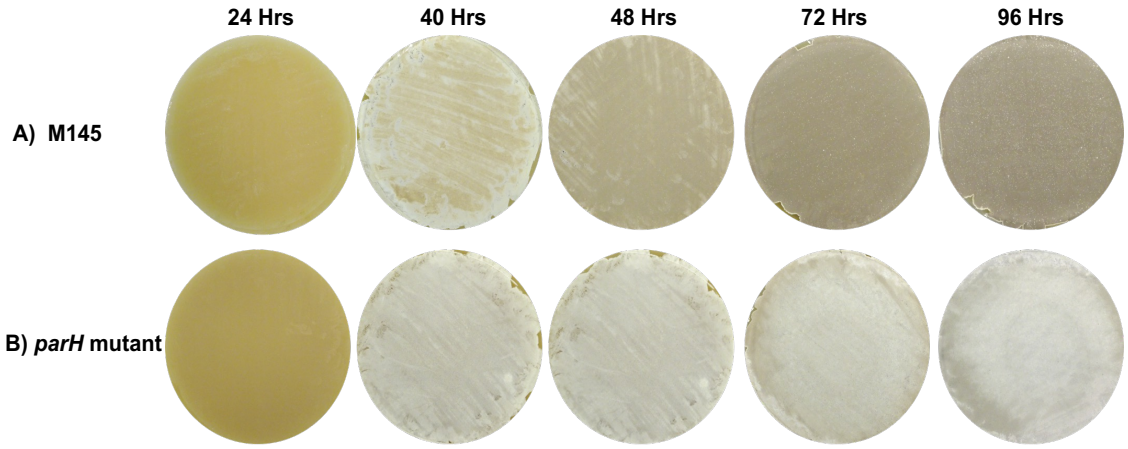

Figure 6.3 Following morphological differentiation during *S. coelicolor* growth

Approximately 10^6 spores of M145 (wild type) and the *parH* mutant strains were plated onto SFM medium. The plates were incubated at 30˚C. the *parH* mutant is developmentally delayed compared to the wild type. While all strains develop vegetative at 24 hours and aerial hyphae at 40 hrs and 48 hrs at the same rate, the *parH* mutant are delayed in sporulation (72 hrs and 96 hrs). As well as at 72 hrs and 96 hrs, the *parH* mutant are also unable to produce the grey pigments related to spore maturation.

However, the *parH* mutant exhibited a developmental delay in morphological differentiation compared to wild type strains, M145, from 48 hours. Compared to wild type strains, *parH* mutant strains develop vegetative and aerial hyphae after 24 and 40 hours of growth, respectively. However, after 48 hours, when the wild type strain turned grey, the *parH* mutant stayed white even at 72 and 96 hours of growth (Figure 6.3 B). The “white” morphology of suggests that the *parH* mutant either does not sporulate or does not generate mature spores. The studies conducted by Gillespie, 2017, a fluorescent microscopy analysis indicated that the *parH* mutant strain had irregular septation and abnormal branching within the aerial hyphae compared

to the wild type strain. In the other words, *parH* affected cell division, during sporulation (Gillespie, Unpublished 2017).

6.2.2 RNA extraction using Trizol

The distinctive morphological differences observed between the wild type and *parH* mutant strains (Figure 6.3, A and B) prompted us to investigate the gene expression profiles in these strains using RNA-Seq. In order to get good quality RNA prepared from our samples first we evaluated the performance of the RNA extraction protocol many times to obtain a high quality of total RNA with minimal DNA contamination. In order to extract high quality RNA from cells, the cellular structure must be disrupted effectively and RNases must be inhibited simultaneously to minimize RNA degradation (Shedlovskiy, Shcherbik and Pestov, 2017). Whilst cell disruption of vegetative hyphae is straightforward, disruption of aerial hyphae and spores are a challenge due to a thickened cell wall at these later developmental stages. Standard kit procedures are not sufficient to break the cell wall of spores and using those will result in incomplete RNA samples. We have tried several methods, and we finally achieved reasonable RNA quality when we disrupt the cells using grinding with glass beads of frozen cells with liquid nitrogen.

Total RNA was prepared at different time points of growth on solid SFM medium from the *parH* mutant strain with the wild type M145 strain for comparison. *S. coelicolor* grown on cellophaned SFM were harvested using a clean (sterilised) medium sized spatula at five different time points 24 hours, 40 hours, 48 hours, 72 hours, and 96 hours after inoculation. Each time point had three independent replicates. As the cell wall of aerial hyphae and spores is difficult to break, RNA extraction requires tedious and labour-intensive steps, such as homogenising cells with glass beads. Therefore, all cells were moved into a sterile tube containing ~ 100 µl washed glass beads and 500 µl Trizol reagent. Then, all tubes were kept in liquid nitrogen/ dry ice environment as much as possible to not allow gene expression to change in response to environmental changes and to prevent RNA degradation. In a liquid nitrogen environment, the cells were grinded in a screw-top Eppendorf using a conical pestle similar to that of standard Eppendorf. To further homogenise cells, all

tubes were moved to the cell lyser fastprep machine and two 30-second bursts were applied at 7.5 m/s with a rest time of 5 minutes between bursts using FastPrep^{R} -24 Tissue and Cell Homogeniser (MP Biomedical). Further Trizol reagent (500 µl), SDS (1%) were added to each sample followed by 1 minute vortex and incubation at 65°C for 10 minutes. When all samples were cooled, 200 µl of chloroform was added to each sample and vortexed for 30 sec, then all tubes were incubated for 5 minutes at room temperature. After that, the samples were centrifuged at maximum speed for 15 minutes at room temperature. After centrifugation, three phases were developed, the bottom, organics phase contains proteins, the interphase contains DNA and the top layer contains RNA. Accordingly, the clear top phase was transferred into a new tube, and further phenol and chloroform extraction were performed. Finally RNA was precipitated using isopropyl overnight at -20°C.

Then, all samples were centrifuged at room temperature for 15 minutes, and the white pellet was formed, indicating RNA. After removing the supernatant, 700 µl of cooled 80% Ethanol were added to all tubes, and briefly vortex. To remove all Ethanol, the samples were centrifuged at maximum speed for 5 minutes. Previous RNA isolation attempts indicated that although the Trizol reagent supposed to eliminate DNA in the interphase during extraction, we still had lots of DNA contamination in the samples. To eliminate DNA we performed selective RNA precipitation using 4M NaOAc. Therefore, 1.5 to 2 ml of water was added to each RNA pellet and incubated for 10 minutes at 50°C to confirm that all RNA has dissolved. To the dissolved samples 3X volume of 4 M NaOAc was added and RNA was precipitated by incubation at -20°C and collected by centrifugation. After removal of the supernatant, the RNA pellet was washed using 80% ethanol and finally RNA was dissolved in 300 µl specially clean water.

6.2.3 Agarose Gel Electrophoresis

The high integrity of the RNA was impeded by the difficulties of extracting total RNA. Therefore, several modifications were made to optimise the RNA extraction procedure and obtain a good resolution on agarose gel. One of these modifications was the addition of formamide in order to stabilise RNA

during electrophoresis. RNA could be effectively protected from degradation by RNases during electrophoresis by storing it in formamide (Chomczynski, 1992). The samples for the loading of the agarose gel were prepared (5 µl RNA sample, 2 µl loading dye (10x), 6 µl formamide), then incubated at 75°C for 10 minutes. All samples were loaded into 1% agarose gel and ran for 1 to 2 hours at 50 V (Figure 6.4 and Figure 6.5)

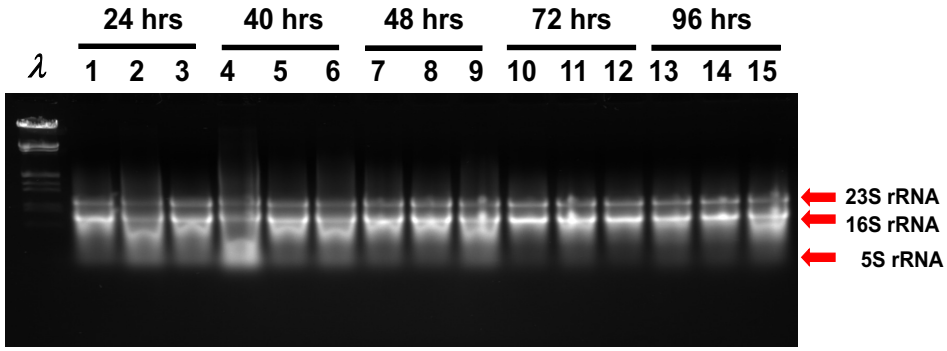

Figure 6.4 Agarose gel of RNA from the wild type of *S. coelicolor* M145

RNA samples isolated from *S.coelicolor* wild type M145 at five time points electrophoresed on a 1% agarose gel before DNA treatment. M145 was grown on cellophaned SFM plates which incubated at 30° C. Lanes 1,2 & 3 performed the harvesting after 24 hours of incubation. Lanes 4,5, & 6 performed the harvesting after 40 hours. Lanes 7,8 &9 performed the harvesting after 48 hours. Lane 10,11 & 12 performed the harvesting after 72 hours. Lanes 13, 14, and 15 performed the harvesting after 96 hours of growth.

The first set of data (Figure 6.4) represents the wild type M145 RNA samples from *S. coelicolor* at five different time points of growth 24, 40, 48, 72, and 96 hours. For each time point, three independent replicates were generated to exclude experimental errors. We expected to find three bands on the agarose gel, each corresponding to one subunit of rRNA, 23S, 16S, and 5S rRNA.

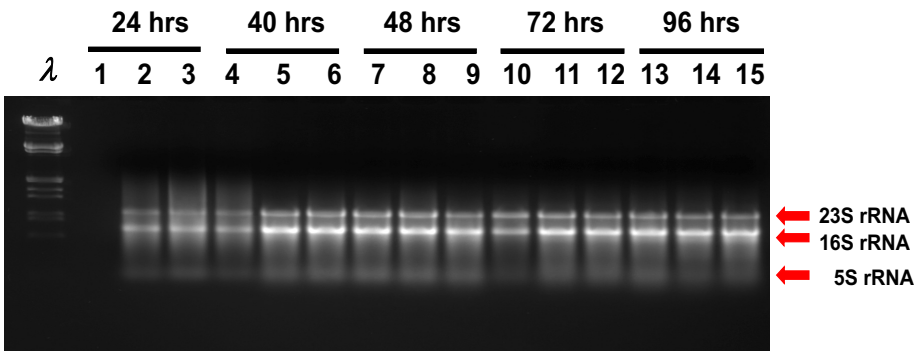

Figure 6.5 Agarose gel of RNA from the *parH* mutant

RNA samples isolated from *S.coelicolor parH* mutant at five time points electrophoresed on a 1% agarose gel before DNA treatment. *parH* mutant was grown on cellophaned SFM plates which incubated at 30° C. Lanes 1,2 & 3 performed the harvesting after 24 hours of incubation. Lanes 4,5, & 6 performed the harvesting after 40 hours. Lanes 7,8 &9 performed the harvesting after 48 hours. Lane 10,11 & 12 performed the harvesting after 72 hours. Lanes 13, 14, and 15 performed the harvesting after 96 hours of growth.

Performing an RNA gel electrophoresis is one of the most affordable and quickest methods to verify the RNA quality, but not enough evidence for RNA integrity. From the gel it is clearly seen the 23S and 16S RNA bands which initially indicated acceptable quality RNA. There was some high molecular wight smear in some of the samples (Figure 6.5) indicating the presence of residual DNA in some of the samples.

6.2.4 Removal of DNA contaminating by DNase

In order to obtain high quality and purity of total RNA, all samples were treated further to minimise genomic DNA contamination. To achieve this we used a TURBO DNA-free kit (Invitrogen). After the DNase treatment the RNA samples (3 µl) were analysed again using agarose gel electrophoresis (Figure 6.6 and Figure 6.7).

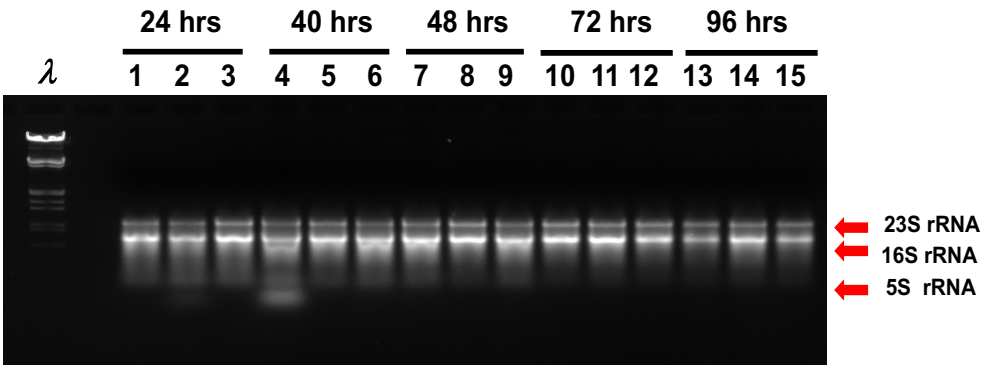

Figure 6.6 Agarose gel of DNAsed RNA from the wild type of *S. coelicolor* M145

RNA samples isolated from wild type of *S. coelicolor* M145 at five time points electrophoresed on a 1% agarose gel after DNase treatment. M145 was grown on cellophaned SFM plates which incubated at 30° C. Lanes 1,2 & 3 performed the harvesting after 24 hours of incubation. Lanes 4,5, & 6 performed the harvesting after 40 hours. Lanes 7,8 &9 performed the harvesting after 48 hours. Lane 10,11 & 12 performed the harvesting after 72 hours. Lanes 13, 14, and 15 performed the harvesting after 96 hours of growth.

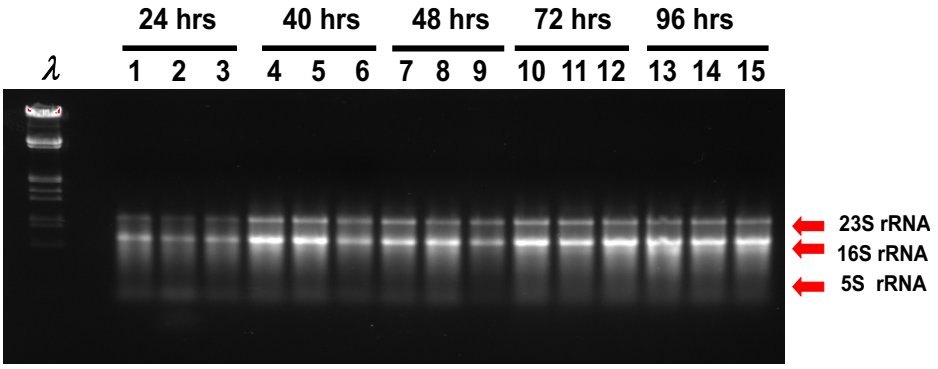

Figure 6.7 Agarose gel of DNAsed RNA *parH* mutant

RNA samples isolated from *parH* mutant at five time points electrophoresed on a 1% agarose gel after DNA treatment. *parH* mutant was grown on cellophaned SFM plates which incubated at 30° C. Lanes 1,2 & 3 performed the harvesting after 24 hours of incubation. Lanes 4,5, & 6 performed the harvesting after 40 hours. Lanes 7,8 &9 performed the harvesting after 48 hours. Lane 10,11 & 12 performed the harvesting after 72 hours. Lanes 13, 14, and 15 performed the harvesting after 96 hours of growth.

The final DNase treatment did remove the DNA contamination of the samples, but in some cases we observed some degree of RNA degradation. Namely, if there is no RNA degradation, the 23S , 16S and 5S rRNA are generated in equimolar quantities, which due to staining with ethidium bromide, should generate more intense 23S bands, compared to the 16S bands. However, we often found that the 16S rRNA bands were more intense, which might indicate some degree of RNA degradation. We have repeated the RNA preparations but we could never completely eliminate some level of RNA degradation. Also, we collect all samples by scraping all cell material from the surface of cellophane and we cannot rule out that the collected samples contain dead cells where RNA degradation might be a natural process (Manteca *et al.*, 2007).

6.2.5 Determination of RNA integrity

The RNA quality should be sufficiently high to generate a library for sequencing, to ensure a successful RNA-Seq experiment. Therefore, an Agilent bioanalyzer was used to measure the quality of the RNA, which shows that the RNA integrity number (RIN) ranges from 1 to 10, with 10 being the highest quality samples representing low degradation and contamination (Kukurba and Montgomery, 2015). The integrity of RNA samples of this study was determined by Novogene lab. The Novogene Lab were run in an Agilent 5400 Bioanalyzer following the manufacturer's instructions (Table 6.1).

Table 6.1 Quality control of RNA samples of the wild type M145 and *parH* mutant
This table represents the integrity values (RIN) of M145 and *parH* mutant, for each time point three independent replicates.

Sample	*S. coelicolor*	Time point of growth	Concentration (ng/ul)	Integrity value RIN
1	M145		1100	7.2
2	M145	24 hours	1050	6
3	M145		870	6.80
4	M145		1180	6.90
5	M145	40 hours	1140	7.20
6	M145		2140	7
7	M145		1230	7
8	M145	48 hours	1233	7.90
9	M145		1060	7.10
10	M145		698	7.60
11	M145	72 hours	830	7.6
12	M145		1060	7.7
13	M145		976	6.7
14	M145	96 hours	917	7
15	M145		540	6.4
16	*parH mutant*		335	6.30
17	*parH mutant*	24 hours	525	5.70
18	*parH mutant*		545	6.00
19	*parH mutant*		1106	6.80
20	*parH mutant*	40 hours	1067	7.30
21	*parH mutant*		1059	7.00
22	*parH mutant*		920	7.50
23	*parH mutant*	48 hours	971	6.10
24	*parH mutant*		541	7.50
25	*parH mutant*		976	6.70
26	*parH mutant*	72 hours	1061	7.20
27	*parH mutant*		1004	6.50
28	*parH mutant*		1079	6.00
29	*parH mutant*	96 hours	1108	6.40
30	*parH mutant*		1110	6.20

6.2.6 Next-generation sequencing (RNA-Seq)

We analysed total RNA harvested from *S. coelicolor*, the wild type M145 and *parH* mutant, were grown on cellophaned SFM medium for 24 hours, 40 hours, 48 hours, 72 hours, and 96 hours. The typical RNA-Seq procedure begins with isolation of RNA, conversion to complementary DNA (cDNA), preparation of libraries, and sequencing with an NGS system (Kukurba and Montgomery, 2015). RNA samples were sequenced by Novogene lab.

6.2.6.1 Library Preparation and Sequencing

From the RNA samples to the final data, each step, including sample test, library preparation, and sequencing, influences the quality of the data, and data quality directly impacts the analysis results. To guarantee the reliability of the data, quality control (QC) is performed at each step of the procedure (Figure 6.8).

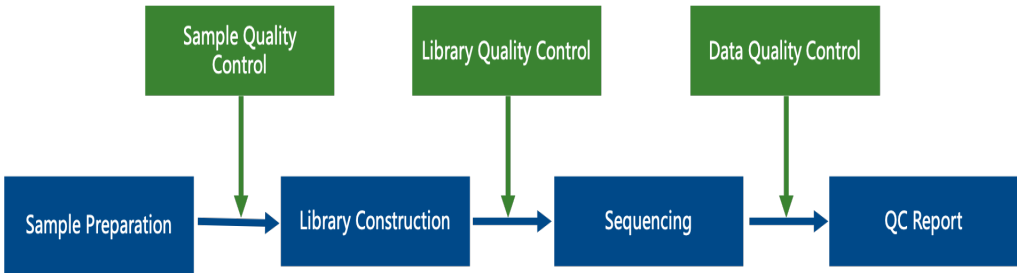

Figure 6.8 An overview of processing sample quality

6.2.6.2 Library Construction, Quality Control and Sequencing

Following is the workflow of library construction (Figure 6.9):

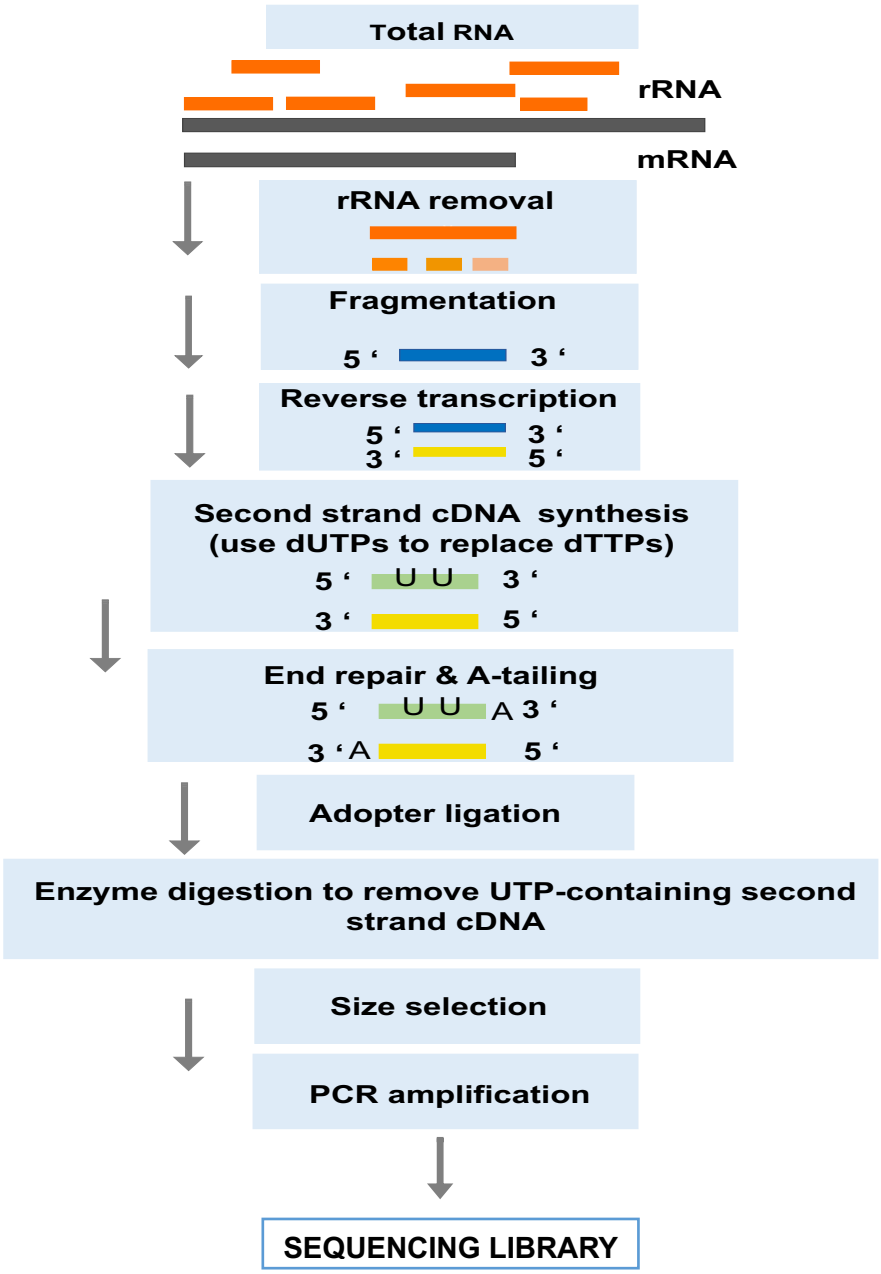

Figure 6.9 The sequencing library construction process for RNA-Seq (Novogene, 2023)

Firstly, ribosomal RNA was removed from total RNA, followed by ethanol precipitation. After fragmentation, the first strand cDNA was synthesized using random hexamer primers. During the second strand cDNA synthesis, dUTPs were replaced with dTTPs in the reaction buffer. The directional library was ready after end repair, adapter ligation, size selection, USER enzyme digestion, amplification, and purification (Novogene,2023) (Figure 6.9).

6.2.6.3 Results of Raw Data

The sequenced reads (raw reads) often contain low quality reads and adapters, which will affect the analysis quality. Thus, it's necessary to trim and filter the raw reads to obtain the clean reads. The filtering process is as follows:
1- Remove reads containing adapters.

2- Remove reads containing N > 10% (N represents the base cannot be determined).

3- Remove reads containing low quality.

The sequenced reads results were represented in (Figure 6.12, and Figure 6.13) after filtration to achieve the clean read. The numbers RNA-1 to RNA-15 represent the RNA of the wild type M145 at five distinct times of growth, where each time point had three independent replicates. Therefore, (RNA_1 to RNA_3) for 24 hours, (RNA_4 to RNA_6) for 40 hours, (RNA_7 to RNA_9) for 48 hours, (RNA_10 to RNA_12) for 72 hours, and (RNA_13 to RNA_15) for 96 hours (Figure 6.10). While the numbers RNA-16 to RNA-30 represent the RNA of *parH* mutant at five time points of growth, where each time point had three independent replicates. Therefore, (RNA_16 to RNA_18) for 24 hours, (RNA_19 to RNA_21) for 40 hours, (RNA_22 to RNA_24) for 48 hours, (RNA_25 to RNA_27) for 72 hours, and (RNA_28 to RNA_30) for 96 hours (Figure 6.11).

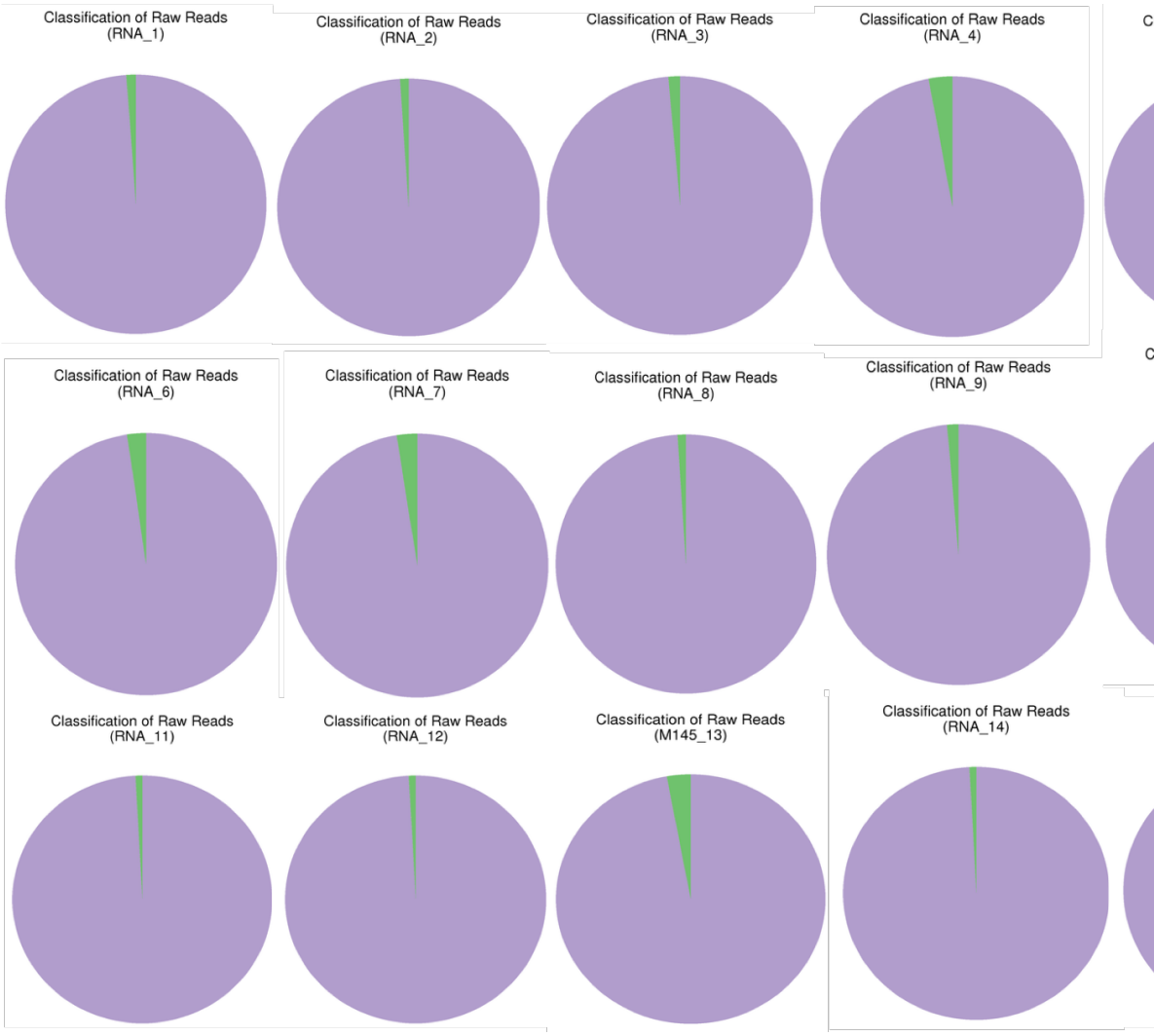

Figure 6.10 Sequencing and composition raw data of M145 RNA.

The purple colours represent the clean reads: (clean reads) / (total raw rea
show the adapters related (Novogene).

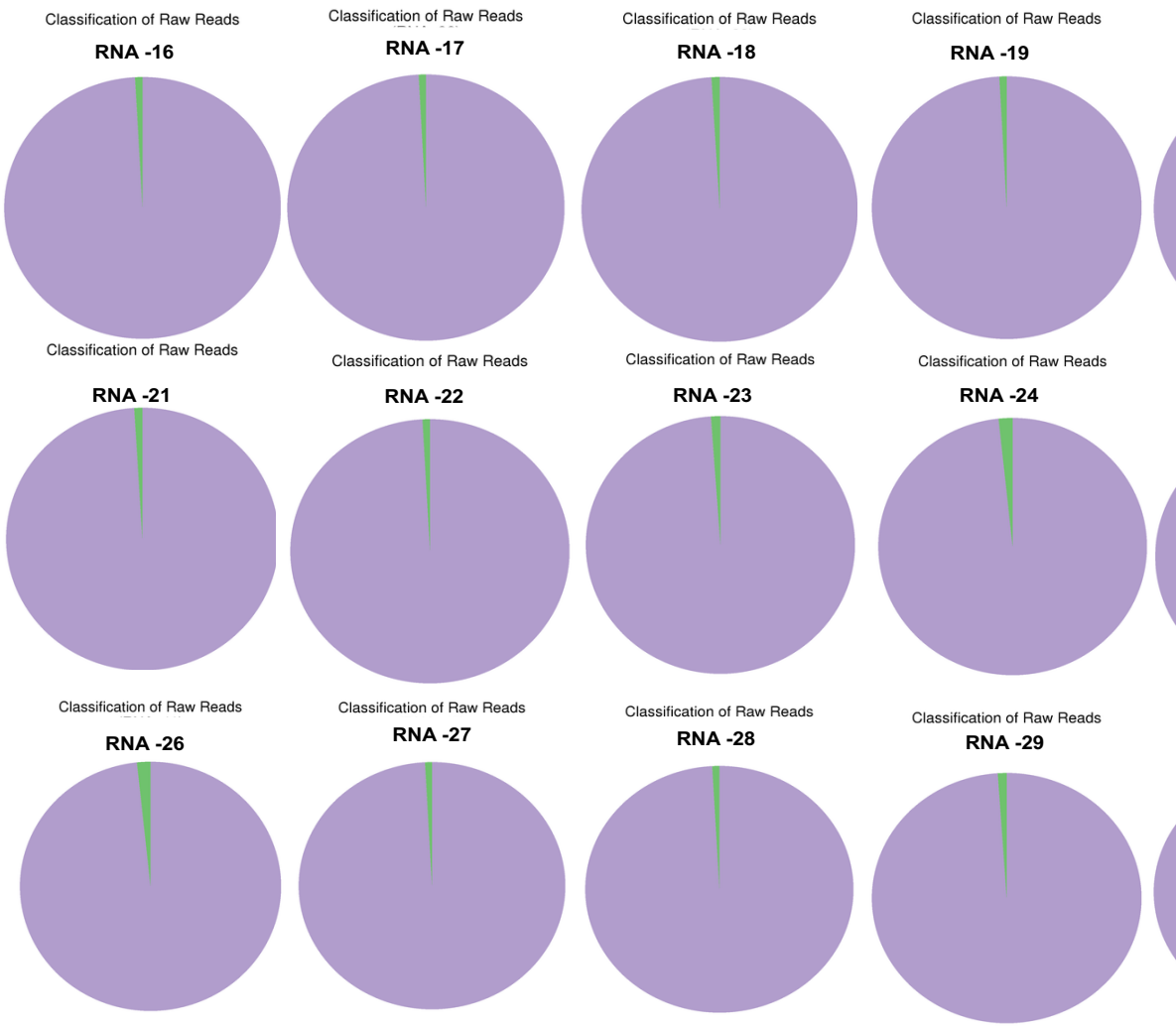

Figure 6.11 Sequencing and composition raw data of *parH* mutant

The purple colour represents the clean reads: (clean reads) / (total raw r
show the adapters related (Novogene).

6.2.7 Bioinformatic (RNA-Seq) analysis

The comparison of gene expression levels was undertaken by comparing levels of expression between the wild type M145 and *parH* mutant across each five time points 24 hours, 40 hours, 48 hours, 72 hours, and 96 hours. We have chosen the time points which corresponds with vegetative growth (24 hours), aerial mycelium formation (40 hours), and sporulation (from 48 hours). Moreover, for RNA-Seq data analysis the edgeR tool was applied. A total of 7848 transcripts were identified in this study, corresponding to the 7848 genes identified when the genome sequence was annotated (Bentley et at., 2002). This chapter summarizes and discusses those the results, which support some observations stated in the previous chapters. An overall, large scale analysis of the RNA-Seq data was not possible due to late arrival of the RNA-Seq data from Novogene. The result from edgeR is summarised in (Table 6.2, Table 6.3, Table 6.4, Table 6.5, Table 6.6, and Table 6.7).

The comparison of the wildtype M145 and *parH* mutant strains was carried out using RNA sequencing analysis, and the findings were analysed based on the following:

- The use of a heatmap to show the differences between the upregulated and downregulated genes based on the computational LogFold calculations.
- For upregulated genes, the LogFC value was found to be greater than 1. Moreover, the P-value was found to be less than 0.05, indicating significance. Additionally, the False Discovery Rate (FDR) was analysed, as the FDR provides a more detailed analysis of the p-value.
- For downregulated genes, the LogFC value was found to be less than -1. Moreover, the P-value was found to be less than 0.05, indicating significance. In addition, the False Discovery Rate (FDR) was analysed, as the FDR provides a more detailed analysis of the p-value.

Nevertheless, based on the heatmap the coloured keys show the following:

- The green boxes indicate that the expression level of the particular gene was higher in the *parH* mutant than in the wild type M145.

- The red boxes indicate higher expression levels in the wild type M145 and decreased expression in the *parH* mutant.

6.2.7.1 Identification of cell division gene expression level in *parH* mutant strain

The heat map (Table 6.2) indicates the expression level of the cell division proteins, SepF and FtsZ, across the representative five time points of growth.

Table 6.2 Transcriptome dynamic of SepF and FtsZ at different time point of growth. The table represents the expression pattern of cell division proteins in *parH* mutant.

Geneid	Length	Product	24 hrs	40 hrs	48 hrs	72 hrs	96 hrs
SCO2079	642	cell division protein	0.44906	-0.220281	-0.017441	-0.213014	-0.344126
SCO2082	1200	cell division protein	-0.155124	-0.649912	-0.133868	-0.346764	-0.327092

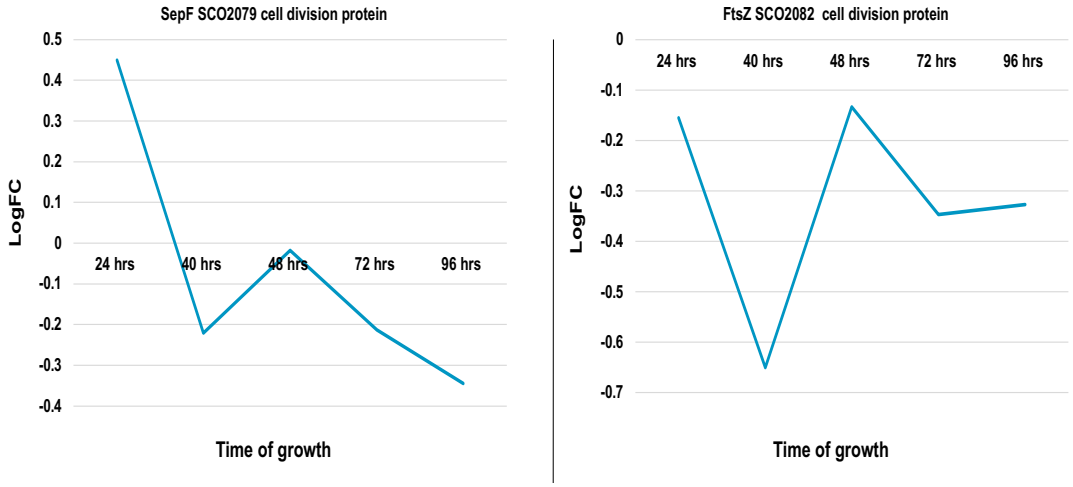

Figure 6.12 Expression level of SepF and FtsZ in the *parH* mutant across five times of growth

SepF (SCO2079) and FtsZ (SCO2082) expression was compared between the wild type and the *parH* mutant. The y axis represents $\log_2$[raw reads in *parH*/raw read in M145] at any given time point (graphs at the bottom).

The cell division protein SepF (SCO2079) showed higher expression levels at 24 hrs in the *parH* mutant compared to the wild type M145 strain (Figure 6.12). However, in the second time point when FtsZ expression is

upregulated in the wild type strain, SepF levels drop in the *parH* mutant, suggesting a lack of upregulation of SepF at the time when cells prepare for sporulation septation. This might be consistent with the delay of sporulation in the *parH* mutant. Similarly, the FtsZ protein (SCO2082) had the reduction in the expression at the second time of growth (40 hrs) in *parH* mutant strain, while had increased expression in the M145 at the similar time of growth, 40 hrs. Again, this is consistent with delayed sporulation in the *parH* mutant.

6.2.7.2 The dynamic transcriptome of antibiotic actinorhodin gene in *parH* mutant

In *S. coelicolor,* several hundred secondary metabolic genes are encoded*,* which are involved in the synthesis of a wide variety of antibiotics (Jeong *et al.*, 2016). Thus, in this chapter the dynamic of expression of the different transcripts of genes for production of the antibiotic actinorhodin were compared between the *parH* mutant and the wild type M145 (Table 6.3, Figure 6.13). The results of this investigation show that the majority of actinorhodin genes were upregulated in *parH* mutant at 96 hrs of growth. Interestingly, Gillespie (2017) investigated the macroscopic phenotype of the *parH* mutant on SFM medium, which indicated that after 4 days of growth *parH* lacked the grey spore pigments, but it exhibited the strong blue colour of the antibiotic actinorhodin (Figure 6.14 B).

Table 6.3 Transcriptome dynamic of actinorhodin production at five different time points. All actinorhodin production genes are clustered from SCO5071 to SCO5092. The values in the table represent log_2[raw reads in parH/raw read in M145] at any given time point.

Geneid	Length	Product	24 hrs	40 hrs	48 hrs	72 hrs	96 hrs
SCO5071	441	hydroxylacyl-CoA dehydrogenase	-2.421286	-0.569535	-0.465834	1.219903	4.412728
SCO5072	924	hydroxylacyl-CoA dehydrogenase	-2.227851	1.560232	0.880913	1.108262	4.330665
SCO5073	990	putative oxidoreductase	-0.35793	0.333348	0.673505	0.576568	3.880704
SCO5074	645	putative dehydratase	-1.902331	1.267087	0.702744	0.935912	4.656746
SCO5075	921	putative oxidoreductase	-1.452257	1.396144	0.710773	1.421363	4.511502
SCO5076	1602	integral membrane protein	0.29515	0.48516	0.239588	-0.347702	0.571469
SCO5077	396	hypothetical protein	0.375867	0.590943	0.673359	-0.071614	0.987193
SCO5078	846	hypothetical protein	0.515549	0.253102	0.271668	-0.29461	2.110622
SCO5079	885	conserved hypothetical protein	-0.285717	0.753352	0.80018	0.452331	4.061336
SCO5080	1146	putative hydrolase	-0.375714	0.465976	0.535722	0.23524	3.896465
SCO5081	342	hypothetical protein	0.137244	0.002689	0.202764	-0.35054	2.370415
SCO5082	780	putative transcriptional regulatory protein	0.517227	-0.278283	-0.252084	-0.417814	1.066516
SCO5083	1737	putative actinorhodin transporter	-0.244264	0.018876	0.143727	0.392884	4.303949
SCO5084	2136	putative membrane protein	-0.226858	-0.012463	0.151334	0.572407	4.550583
SCO5085	768	actinorhodin cluster activator protein	0.219985	1.038639	0.938489	0.784172	1.844968
SCO5086	786	ketoacyl reductase	-1.614226	0.049512	0.064539	0.413804	4.315209
SCO5087	1404	actinorhodin polyketide beta-ketoacyl synthase alpha subunit	-1.105381	-0.100883	0.717912	0.309674	3.964441
SCO5088	1224	actinorhodin polyketide beta-ketoacyl synthase beta subunit	0.107166	-0.011963	0.737461	-0.02754	4.58537
SCO5089	261	actinorhodin polyketide synthase acyl carrier protein	-0.507109	0.261593	0.544656	-0.544038	4.895743
SCO5090	951	actinorhodin polyketide synthase bifunctional cyclase/dehydratase	-0.66269	-0.978599	0.50169	-0.464519	4.319801
SCO5091	894	cyclase	-0.177419	-0.293849	-0.129226	-0.210961	3.502649
SCO5092	534	actinorhodin polyketide putative dimerase	-0.415332	-0.247249	-0.198123	0.476876	3.275188

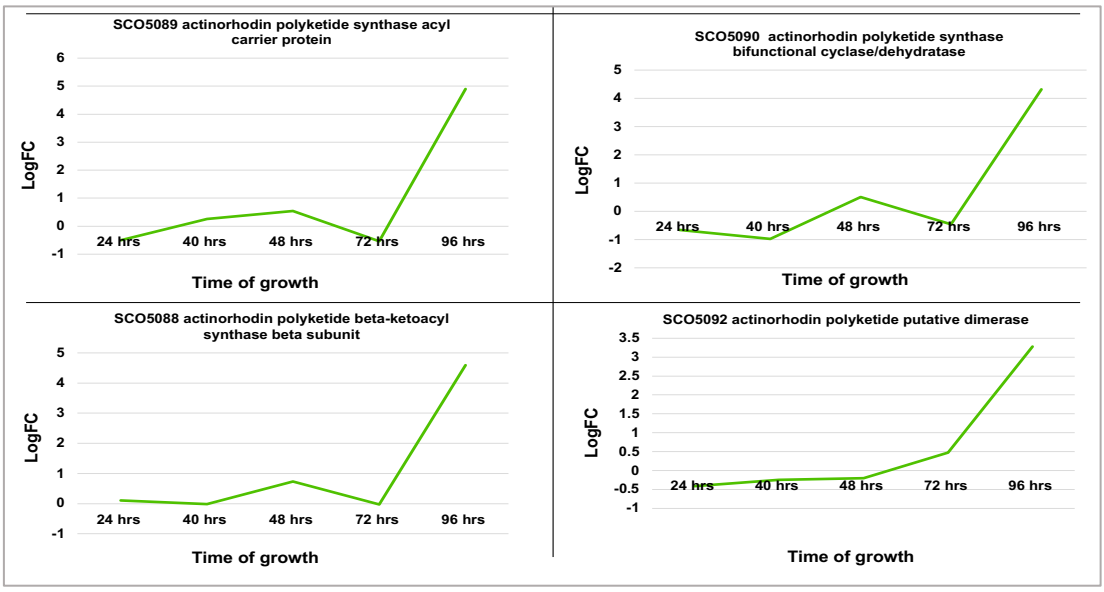

Figure 6.13 Expression level of antibiotic actinorhodin across representative times of growth in *parH* mutant.

The y axis represents $\log_2$[raw reads in parH/raw read in M145] at any given time point. Actinorhodin genes show increased level of expression after 96 hrs of growth in *parH* mutant compared to the wild type M145.

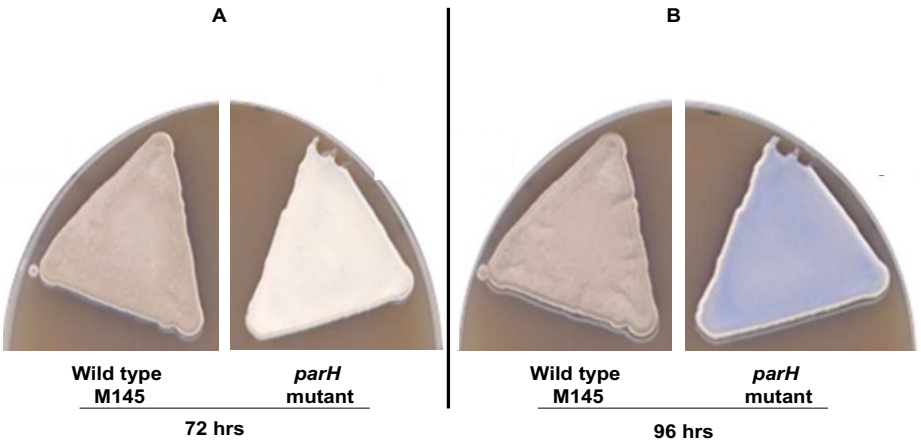

Figure 6.14 Morphological analysis of *parH* mutant strain.

Approximately 10^6 spores of the wild type M145 and the *parH* mutant strains were plated in a triangle patch on SFM medium. The plates were incubated at 30° C and images were taken at 72 hrs (A) & 96 hours (B) of growth. Taken and modified from Gillespie, Unpublished 2017.

This previous observation (Figure 6.15) is clearly supported by the current findings of RNA-Seq. The SFM medium used in this study is not particularly optimal for antibiotic production, but in the *parH* mutant actinorhodin production is de-regulated and there is an upregulation of actinorhodin production at late stages, after 96 hrs growth.

Next, we investigated the expression of the *whiE* genes by analysing the RNA-Seq data. The *whiE* gene cluster encodes the enzymes responsible for synthesizing grey sporulation pigments in *S. coelicolor* (Chater, 1972). When investigating the *parH* mutant phenotype we found that it stayed white even after 3 days growth (Figure 6.3 B and Figure 6.14 A), the time when the wild type strain acquired the dark grey colour due to sporulation and the production of the dark grey spore pigment by the enzymes encoded in the *whiE* gene cluster. This is consistent with the RNA-Seq data analysis (Table 6.4 and Figure 6.15) indicates that at 40 hrs of growth the expression of the *whiE* gene cluster was downregulated.

Table 6.4 Transcriptome dynamic of the expression of the *whiE* gene cluster at five time points of growth. The *whiE* genes are spanning from SCO5314 to SCO55322 The values in the table represent $\log_2$[raw reads in parH/raw read in M145] at any given time point.

Geneid	Length	Product	24 hrs	40 hrs	48 hrs	72 hrs	96 hrs
SCO5314	336	whiE protein VII	0.66256213	-5.067106	-1.5850844	-2.3414159	-1.2117338
SCO5315	480	polyketide cyclase	0.55930041	-5.0077666	-1.5785852	-2.240402	-1.1902219
SCO5316	273	acyl carrier protein	0.82733124	-4.8289158	-1.5345814	-2.1652723	-1.1210045
SCO5317	1275	polyketide beta-ketoacyl synthase beta	0.41566744	-5.1658888	-1.6533353	-2.2551368	-0.9973248
SCO5318	1272	polyketide beta-ketoacyl synthase alpha	0.55535035	-4.5612364	-1.3626318	-2.1805243	-1.0737521
SCO5319	474	whiE protein II	-0.0553242	-4.6527042	-1.3905517	-1.9537885	-1.0494621
SCO5320	1194	whiE protein I	1.04039885	-4.6984416	-1.5723363	-2.1425985	-1.2044178
SCO5321	1884	polyketide hydroxylase	0.64712419	-3.8262218	-1.0840804	-1.7620655	-1.3104843
SCO5322	870	conserved hypothetical protein	0.41934432	-1.6295672	-0.9678969	-0.5733314	-0.7664127

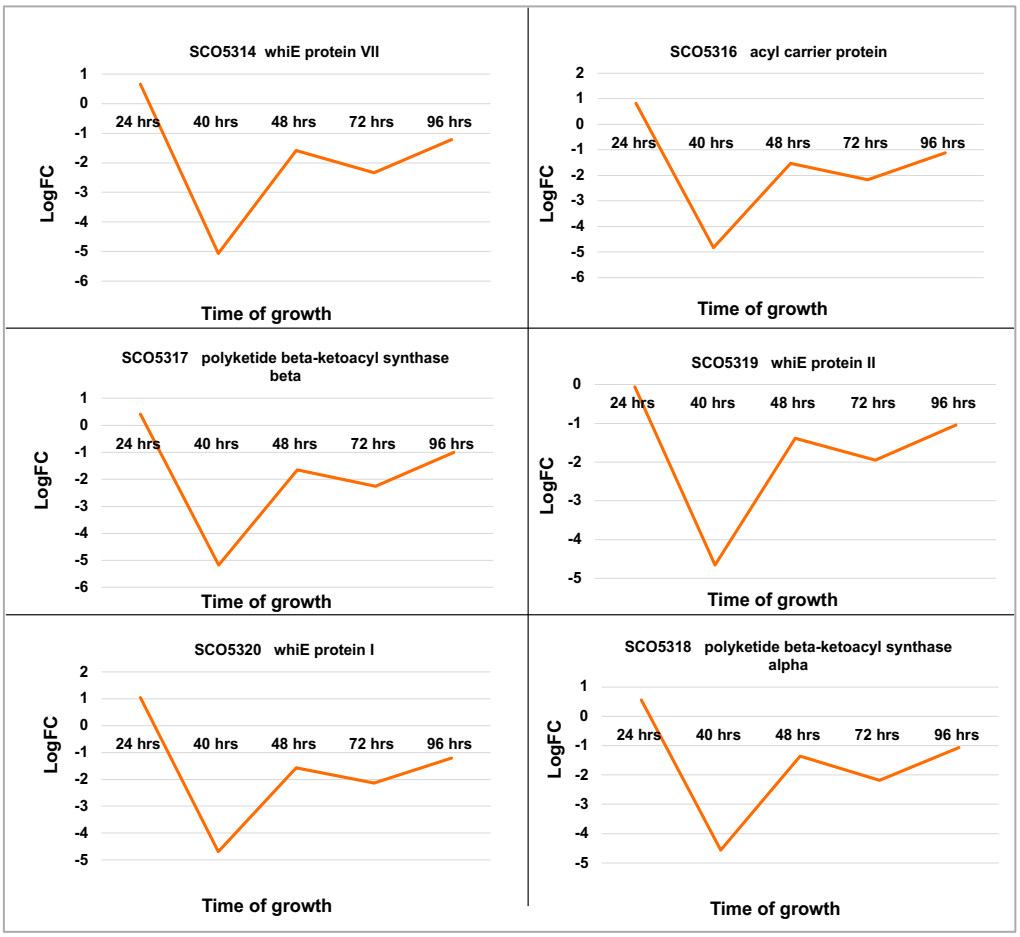

Figure 6.15 Expression level of several *whiE* genes across representative times of growth phases in *parH* mutant.

The graph represents the majority of *whiE* gene have upregulation at the beginning time of growth in *parH* mutant stain. While the second time of growth shows downregulation of these genes compared to M145.

6.2.7.3 Analysis of the expression level of the TIPOC proteins in the *parH* mutant strain

As the bacterial two hybrid analysis in Chapter 3 identified direct link between ParH and Scy together with the ParH and Dia interaction (Chapter 3, Figure 3.11, and Figure 3.15) . This interaction does not necessarily mean that the expression of these genes might change in the *parH* mutant. However, when we investigated the *parH* mutant phenotype using scanning electron microscopy (Figure 6.2), we found branching defects of spore chains, suggesting that there might be differences in Scy and/or Dia levels in the *parH*

mutant. We found that *dia* (SCO5569) expression was downregulated at the early time of growth of 24 hrs in the *parH* mutant compared to the wild type M145. On the other word, in M145 strain at 24 hrs the Dia protein tend to be upregulated during this active growth phase. While at the second time point after 40 hrs of growth, there is the higher expression of *dia* gene in the *parH* mutant strain and decreased expression in the M145 strain. Further, 48 hrs, 72 hrs, and 96 hrs of growing revealed no significant difference in the level of expression between *parH* mutant and M145 strains (Table 6.5).

Table 6.5 Transcriptome dynamic of the expression of Dia at different time points of growth in the *parH* mutant. At 24 hrs of growth Dia was downregulated, then has rapid upregulation at the next time of growth 40 hrs. The values in the table represent $\log_2$[raw reads in parH/raw read in M145] at any given time point.

Geneid	Length	Product	24 hrs	40 hrs	48 hrs	72 hrs	96 hrs
SCO5569	1140	hypothetical protein SC7A1.13	-0.056976	0.510113	0.247757	0.300304	0.115467

Scy, initially had slightly higher expression in the *parH* mutant strain whereas at later time point of growth, at 72 hrs Scy expression was significantly lower than in the wild type strain (Table 6.6).

Table 6.6 Transcriptome dynamic of expression of Scy at five time points of growth in *parH* mutant. The values in the table represent $\log_2$[raw reads in parH/raw read in M145] at any given time point. Expression of Scy is lower in the *parH* mutant at the late time points of 72 and 96 hrs.

Geneid	Length	Product	24 hrs	40 hrs	48 hrs	72 hrs	96 hrs
SCO5397	3981	large Ala/Glu-rich protein	0.245489	0.18265	0.146478	0.023691	0.065346

Low Scy levels are associated with branching defects, therefore, the branching spore chains of the *parH* mutant (Figure 6.2) can be explained by low level of Scy expression at the time of sporulation in the *parH* mutant.

6.2.7.4 Expression level of proteins controlling chromosome segregation in the *parH* mutant

ParA and ParB play important role in chromosome segregation during sporulation in *S. coelicolor*. Therefore, it is worth to investigate their dynamic expression profile in the *parH* mutant strain (Table 6.7 and Figure 6.16).

Table 6.7 Transcriptome dynamic of the ParA and ParB chromosome segregation genes at five time points of growth. Heat map showing the dynamic of expression level of ParA (SCO3886) and ParB (SCO3887). The values in the table represent log_2[raw reads in parH/raw read in M145] at any given time point.

Geneid	Length	Product	24 hrs	40 hrs	48 hrs	72 hrs	96 hrs
SCO3886	828	partitioning or sporulation protein	-0.322983	-0.222186	-0.014598	0.00585	-0.126889
SCO3887	987	partitioning or sporulation protein	-0.076971	-0.191921	0.183399	0.2042	0.030683

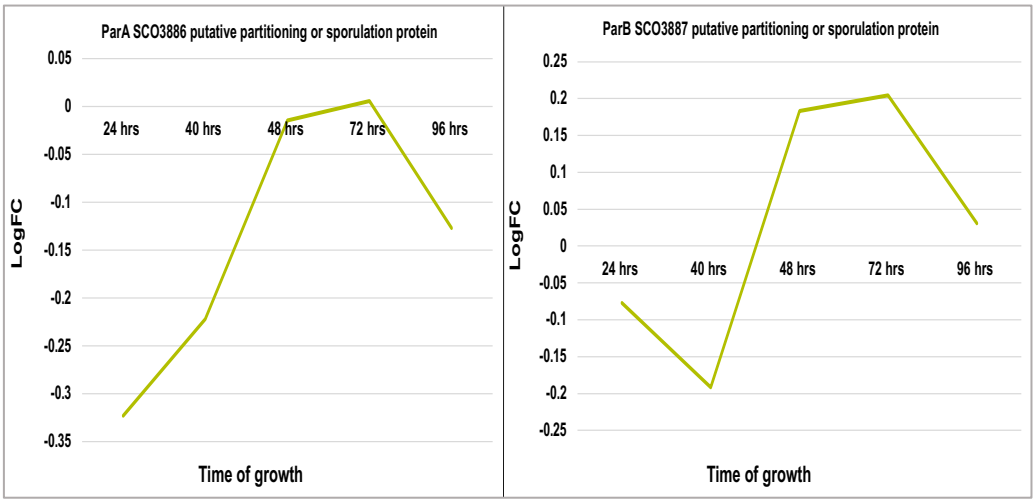

Figure 6.16 Expression level of ParA and ParB across five times of growth phases in *parH* mutant

The y axis represents log_2[raw reads in parH/raw read in M145] at any given time point (as shown in Table 6.7).

Interestingly, the RNA-Seq data revealed that the expression level of ParA and ParB proteins in *parH* mutant was different. Whilst ParA expression was lower at the early timepoint of 24 and 40 hrs, at 48 and 72 hrs expression was comparable with expression of ParA in the wild type strain. However, ParB showed somewhat different expression profile, lower expression at 24 and 40 hrs, but somewhat increased expression at 48 and 72 hrs. The common pattern though is the lower expression at 40 hrs of both portioning protein in

the *parH* mutant, at the time when the wide type strain is in preparation for sporulation. This suggests that expression of both ParA and ParB are de-regulated in the *parH* mutant that leads to segregation defects in the *parH* mutant as seen in the scanning electron microscopy images (Figure 6.2).

6.3 Summary

In this chapter we set out to characterise the gene expression profile throughout development in *S. coelicolor* wild type M145 and *parH* mutant strains, when grown on solid SFM medium. This allowed us to visualise in unprecedented depth the expression profile of the *S. coelicolor* genome and to rationalise the microscopic and macroscopic morphology of *parH* mutant across five representative growth phases.

We successfully achieved the isolation of total RNA from M145, the *parH* mutant, and *hyp* mutant strains using a method we developed to efficiently lyse the cells using a combination of grinding and cell disruption with glass beads in the presence of Trizol and SDS. We have collected samples at 5 distinct time points representing different stages of development and for each time point we collected three biological replicates. The purified RNA samples were analysed at the Novogene Lab using an Agilent 5400 Bioanalyzer. This method determines the RNA Integrity Number (RIN) of an RNA sample. Likewise, the sequencing was performed successfully by Novogene lab. Each RNA sample which were converted to cDNAs and sequenced yielded approximately 14-29 million reads of raw data. Analysing data was performed using edgeR program.

The RNA sequencing covered around 7,842 genes (which covers all predicted ORFs in *S. coelicolor*) which will need more in depth analysis. As we received the RNA-Seq data well into the write up period of my PhD, we did not have time to fully analyse the data generated. Here we decided to represent some of the data that support relevant observations in the present study and previous studies.

- First we focussed on the transcriptional dynamics of cell division proteins SepF and FtsZ. Both genes were down regulated in the *parH* mutant at 40 hrs, that is the time for transitioning of the aerial hyphae into spore chains.
- Previous characterisation of the *parH* mutant showed that the blue pigmented actinorhodin was overproduced in older, 96 hrs samples

(Gillespie, Unpublished 2017). Here we found that the RNA-Seq data confirmed the upregulation of genes for actinorhodin biosynthesis spanning from SCO5071 to SCO5092.

- Moreover, the *whiE* genes spanning from SCO5314 to SCO55322, encoding enzymes for the synthesis of the grey spore pigment were also downregulated in the *parH* mutant, explaining the fact that the *parH* mutant stayed white at the time when the wild type strain turns grey.
- The expression of Dia and Scy that are involved in polar growth were slightly altered in the *parH* mutant, which might explain the unusual branching of spore chains in the *parH* mutant.
- Finally, we focussed on ParA and ParB, known to control chromosome segregation during sporulation. Both ParA and ParB were downregulated at 24 and 40 hrs of growth, the time when these genes are needed in readiness for chromosome organisation prior to sporulation. This is consistent with the finding that the *parH* mutant is delayed in sporulation.

6.4 Acknowledgment

The primary RNA-Seq data analysis files were generated by Govind Chandra, John Innes Centre, Norwich.

CHAPTER 7

7. Discussion

In *Streptomyces*, cell division and its regulation are crucial parts of the life cycle and our understanding is still limited about the complex process of regularly space, synchronous septation event in the multinucleoidal hyphae that generates pre-spore compartments with a single chromosome during sporulation. Chromosome segregation during sporulation in *Streptomyces* requires the accurate positioning of tens of chromosomes in each sporogenic hyphae (Chater *et al.*, 2007). ParA and ParB are the main key proteins associated in this process, although other proteins such as SMC has also been implicated. Through bioinformatic studies in Kelemen's lab, in addition to ParA/B there were several ParA-like proteins identified in *S.coelicolor* that have not been fully characterised. One of these proteins, designated ParH, has a 49% identity with Soj and 30% identity with MinD from *Bacillus subtilis.* The knockout mutant of *parH* showed delayed sporulation and irregularities in septum placement, suggesting that in addition to ParA and SMC, ParH might also contribute to correct chromosome organisation in *Streptomyces.* Therefore, in the present study we build on the preliminary data generated before (Gillespie, Unpublished, 2017), and continue the characterisation of the role of ParH during *Streptomyces* development.

In spite of the fact that the process of bacterial cell division is not fully understood, many previous studies have explored the characterisation of the links of proteins that regulate the process. Chromosome segregation within bacteria is often synchronised with the placement of the septum site. For instance, the nucleoid occlusion proteins SlmA in *E. coli* and Noc in *B. subtilis;* inhibit the formation of FtsZ rings over the chromosome (Lutkenhaus, 2012). Similarly, some bacteria proceed with this segregation employing other proteins, such as cell division and polar growth proteins.

Monitoring the macroscopic morphology of *parH* mutant when grown on solid SFM medium, both in the previous studies and the current investigations,

we established that this mutant is delayed in sporulation as it stayed white even after 4 days growth . This suggested that ParH plays a role in cell division. A novel positive interaction between ParH and SepF has been observed in *vivo* using bacterial two hybrid assay (Chapter 3, Figure 3.3). To understand how the SepF protein influences the interaction with ParH, we aimed to investigate some important point mutations. The K46A mutation did not alter the ParH-SepF interaction, while the F71A mutation has impaired the ParH-SepF interaction (Chapter 3, Figure 3.4 and Figure 3.5). A recent study by Cassettari, 2021 detected that the F71A mutation also abolished the SepF-FtsZ interaction. Interestingly, the SepF F71A is believed to be involved in both the ParH-SepF interaction and the SepF-FtsZ interaction. Together, these results provide important insights into the possibility that SepF switches between ParH and FtsZ for binding. Alternatively, the F71A mutation might affect the structure of the cell division protein SepF which influences the interaction with the ParH protein (Cassettari, Unpublished 2021).

We also examined whether the ParH mutations, G95A, K99A, D121A, and K94A, affected its interaction with SepF (Chapter 3). These G95A, K99A, and D121A are implicated in dimerisation, ATP binding, and ATP hydrolysis, respectively. The G95A mutation did not alter the interaction ParH-SepF, which means that the dimerisation residue is not important for the ParH-SepF interaction (Chapter 3, Figure 3.7). While the mutations affecting ATP binding and hydrolysis, K99A, D121A, and K94A, abolished the ParH-SepF interaction (Chapter 3, Figures 3.8, 3.9, and 3.10). Hence, these residues (K99, D121, and K94) are involved in the interaction of ParH-SepF. This observation might suggest that the presence of ATP is required to keep ParH in dimer form, and this form allows the interaction with SepF to occur. However, when investigating the SepF and ParH interaction *in vitro*, we found that SepF promoted ParH oligomerisation in the absence of ATP, whilst ATP was promoting ParH depolymerisation. This apparent inconsistency needs further investigations, for example by performing the *in vitro* polymerisation assays and native PAGE using overexpressed and purified mutant ParH proteins.

The link between growth and division has been previously observed in *S. coelicolor*. This was demonstrated through the interaction between Scy, a TIPOC component protein, and ParA (B. Ditkowski *et al.*, 2013). Therefore, the interaction between ParH and Scy was tested in this study (Chapter 3). Interestingly, bacterial two hybrid confirmed the positive interaction between ParH and Scy (Chapter 3, Figure 3.11). This finding illustrated that the growth defect observed in the *parH* mutant strain is caused by an impact on TIPOC component from ParH depletion (Chapter 6, Figure 6.2). Furthermore, investigations into the impact of ParH mutations on the ParH-Scy interaction were conducted. The bacterial two-hybrid assay revealed that neither the G95A nor the K99A mutants abolished the ParH-Scy interaction. Therefore, it can be concluded that neither the glycine residue at position 95 nor the lysine residue at position 99 of ParH are involved in the interaction (Chapter 3, Figure 3.12 A , B). However the interaction between ParH and Scy was disrupted when the D121A mutant was tested, indicating the involvement of the aspartate residue (D121) of ParH in this interaction under the tested conditions (Chapter 3, Figure 3.12 C).

We next aimed to investigate a possible link between ParH and chromosome segregation component ParB. We were able to confirm ParH-ParB interaction in *vivo* using bacterial two hybrid assay (Chapter 3, Figure 3.13). Both ParH mutants, G95A and K99A, failed to abolish ParH-ParB interaction (Chapter 3, Figure 3.14 A and B). Nevertheless, the D121A mutation, which corresponds to a ParA mutation that abolishes the ability of ParA to hydrolyse ATP, impaired the two-hybrid interaction indicating that ATP hydrolysis residue might be important for ParH-ParB interaction (Chapter 3, Figure 3.14 C). The fact that ParH can interact with ParB suggests that there is a crosstalk between the ParH-Hyp and the ParA-ParB system.

The possible interaction between ParH with Dia, a new novel TIPOC component that was recently established in Kelemen laboratory has been examined in *vivo*. The bacterial two-hybrid assay has confirmed the interaction between ParH and the Dia coiled coil protein (SCO5569) (Chapter 3; Figure 3.15). The ParH K99A and D121A mutants failed to interact with Dia (Chapter

3.17 A and B). The K99A mutation affected the interaction but was not fully abolished. This indicates that both ATP binding and ATP hydrolysis, are essential for the ParH-Dia interaction.

A key feature of the ParA and MinD proteins is their ability to dimerise, usually in the presence of ATP. These polymerisation states usually affect the function of proteins in a cell by switching between different states that act as regulators for cell division and chromosome segregation. For example, in *E. coli,* MinD binds to the membrane in an ATP form (dimer) and then binds to MinC. This interaction activates the inhibition of FtsZ polymerisation. A monomeric MinD form, on the other hand, is not capable of binding to MinC. MinCD complexes are bound to the poles; this location drives the FtsZ ring to be localised at the mid-cell (Ramm, Heermann and Schwille, 2019). In case of *S. coelicolor* and *C. crescentus*, when ParA retracts its filament or dimer form during segregation, it pulls ParB bound chromosomes into desired positions in the cell (Ptacin *et al.*, 2014).

Therefore, our objective was to characterise the biochemical characteristics of ParH in *vitro* using the native PAGE method (Chapter 5). We provided evidence that ParH assembles into multiple oligomers (Chapter 5, Figure 5.1, and Figure 5.2) but not specifically into dimers. We examined whether ParH oligomerisation was affected in the presence of ATP. Surprisingly, under these tested conditions, ATP had an effect on His-ParH oligomerisation through promoting depolymerisation (Chapter 5, Figure 5.3). This is very different from observations of other ParA-like proteins, where dimerisation of ParA like proteins is dependent on ATP binding. Overall, our data revealed that ParH does not generate specifically dimers, but instead there is an equilibrium of its different oligomer form in solution. Moreover this oligomerisation takes place in the absence of any co-factors, while de-polymerisation is promoted in the presence of ATP. In spite of the fact that ParH is a ParA like protein, its biochemical characteristics are very different from that of ParA. What is responsible for this different behaviour could be answered by studying the structure of ParH and compare it to that of ParA.

Through native-PAGE we were able to detect the positive interaction of ParH-Hyp. This interaction occurred only between the higher order oligomerisation of ParH and Hyp (Chapter 5, Figure 5.5). The same technique also revealed that there is no evidence that ATP plays a role in the interaction between ParH and Hyp. The present study has also confirmed the findings of Gillespie (2017), who found that the oligomerisation state of ParH is essential for interaction with Hyp. Hence, a regulatory mechanism may exist that regulates the oligomerisation of ParH and regulates the interaction of ParH-Hyp (Gillespie, Unpublished 2017).

We then turned to observe interaction between ParH and coiled coil protein Dia, ParH and cell division protein SepF. In (Chapter 3, Figure 3.15) the bacterial two hybrid assay detected positive interaction between ParH and Dia. Intriguingly, in this study (Chapter 5, Figure 5.7) native-PAGE suggests that the presence of Dia might have inhibited His-ParH depolymerisation in the presence of ATP in *vitro*. Comparing lanes 2 and 3 in (Figure 5.3 A & B) with lanes 2 and 3 in (Figure 5.7 C) (Chapter 5), the presence of Dia inhibited ParH depolymerisation. Likewise, the interaction of ParH with SepF was examined in *vitro* by the native-PAGE technique. The bacterial two hybrid assay confirmed the positive interaction between His-ParH and His-SepF (Chapter 4, Figure 4.3), and the native PAGE showed that SepF promoted ParH polymerisation dramatically when the reaction was allowed to progress for hours. Taken together, these results would suggest that SepF and Dia promote ParH polymerisation or prevent depolymerisation of ParH in the presence of ATP. As discussed in the literature, SepF is linked to FtsZ filaments bonded to the membrane (Chapter 1, Figure 1.7). Hence, its sign that led to a possible suggestion the ParH-SepF interaction stimulates the ParH function by precise the position of the septa.

The DNA binding activity of ParH was established in the present study using both native-PAGE techniques and electrophoretic mobility shift assays (Chapter 5). Previous studies revealed that Soj (ParA) binding to DNA required the presence of ATP to stimulate Soj dimerisation (Scholefield *et al.*, 2011). However, our finding through the native-PAGE technique suggested

that ParH oligomers might have higher affinity for DNA (Chapter 5, Figure 5.4 B). In addition, another possible explanation that DNA binding might be promoted the depolymerisation of ParH (Chapter 5, Figure 5.4 B). Moreover, In the presence of DNA, there were slightly less higher oligomers and this depolymerisation was further promoted in the presence of ATP.

The ParH-DNA binding activity was further tested in *vitro* using electrophoretic mobility shift assay (EMSA). We were able to observe a clear shift in the assay when ParH was incubated with DNA (Chapter 5, Figure 5.10). Likewise, this technique was able to confirm that ParH is a nonspecific DNA binding protein. Overall, considering the different oligomers' affinity for DNA, we cannot conclusively say whether they interact differently with DNA. Further investigation is required to establish these interactions. We also showed that the coiled-coil protein Dia, unexpectedly, also interacted with DNA and when together with ParH, generated a super shift. It is not clear at this stage how these DNA binding activities of not only ParH and Dia , but also Hyp, ParB and ParA contribute to the interplay between these proteins and chromosome organisation in *Streptomyces*.

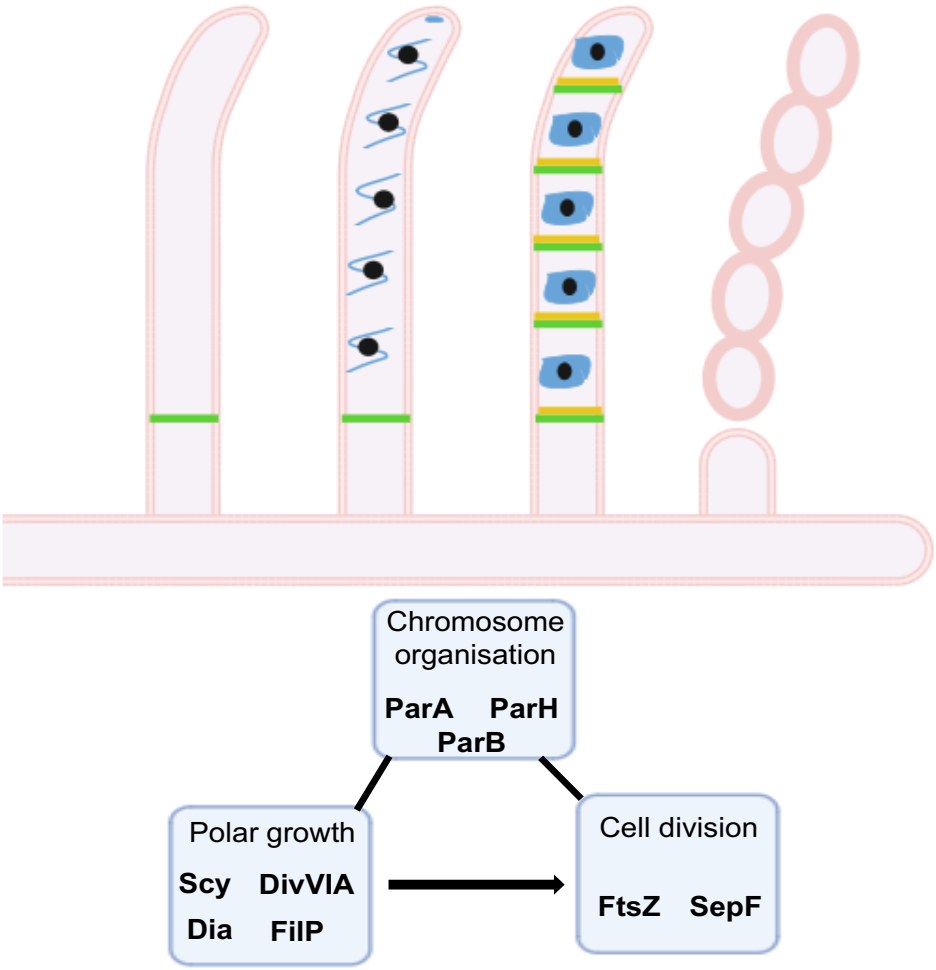

Figure 7.1 Putative model of ParH function in chromosome organisation

Aerial hyphae grow by polar growth at their tips. The process of chromosome segregation relies on the established ParAB machinery. Throughout this study observation (Chapter 3, Figure 3.13 , Chapter 5, Figure 5.10 and Chapter 6, Figure 6.2) expected that ParH (blue) becomes localised to the chromosomes, facilitated by the presence of ParB (black) foci bound to the chromosomes. After the cessation of growth and chromosome organisation by ParA , ParH and ParB, cell division is initiated by the activity of FtsZ (green) and SepF (yellow). Notably, ParH-SepF interaction (Chapter 3, Figure 3.3) suggested that ParH involvement significantly impacts the positioning of septa, ensuring the enclosure of each chromosome between two septa.

Drawing from the findings of this study, we present a putative model for the division process (Figure 7.1). Scy interacts with TIPOC components DivIVA, FilP and the chromosomal organisation component, ParA (Ditkowski *et al.,* 2013; Fuchino *et al.,* 2013; Holmes *et al.,* 2013; Kelemen, 2017). The division occurs subsequent to countering polymerisation inhibition by Scy. ParA then forms filaments along the aerial hyphae, arranging ParB, which is

attached to the *parS* sites of individual chromosomes. This orderly arrangement facilitates the segregation of chromosomes before septation takes place. Considering the observations of unevenness in spore size in the *parH* mutant (Chapter 6, Figure 6.2) and the confirmed ParH-ParB interaction (Chapter 3, Figure 3.13), it is likely that ParH becomes localised to the chromosome through its interaction with ParB. This localisation process further aids in orchestrating the positioning of septa on both sides of the chromosome, although the precise mechanism remains to be elucidated.

The study by Duman *et al*. (2013) and Singh *et al*. (2008) has elucidated the interaction between SepF and FtsZ, demonstrating their binding via C-terminal, which in turn stimulates FtsZ polymerisation. In the context of our research, the established interaction between ParH and SepF underscores an intriguing connection. This connection prompts speculation about a potential linkage between ParH and FtsZ. Consequently, it's plausible to propose that ParH might contribute to cell division through its association with both FtsZ and SepF, further enhancing the complexity of the interplay within the cell division machinery.

An unanticipated finding through the native PAGE technique applied for studying ParH polymerisation was that we observed a new band, just below the monomeric ParH, in the presence of ATP (Chapter 5, Figure 5.13). Using mass spectrometry, we detected numerous putative phosphorylated residues in the samples of ParH that was running below the monomeric form of ParH. In *Streptomyces,* several phosphorylated proteins have been identified as regulators of aerial mycelium sporulation and differentiation (Manteca *et al.*, 2011). However, this preliminary finding in the present study needs further confirmatory study.

The question of whether ParH possesses a kinase domain is an intriguing one, given the complex interplay of protein interactions and phosphorylation events observed in the study. If ParH were found to possess a kinase domain, it could have significant implications for its role in cell division and chromosome organization. Kinases are well-known regulators of cellular processes, including signal transduction pathways and protein interactions. In

the context of Streptomyces development, a ParH kinase domain could potentially phosphorylate specific target proteins, affecting their functions and interactions. This could further modulate processes such as chromosome segregation, cell division, and other developmental transition.

Considering the observed overrepresentation of Ser/Thr/Tyr kinases and phosphorylation during sporulation, suggesting their role in differentiation and sporulation regulation (Rioseras *et al.*, 2018). Thus, the presence of a ParH kinase domain could contribute to the finely tuned regulatory network underlying *Streptomyces* differentiation. If ParH were to phosphorylate partner proteins involved in cell division, chromosome organisation, or other developmental events, it could provide a means of coordination and synchronisation between these processes. This is especially relevant given the identified interactions of ParH with key proteins like SepF, Dia, and Scy.

However, it's important to note that this discussion is speculative, as the study does not directly address the presence or absence of a kinase domain in ParH. To definitively answer this question, further research such as protein domain analysis or biochemical assays would be required. Nonetheless, exploring the potential implications of a ParH kinase domain adds an exciting dimension to understanding the intricate regulatory mechanisms governing *Streptomyces* development and could inspire future investigations in this field.

The final chapter of the project aimed to characterise the gene expression profile in the *parH* mutant and in the wild type M145, for comparison. This allows us to visualise in unprecedented depth the expression of the *S. coelicolor* genome and to elucidate the gene expression profile to explain the microscopic and macroscopic morphologies of the *parH* mutant across five representative growth phases.

We successfully accomplished total RNA extraction from a large number of biological samples of *S. coelicolor* strains, including M145, *parH* and *hyp* mutants grown on solid SFM medium. We used cells from three independent

replicates of each five time points of growth phases of each strain (Figure 6.4 and Figure 6.5). We optimised RNA extraction and the elimination of contaminating DNA (Figure 6.6 and Figure 6.7). After, The RNA concentration and quality was measured using the RNA nanodrop Novogene lab (Table 6.1). The Novogene Lab were run in an Agilent 5400 Bioanalyzer following the manufacturer's instructions. This method determines the RNA Integrity Number (RIN) of an RNA sample. Likewise, the sequencing was performed successfully by Novogene lab. An overview of the preparation of transcriptomic data is illustrated in (Figure 6.8). A total of 14 to 29 million raw reads for RNA-Seq were obtained. Then, analysing data was performed using edgeR program.

Using the RNA-Seq data we could rationalise all the macroscopic and microscopic phenotype we observed, including delayed sporulation, lack of spore pigment production and somewhat elevated actinorhodin production at late stages in the *parH* mutant. Altered expression of the TIPOC components Scy and possibly Dia can explain the unusual branching spore chains observed using scanning electron microscopy. However, further in depth analysis of the RNA-Seq data was prevented by lack of time. Nevertheless, the data generated is of good quality and will be a rich source of further data mining, including not only the identification of further differences in gene expression between the wild type and the *parH* mutant, but also to detect multiple promoter activities during the life cycle of *Streptomyces*. The question still remains of the cause of the altered gene expression in the *parH* mutant, as ParH is not a transcription factor, so if it controls gene expression it will do so indirectly, by perhaps altering chromosome packaging during the transition from the multinucleoidal aerial hyphae to the unigenomic prespore compartments.

In this study, taking all together, the intricate process of cell division and its regulation in *Streptomyces* were meticulously investigated. *Streptomyces* exhibit a unique sporulation process requiring precise chromosome positioning within multinucleoidal hyphae, and ParH, a ParA-like protein, was identified as an essential player in this complex orchestration. ParH involvement in regulating chromosome organisation and septum placement was evident from the delayed sporulation and irregular septa observed in the *parH* mutant. The interactions between ParH and key proteins such as SepF, Scy, ParB, and Dia were extensively explored, shedding light on the interplay between various cellular processes. Notably, the finding that SepF stimulates ParH polymerisation while Dia and Hyp may hinder its depolymerisation unveils potential roles of these proteins in coordinating division and morphogenesis. The ParH-DNA interactions also added to the complexity, hinting at potential mechanisms underlying chromosome organization.

Through a comprehensive exploration of ParH mutations, including those affecting dimerization, ATP binding, and hydrolysis, the intricacies of ParH interactions were illuminated. The fact that different mutations influenced interactions differently highlighted the multifaceted nature of these associations. The unexpected observation of phosphorylated residues in ParH below the monomeric form opened up new questions about the potential regulatory role of phosphorylation in ParH function.

Furthermore, the investigation extended to the transcriptomic level, where the parH mutant's altered gene expression profile was assessed. This approach allowed the rationalization of various observed phenotypic changes and provided insights into the potential indirect role of ParH in gene expression modulation, potentially through chromosomal packaging changes. Despite these remarkable advances, the exact function of ParH remains elusive, representing a compelling avenue for further investigation.

In conclusion, this study substantially advances our understanding of the intricate molecular mechanisms governing *Streptomyces* cell division and chromosome organisation. The multifaceted interactions involving ParH and its partners provide a compelling foundation for further investigations. The

results obtained here not only contribute to elucidating the role of ParH in *Streptomyces* development but also pave the way for future studies, such as 3D chromosomal architecture analyses, to comprehensively unravel the complex regulatory network at play.

8. References

Adams, D. W., Wu, L. J. and Errington, J. (2015) 'Nucleoid occlusion protein Noc recruits DNA to the bacterial cell membrane', *The EMBO Journal*, 34(4), pp. 491–501. doi: 10.15252/embj.201490177.

Ausmees, N. (2013) 'Coiled coil cytoskeletons collaborate in polar growth of Streptomyces', *Bioarchitecture*, 3(4), pp. 110–112. doi: 10.4161/bioa.26194.

Badrinarayanan, A. and Laub, M. T. (2016) 'Bacterial chromosome organization and segregation', *Annu Rev Cell Dev Biol.*, 31, pp. 171–199. doi: 10.1146/annurev-cellbio-100814-125211.Bacterial.

Baer, C. E. *et al.* (2014) 'Subpolar addition of new cell wall is directed by DivIVA in mycobacteria', *Proceedings of the National Academy of Sciences*, 111(31), pp. E3243–E3251. doi: 10.1073/pnas.1402158111.

Barák, I. *et al.* (2008) 'Lipid spirals in Bacillus subtilis and their role in cell division', *Molecular Microbiology*, 68(5), pp. 1315–1327. doi: 10.1111/j.1365-2958.2008.06236.x.

Barka, E. A. *et al.* (2016) 'Taxonomy, Physiology, and Natural Products of Actinobacteria', *Microbiology and Molecular Biology Reviews*, 80(4). doi: 10.1128/mmbr.00044-16.

Baxter, J. C. and Funnell, B. E. (2015) 'Plasmid Partition Mechanisms', *Plasmids: Biology and Impact in Biotechnology and Discovery*, pp. 133–155. doi: 10.1128/9781555818982.ch8.

Beall, B. and Lutkenhaus, J. (1992) 'Impaired cell division and sporulation of a Bacillus subtilis strain with the ftsA gene deleted', *Journal of Bacteriology*, 174(7), pp. 2398–2403. doi: 10.1128/jb.174.7.2398-2403.1992.

Begg, K. J., Dewar, S. J. and Donachie, W. D. (1995) 'A new Escherichia coli cell division gene, ftsK', *Journal of Bacteriology*, 177(21), pp. 6211–6222. doi: 10.1128/jb.177.21.6211-6222.1995.

Bendezú, F. O. and De Boer, P. A. J. (2008) 'Conditional lethality, division defects, membrane involution, and endocytosis in mre and mrd shape mutants of Escherichia coli', *Journal of Bacteriology*, 190(5), pp. 1792–1811. doi: 10.1128/JB.01322-07.

Bentley, S. D. *et al.* (2002) 'Complete genome sequence of the model actinomycete Streptomyces', *Nature*, 417(2), pp. 141–147. doi: 10.1038/417141a.

Bernhardt, T. G. and De Boer, P. A. J. (2005) 'SlmA, a nucleoid-associated, FtsZ binding protein required for blocking septal ring assembly over chromosomes in E. coli', *Molecular Cell*, 18(5), pp. 555–564. doi: 10.1016/j.molcel.2005.04.012.

Bi, E. and Lutkenhaus, J. (1991) 'FtsZ ring structure associated with division in Escherichia coli', *Nature*. Nature Publishing Group, 354, p. 161. Available at: https://doi.org/10.1038/354161a0.

Bignell, C. and Thomas, C. M. (2001) 'The bacterial ParA-ParB partitioning proteins', *Journal of Biotechnology*, 91(1), pp. 1–34. doi: 10.1016/S0168-1656(01)00293-0.

de Boer, P. A. and Raskin, D. M. (1999) 'Rapid pole-to-pole oscillation of a protein required for directing division to the middle of Escherichia coli.', *Proceedings of the National Academy of Sciences of the United States of America*, 96(9), pp. 4971–6. doi: 10.1073/pnas.96.9.4971.

de Boer, P. A. J. *et al.* (2009) 'Self-Enhanced Accumulation of FtsN at Division Sites and Roles for Other Proteins with a SPOR Domain (DamX, DedD, and RlpA) in Escherichia coli Cell Constriction', *Journal of Bacteriology*, 191(24), pp. 7383–7401. doi: 10.1128/jb.00811-09.

de Boer, P. A. J. (2010) 'Advances in understanding E. coli cell fission', *Current Opinion in Microbiology*. Elsevier Ltd, 13(6), pp. 730–737. doi: 10.1016/j.mib.2010.09.015.

de Boer, P. A. J., Crossley, R. E. and Rothfield, L. I. (1989) ‘A division inhibitor and a topological specificity factor coded for by the minicell locus determine proper placement of the division septum in E. coli’, *Cell*, 56(4), pp. 641–649. doi: 10.1016/0092-8674(89)90586-2.

De Boer, P. A. J., Crossley, R. E. and Rothfield, L. I. (1992) ‘Roles of MinC and MinD in the site-specific septation block mediated by the MinCDE system of Escherichia coli’, *Journal of Bacteriology*, 174(1), pp. 63–70. doi: 10.1128/jb.174.1.63-70.1992.

Brown, D. R. *et al.* (2008) ‘Selective Anti-Staphylococcal Activity’, (September), pp. 1673–1676.

Brun, Y. V. *et al.* (2012) ‘Polar growth in the Alphaproteobacterial order Rhizobiales’, *Proceedings of the National Academy of Sciences*, 109(5), pp. 1697–1701. doi: 10.1073/pnas.1114476109.

Buddelmeijer, N. and Beckwith, J. (2004) ‘A complex of the Escherichia coli cell division proteins FtsL, FtsB and FtsQ forms independently of its localization to the septal region’, *Molecular Microbiology*, 52(5), pp. 1315–1327. doi: 10.1111/j.1365-2958.2004.04044.x.

Busiek, K. K. and Margolin, W. (2015) ‘Bacterial actin and tubulin homologs in cell growth and division’, *Current Biology*. Elsevier Ltd, 25(6), pp. R243–R254. doi: 10.1016/j.cub.2015.01.030.

Cabré, E. J. *et al.* (2015) ‘The nucleoid occlusion SlmA protein accelerates the disassembly of the FtsZ protein polymers without affecting their GTPase activity’, *PLoS ONE*, 10(5), pp. 1–21. doi: 10.1371/journal.pone.0126434.

Cameron, T. A. *et al.* (2014) ‘Peptidoglycan Synthesis Machinery in Agrobacterium tumefaciens During Unipolar Growth and Cell Division’, *mBio*, 5(3), pp. 1–10. doi: 10.1128/mbio.01219-14.

Cameron, T. A., Zupan, J. R. and Zambryski, P. C. (2015) ‘The

essential features and modes of bacterial polar growth', *Trends in Microbiology*. Elsevier Ltd, 23(6), pp. 347–353. doi: 10.1016/j.tim.2015.01.003.

Cha, J. H. and Stewart, G. C. (1997) 'The divIVA minicell locus of Bacillus subtilis', *Journal of Bacteriology*, 179(5), pp. 1671–1683. doi: 10.1128/jb.179.5.1671-1683.1997.

Chater, K. F. (1972) 'A morphological and genetic mapping study of white colony mutants of Streptomyces coelicolor.', *Journal of general microbiology*, 72(1), pp. 9–28. doi: 10.1099/00221287-72-1-9.

Chater, K. F. *et al.* (2007) 'Alignment of multiple chromosomes along helical ParA scaffolding in sporulating Streptomyces hyphae', *Molecular Microbiology*, 65(3), pp. 625–641. doi: 10.1111/j.1365-2958.2007.05815.x.

Chen, C. W. *et al.* (1993) 'The chromosomal DNA of Streptomyces lividans 66 appears to be linear (abstract)', *J. Cell. Biochem.*, Suppl 17E, p. 291.

Chen, J. C. and Beckwith, J. (2001) 'FtsQ, FtsL and Ftsl require FtsK, but not FtsN, for co-localization with FtsZ during Escherichia coli cell division', *Molecular Microbiology*, 42(2), pp. 395–413. doi: 10.1046/j.1365-2958.2001.02640.x.

Cho, H. *et al.* (2011) 'Nucleoid occlusion factor SlmA is a DNA-activated FtsZ polymerization antagonist', *Proceedings of the National Academy of Sciences*, 108(9), pp. 3773–3778. doi: 10.1073/pnas.1018674108.

Chomczynski, P. (1992) 'Solubilzation in formamide protects RNA from degradation', *Nucleic Acids Research*, 20(14), pp. 3791–3792. doi: 10.1093/nar/20.14.3791.

Daniel, R. A. *et al.* (2006) 'Characterization of the essential cell division gene ftsL (yllD) of Bacillus subtilis and its role in the assembly of the division

apparatus', 29(1998), pp. 593–604.

Daniel, R. A. and Errington, J. (2003) 'Control of Cell Morphogenesis in Bacteria: Two Distinct Ways to Make a Rod-Shaped Cell termining cell shape. The relative roles of these closely- related proteins are partially resolved in this paper. The precursor for PG synthesis is a disaccharide pen', *Cell*, 113, pp. 767–776. doi: 10.1016/S0092-8674(03)00421-5.

Defeu Soufo, H. J. and Graumann, P. L. (2006) 'Dynamic localization and interaction with other Bacillus subtilis actin-like proteins are important for the function of MreB', *Molecular Microbiology*, 62(5), pp. 1340–1356. doi: 10.1111/j.1365-2958.2006.05457.x.

Ditkowski, B. *et al.* (2010) 'The actinobacterial signature protein ParJ (SCO1662) regulates ParA polymerization and affects chromosome segregation and cell division during Streptomyces sporulation', *Molecular Microbiology*, 78(6), pp. 1403–1415. doi: 10.1111/j.1365-2958.2010.07409.x.

Ditkowski, B. *et al.* (2013) 'Dynamic interplay of ParA with the polarity protein, Scy, coordinates the growth with chromosome segregation in Streptomyces coelicolor', *Open Biology*, 3(3), pp. 130006–130006. doi: 10.1098/rsob.130006.

Ditkowski, Bartosz *et al.* (2013) 'Dynamic interplay of ParA with the polarity protein, Scy, coordinates the growth with chromosome segregation in Streptomyces coelicolor', *Open Biology*, 3(MAR). doi: 10.1098/rsob.130006.

Dominguez-Escobar, J. *et al.* (2011) 'Processive Movement of', *Science*, 333(July), pp. 225–228. doi: 10.1126/science.1203466.

Donczew, M. *et al.* (2016) 'ParA and ParB coordinate chromosome segregation with cell elongation and division during Streptomyces sporulation', *Open Biology*, 6(4), p. 150263. doi: 10.1098/rsob.150263.

Donovan, C. *et al.* (2008) ' A novel component of the division-site selection system of Bacillus subtilis and a new mode of action for the division

inhibitor MinCD ', *Molecular Microbiology*, 70(6), pp. 1556–1569. doi: 10.1111/j.1365-2958.2008.06501.x.

Du, S. and Lutkenhaus, J. (2014) 'SlmA Antagonism of FtsZ Assembly Employs a Two-pronged Mechanism like MinCD', *PLoS Genetics*, 10(7). doi: 10.1371/journal.pgen.1004460.

Duman, R. *et al.* (2013) 'Structural and genetic analyses reveal the protein SepF as a new membrane anchor for the Z ring', *Proceedings of the National Academy of Sciences of the United States of America*, 110(48). doi: 10.1073/pnas.1313978110.

Easter, J. and Gober, J. W. (2002) 'ParB-stimulated nucleotide exchange regulates a switch in functionally distinct ParA activities', *Molecular Cell*, 10(2), pp. 427–434. doi: 10.1016/S1097-2765(02)00594-4.

Ebersbach, G. and Gerdes, K. (2005) 'Plasmid Segregation Mechanisms', *Annual Review of Genetics*, 39(1), pp. 453–479. doi: 10.1146/annurev.genet.38.072902.091252.

Edwards, D. H. and Errington, J. (1997) 'The Bacillus subtilis DivIVA protein targets to the division septum and controls the site specificity of cell division', *Molecular Microbiology*, 24(5), pp. 905–915. doi: 10.1046/j.1365-2958.1997.3811764.x.

van den Ent, F. (2002) 'Crystal structure of the cell division protein FtsA from Thermotoga maritima', *The EMBO Journal*, 19(20), pp. 5300–5307. doi: 10.1093/emboj/19.20.5300.

van den Ent, F. *et al.* (2014) 'Bacterial actin MreB forms antiparallel double filaments', *eLife*, 2014(3), pp. 1–22. doi: 10.7554/eLife.02634.

Erickson, H. P. (1998) 'Atomic structures of tubulin and FtsZ', *Trends in Cell Biology*, 8(4), pp. 133–137. doi: 10.1016/S0962-8924(98)01237-9.

Erickson, H. P., Anderson, D. E. and Osawa, M. (2010) 'FtsZ in

Bacterial Cytokinesis: Cytoskeleton and Force Generator All in One', *Microbiology and Molecular Biology Reviews*, 74(4), pp. 504–528. doi: 10.1128/mmbr.00021-10.

Errington, J. (2015) 'Bacterial morphogenesis and the enigmatic MreB helix', *Nature Reviews Microbiology*. Nature Publishing Group, 13(4), pp. 241–248. doi: 10.1038/nrmicro3398.

Eswaramoorthy, P. *et al.* (2011) 'Cellular architecture mediates DivIVA ultrastructure and regulates min activity in Bacillus subtilis', *mBio*, 2(6), pp. 1–9. doi: 10.1128/mBio.00257-11.

Fenton, A. K. and Gerdes, K. (2013) 'Direct interaction of FtsZ and MreB is required for septum synthesis and cell division in Escherichia coli', *EMBO Journal*. Nature Publishing Group, 32(13), pp. 1953–1965. doi: 10.1038/emboj.2013.129.

Fero, M. J. *et al.* (2011) 'Assembly of the Caulobacter cell division machine', *Molecular Microbiology*, 80(6), pp. 1680–1698. doi: 10.1111/j.1365-2958.2011.07677.x.

Figge, R. M., Divakaruni, A. V and Gober, J. W. (2004) 'MreB, the cell-shape determining bacterial actin homolog, coordinates cell wall morphogenesis in', *Genomics*, 51, pp. 1–47. doi: 10.1046/j.1365-2958.2003.03936.x.

Flärdh, K. (2003a) 'Essential role of DivIVA in polar growth and morphogenesis in Streptomyces coelicolor A3(2)', *Molecular Microbiology*, 49(6), pp. 1523–1536. doi: 10.1046/j.1365-2958.2003.03660.x.

Flärdh, K. (2003b) 'Growth polarity and cell division in Streptomyces', *Current Opinion in Microbiology*, 6(6), pp. 564–571. doi: 10.1016/j.mib.2003.10.011.

Flärdh, K. *et al.* (2012) 'Regulation of apical growth and hyphal branching in Streptomyces', *Current Opinion in Microbiology*, 15(6), pp. 737–

743. doi: 10.1016/j.mib.2012.10.012.

Flärdh, K. and Buttner, M. J. (2009) ‘Streptomyces morphogenetics: Dissecting differentiation in a filamentous bacterium’, *Nature Reviews Microbiology*, 7(1), pp. 36–49. doi: 10.1038/nrmicro1968.

Fröjd, M. and Flärdh, K. (2019) ‘Dynamic assemblies of intermediate filament-like protein FilP and effects on polar growth determinant DivIVA in Streptomyces venezuelae.’, *submitted to Molecular Microbiology*, 0, pp. 1–15. doi: 10.1111/mmi.14253.

Fu, X. *et al.* (2012) ‘The MinE ring required for proper placement of the division site is a mobile structure that changes its cellular location during the Escherichia coli division cycle’, *Proceedings of the National Academy of Sciences*, 98(3), pp. 980–985. doi: 10.1073/pnas.98.3.980.

Fuchino, K. *et al.* (2013) ‘Dynamic gradients of an intermediate filament-like cytoskeleton are recruited by a polarity landmark during apical growth’, *Proceedings of the National Academy of Sciences*, 110(21), pp. E1889–E1897. doi: 10.1073/pnas.1305358110.

Fung, E., Bouet, J. Y. and Funnell, B. E. (2001) ‘Probing the ATP-binding site of P1 ParA: Partition and repression have different requirements for ATP binding and hydrolysis’, *EMBO Journal*, 20(17), pp. 4901–4911. doi: 10.1093/emboj/20.17.4901.

Garner, E. C. *et al.* (2011) ‘Circumferential Motions of the Cell Wall Synthesis Machinery Drive Cytoskeletal Dynamics in B. subtilis’, *Science*, 333(6039), pp. 222–225.

Gerdes, K., Moller-Jensen, J. and Jensen, R. B. (2000) ‘Plasmid and chromosome partitioning: Surprises from phylogeny’, *Molecular Microbiology*, 37(3), pp. 455–466. doi: 10.1046/j.1365-2958.2000.01975.x.

Ginda, K. *et al.* (2013) ‘ParA of Mycobacterium smegmatis co-ordinates chromosome segregation with the cell cycle and interacts with the polar

growth determinant DivIVA', *Molecular Microbiology*, 87(5), pp. 998–1012. doi: 10.1111/mmi.12146.

Goehring, N. W. and Beckwith, J. (2005) 'Diverse Paths to Midcell : Assembly of the Bacterial Cell Division Machinery', 15, pp. 514–526. doi: 10.1016/j.cub.2005.06.038.

Grantcharova, N., Lustig, U. and Fla, K. (2005) 'Dynamics of FtsZ Assembly during Sporulation in Streptomyces coelicolor A3 (2)', *Society*, 187(9), pp. 3227–3237. doi: 10.1128/JB.187.9.3227.

Gündoğdu, M. E. *et al.* (2011) 'Large ring polymers align FtsZ polymers for normal septum formation', *EMBO Journal*, 30(3), pp. 617–626. doi: 10.1038/emboj.2010.345.

Hale, C. A. and De Boer, P. A. J. (1999) 'Recruitment of ZipA to the septal ring of Escherichia coli is dependent on FtsZ and independent of FtsA', *Journal of Bacteriology*, 181(1), pp. 167–176.

Hale, C. A., Meinhardt, H. and De Boer, P. A. J. (2001) 'Dynamic localization cycle of the cell division regulator MinE in Escherichia coli', *EMBO Journal*, 20(7), pp. 1563–1572. doi: 10.1093/emboj/20.7.1563.

Hale, C. A., Rhee, A. C. and De Boer, P. A. J. (2000) 'ZipA-induced bundling of FtsZ polymers mediated by an interaction between C-terminal domains', *Journal of Bacteriology*, 182(18), pp. 5153–5166. doi: 10.1128/JB.182.18.5153-5166.2000.

Hamoen, L. W. *et al.* (2006) 'SepF, a novel FtsZ-interacting protein required for a late step in cell division', *Molecular Microbiology*, 59(3), pp. 989–999. doi: 10.1111/j.1365-2958.2005.04987.x.

Harry, E. J. (2001) 'Bacterial cell division: Regulating Z-ring formation', *Molecular Microbiology*, 40(4), pp. 795–803. doi: 10.1046/j.1365-2958.2001.02370.x.

Hempel, A. M. *et al.* (2008) 'Assemblies of DivIVA mark sites for hyphal branching and can establish new zones of cell wall growth in Streptomyces coelicolor', *Journal of Bacteriology*, 190(22), pp. 7579–7583. doi: 10.1128/JB.00839-08.

Hester, C. M. and Lutkenhaus, J. (2007) 'Soj (ParA) DNA binding is mediated by conserved arginines and is essential for plasmid segregation', *Proceedings of the National Academy of Sciences of the United States of America*, 104(51), pp. 20326–20331. doi: 10.1073/pnas.0705196105.

Holmes, N. A. *et al.* (2013) 'Coiled-coil protein Scy is a key component of a multiprotein assembly controlling polarized growth in Streptomyces', *Proceedings of the National Academy of Sciences*, 110(5), pp. E397–E406. doi: 10.1073/pnas.1210657110.

Holyoak, T. *et al.* (2011) 'The Min Oscillator Uses MinD-Dependent Conformational Changes in MinE to Spatially Regulate Cytokinesis', *Cell*. Elsevier, 146(3), pp. 396–407. doi: 10.1016/j.cell.2011.06.042.

Hu, Z. *et al.* (2002) 'The MinC component of the division site selection system in Escherichia coli interacts with FtsZ to prevent polymerization', *Proceedings of the National Academy of Sciences*, 96(26), pp. 14819–14824. doi: 10.1073/pnas.96.26.14819.

Hu, Z., Gogol, E. P. and Lutkenhaus, J. (2002) 'Dynamic assembly of MinD on phospholipid vesicles regulated by ATP and MinE', *Proceedings of the National Academy of Sciences*, 99(10), pp. 6761–6766. doi: 10.1073/pnas.102059099.

Hu, Z. and Lutkenhaus, J. (2001) 'Topological regulation of cell division in E. coli: Spatiotemporal oscillation of MinD requires stimulation of its ATPase by MinE and phospholipid', *Molecular Cell*, 7(6), pp. 1337–1343. doi: 10.1016/S1097-2765(01)00273-8.

Huang, K. H., Durand-Heredia, J. and Janakiraman, A. (2013) 'FtsZ ring stability: Of bundles, tubules, crosslinks, and curves', *Journal of*

Bacteriology, 195(9), pp. 1859–1868. doi: 10.1128/JB.02157-12.

Ishikawa, S. *et al.* (2006) 'A new FtsZ-interacting protein, YlmF, complements the activity of FtsA during progression of cell division in Bacillus subtilis', *Molecular Microbiology*, 60(6), pp. 1364–1380. doi: 10.1111/j.1365-2958.2006.05184.x.

Isolation, M. *et al.* (1987) 'Mutant Isolation and Molecular Cloning of mre Genes, Which Determine Cell Shape, Sensitivity to Mecillinam, and Amount of Penicillin-Binding Proteins in Escherichia coli', *Cell*, 169(11), pp. 4935–4940.

Jakimowicz, D., Chater, K. and Zakrzewska-Czerwínska, J. (2002) 'The ParB protein of Streptomyces coelicolor A3(2) recognizes a cluster of parS sequences within the origin-proximal region of the linear chromosome', *Molecular Microbiology*, 45(5), pp. 1365–1377. doi: 10.1046/j.1365-2958.2002.03102.x.

Jakimowicz, D. and Van Wezel, G. P. (2012) 'Cell division and DNA segregation in Streptomyces: How to build a septum in the middle of nowhere?', *Molecular Microbiology*, 85(3), pp. 393–404. doi: 10.1111/j.1365-2958.2012.08107.x.

Jeong, Y. *et al.* (2016) 'The dynamic transcriptional and translational landscape of the model antibiotic producer Streptomyces coelicolor A3(2)', *Nature Communications*. Nature Publishing Group, 7, pp. 1–11. doi: 10.1038/ncomms11605.

Jiménez, M. *et al.* (2011) 'Reconstitution and organization of Escherichia coli proto-ring elements (FtsZ and FtsA) inside giant unilamellar vesicles obtained from bacterial inner membranes', *Journal of Biological Chemistry*, 286(13), pp. 11236–11241. doi: 10.1074/jbc.M110.194365.

Joël, H., Soufo, D. and Graumann, P. L. (2005) 'the replication machinery and requires membrane proteins MreC / D and other actin-like proteins for proper localization', *BMC Cell Biology*, 11, pp. 1–11. doi:

10.1186/1471-2121-6-10.

Kang, C. M. *et al.* (2008) 'Wag31, a homologue of the cell division protein DivIVA, regulates growth, morphology and polar cell wall synthesis in mycobacteria', *Microbiology*, 154(3), pp. 725–735. doi: 10.1099/mic.0.2007/014076-0.

Karimova, G., Dautin, N. and Ladant, D. (2005) 'Interaction network among Escherichia coli membrane proteins involved in cell division as revealed by bacterial two-hybrid analysis', *Society*, 187(7), pp. 2233–2243. doi: 10.1128/JB.187.7.2233.

Karimova, G., Ullmann, A. and Ladant, D. (2000) 'A bacterial two-hybrid system that exploits a cAMP signaling cascade in Escherichia coli.', *Methods in enzymology*, 328(1988), pp. 59–73. doi: 10.1016/S0076-6879(00)28390-0.

El Karoui, M. and Errington, J. (2001) 'Isolation and characterization of topological specificity mutants of minD in Bacillus subtilis', *Molecular Microbiology*, 42(5), pp. 1211–1221. doi: 10.1046/j.1365-2958.2001.02710.x.

Kawai, Y., Asai, K. and Errington, J. (2009) 'Partial functional redundancy of MreB isoforms, MreB, Mbl and MreBHp in cell morphogenesis of Bacillus subtilis', *Molecular Microbiology*, 73(4), pp. 719–731. doi: 10.1111/j.1365-2958.2009.06805.x.

Kawai, Y. and Ogasawara, N. (2006) 'Bacillus subtilis EzrA and FtsL synergistically regulate FtsZ ring dynamics during cell division', *Microbiology*, 152(4), pp. 1129–1141. doi: 10.1099/mic.0.28497-0.

Kelemen, G. H. *et al.* (1998) 'Developmental Regulation of Transcription of whiE , a Locus Specifying the Polyketide Spore Pigment in', *American Society for Microbiology*, 180(9), pp. 2515–2521.

Kim, H. J. *et al.* (2000) 'Partitioning of the linear chromosome during sporulation of Streptomyces coelicolor A3(2) involves an oriC-linked parAB locus', *Journal of Bacteriology*, 182(5), pp. 1313–1320. doi:

10.1128/JB.182.5.1313-1320.2000.

Kois-Ostrowska, A. *et al.* (2016) 'Unique Function of the Bacterial Chromosome Segregation Machinery in Apically Growing Streptomyces - Targeting the Chromosome to New Hyphal Tubes and its Anchorage at the Tips', *PLoS Genetics*, 12(12), pp. 1–25. doi: 10.1371/journal.pgen.1006488.

Koonin, E. V. (1993) 'A superfamily of ATPases with diverse functions containing either classical or deviant ATP-binding motif', *Journal of Molecular Biology*, pp. 1165–1174. doi: 10.1006/jmbi.1993.1115.

Kukurba, K. R. and Montgomery, S. B. (2015) 'RNA sequencing and analysis', *Cold Spring Harbor Protocols*, 2015(11), pp. 951–969. doi: 10.1101/pdb.top084970.

Lackner, L. L., Raskin, D. M. and De Boer, P. A. J. (2003) 'ATP-dependent interactions between Escherichia coli Min proteins and the phospholipid membrane in vitro', *Journal of Bacteriology*, 185(3), pp. 735–749. doi: 10.1128/JB.185.3.735-749.2003.

Di Lallo, G. *et al.* (2003) 'Use of a two-hybrid assay to study the assembly of a complex multicomponent protein machinery: Bacterial septosome differentiation', *Microbiology*, 149(12), pp. 3353–3359. doi: 10.1099/mic.0.26580-0.

Laloux, G. and Jacobs-Wagner, C. (2013) 'How do bacteria localize proteins to the cell pole?', *Journal of Cell Science*, 127(1), pp. 11–19. doi: 10.1242/jcs.138628.

Leonard, T. A., Butler, P. J. and Löwe, J. (2005a) 'Bacterial chromosome segregation: Structure and DNA binding of the Soj dimer - A conserved biological switch', *EMBO Journal*, 24(2), pp. 270–282. doi: 10.1038/sj.emboj.7600530.

Leonard, T. A., Butler, P. J. and Löwe, J. (2005b) 'Bacterial chromosome segregation: Structure and DNA binding of the Soj dimer - A

conserved biological switch', *EMBO Journal*, 24(2), pp. 270–282. doi: 10.1038/sj.emboj.7600530.

Letek, M. *et al.* (2008) 'DivIVA is required for polar growth in the MreB-lacking rod-shaped actinomycete Corynebacterium glutamicum', *Journal of Bacteriology*, 190(9), pp. 3283–3292. doi: 10.1128/JB.01934-07.

Levin, P. A. and Losick, R. (1994) 'Characterization of a cell division gene from Bacillus subtilis that is required for vegetative and sporulation septum formation', *Journal of Bacteriology*, 176(5), pp. 1451–1459. doi: 10.1128/jb.176.5.1451-1459.1994.

Liu, B. *et al.* (2015) 'Roles for both FtsA and the FtsBLQ subcomplex in FtsN-stimulated cell constriction in Escherichia coli', *Molecular Microbiology*, 95(6), pp. 945–970. doi: 10.1111/mmi.12906.

Livny, J., Yamaichi, Y. and Waldor, M. K. (2007) 'Distribution of centromere-like parS sites in bacteria: Insights from comparative genomics', *Journal of Bacteriology*, 189(23), pp. 8693–8703. doi: 10.1128/JB.01239-07.

Lutkenhaus, J. (2007) 'Assembly Dynamics of the Bacterial MinCDE System and Spatial Regulation of the Z Ring', *Annual Review of Biochemistry*, 76(1), pp. 539–562. doi: 10.1146/annurev.biochem.75.103004.142652.

Lutkenhaus, J. (2012) 'The ParA/MinD family puts things in their place', *Bone*, 23(1), pp. 1–7. doi: 10.1016/j.tim.2012.05.002.The.

Lutkenhaus, J., Pichoff, S. and Du, S. (2012) 'Bacterial cytokinesis: From Z ring to divisome', *Cytoskeleton*, 69(10), pp. 778–790. doi: 10.1002/cm.21054.

Lutkenhaus, J. and Sundaramoorthy, M. (2003) 'MinD and role of the deviant Walker A motif, dimerization and membrane binding in oscillation', *Molecular Microbiology*, 48(2), pp. 295–303. doi: 10.1046/j.1365-2958.2003.03427.x.

Ma, X. and Margolin, W. (1999) ‘Genetic and functional analyses of the conserved C-terminal core domain of Escherichia coli FtsZ’, *Journal of Bacteriology*, 181(24), pp. 7531–7544.

Mahone, C. R. and Goley, E. D. (2020) ‘Bacterial cell division at a glance’, *Journal of Cell Science*, 133(7), pp. 1–7. doi: 10.1242/jcs.237057.

Manteca, A. *et al.* (2007) ‘Aerial hyphae in surface cultures of Streptomyces lividans and Streptomyces coelicolor originate from viable segments surviving an early programmed cell death event’, *FEMS Microbiology Letters*, 274(1), pp. 118–125. doi: 10.1111/j.1574-6968.2007.00825.x.

Manteca, A. *et al.* (2011) ‘Phosphoproteome analysis of streptomyces development reveals extensive protein phosphorylation accompanying bacterial differentiation’, *Journal of Proteome Research*, 10(12), pp. 5481–5492. doi: 10.1021/pr200762y.

Margolin, W. (2001) ‘Bacterial cell division: A moving MinE sweeper boggles the MinD’, *Current Biology*, 11(10), pp. 395–398. doi: 10.1016/S0960-9822(01)00217-2.

Margolin, W. (2005) ‘FtsZ and the division of prokaryotic cells and organelles’, *Nature Reviews Molecular Cell Biology*, 6(11), pp. 862–871. doi: 10.1038/nrm1745.

Margolin, W. (2009) ‘Sculpting the Bacterial Cell’, *Current Biology*. Elsevier Ltd, 19(17), pp. R812–R822. doi: 10.1016/j.cub.2009.06.033.

Mazza, P. *et al.* (2006) ‘MreB of Streptomyces coelicolor is not essential for vegetative growth but is required for the integrity of aerial hyphae and spores’, *Molecular Microbiology*, 60(4), pp. 838–852. doi: 10.1111/j.1365-2958.2006.05134.x.

McCormick, J. R. *et al.* (1994) ‘Growth and viability of Streptomyces coelicolor mutant for the cell division gene ftsZ’, *Molecular Microbiology*, 14(2),

pp. 243–254. doi: 10.1111/j.1365-2958.1994.tb01285.x.

Mercer, K. L. N. and Weiss, D. S. (2002) ‘The Escherichia coli cell division protein FtsW is required to recruit its cognate transpeptidase, FtsI (PBP3), to the division site’, *Journal of Bacteriology*, 184(4), pp. 904–912. doi: 10.1128/jb.184.4.904-912.2002.

Misra, H. S. *et al.* (2018) ‘Interdependence of bacterial cell division and genome segregation and its potential in drug development’, *Microbiological Research*. Elsevier, 208(January), pp. 12–24. doi: 10.1016/j.micres.2017.12.013.

Mohammadi, T. *et al.* (2011) ‘Identification of FtsW as a transporter of lipid-linked cell wall precursors across the membrane’, *EMBO Journal*, 30(8), pp. 1425–1432. doi: 10.1038/emboj.2011.61.

Monahan, L. G. *et al.* (2014) ‘Division site positioning in bacteria: One size does not fit all’, *Frontiers in Microbiology*, 5(FEB), pp. 1–7. doi: 10.3389/fmicb.2014.00019.

Monahan, L. G. and Harry, E. J. (2013) ‘Identifying how bacterial cells find their middle: A new perspective’, *Molecular Microbiology*, 87(2), pp. 231–234. doi: 10.1111/mmi.12114.

Motallebi-Veshareh, M., Rouch, D. A. and Thomas, C. M. (1990) ‘A family of ATPases involved in active partitioning of diverse bacterial plasmids’, *Molecular Microbiology*, 4(9), pp. 1455–1463. doi: 10.1111/j.1365-2958.1990.tb02056.x.

Mukherjee, A., Dai, K. and Lutkenhaus, J. (2006) ‘Escherichia coli cell division protein FtsZ is a guanine nucleotide binding protein.’, *Proceedings of the National Academy of Sciences*, 90(3), pp. 1053–1057. doi: 10.1073/pnas.90.3.1053.

Nanninga (1991) ‘Cell division and peptidoglycan assembly in Eschenchia coli’, *Molecular Microbiology*, 5(4), pp. 791–795. doi:

10.1111/j.1365-2958.1991.tb00751.x.

Nguyen, L. *et al.* (2007) ‘Antigen 84, an effector of pleiomorphism in Mycobactenum smegmatis’, *Journal of Bacteriology*, 189(21), pp. 7896–7910. doi: 10.1128/JB.00726-07.

Nodwell, J. R. (2019) ‘Microbe profile: Streptomyces coelicolor: A burlesque of pigments and phenotypes’, *Microbiology (United Kingdom)*, 165(9), pp. 953–955. doi: 10.1099/mic.0.000821.

Oliva, M. A. *et al.* (2010) ‘Features critical for membrane binding revealed by DivIVA crystal structure’, *EMBO Journal*, 29(12), pp. 1988–2001. doi: 10.1038/emboj.2010.99.

Olshausen, P. V. *et al.* (2013) ‘Superresolution imaging of dynamic MreB filaments in B. subtilis - A multiple-motor-driven transport?’, *Biophysical Journal*, 105(5), pp. 1171–1181. doi: 10.1016/j.bpj.2013.07.038.

Osawa, M., Anderson, D. E. and Erickson, H. P. (2008) ‘Reconstitution of contractile FtsZ rings’, *in liposomes, Science (New York, N.Y*, 320(May), pp. 792–794.

Patrick, J. E. and Kearns, D. B. (2008) ‘MinJ (YvjD) is a topological determinant of cell division in Bacillus subtilis’, *Molecular Microbiology*, 70(5), pp. 1166–1179. doi: 10.1111/j.1365-2958.2008.06469.x.

Pease, P. J. *et al.* (2005) ‘Sequence-directed DNA translocation by purified FtsK’, *Science*, 307(5709), pp. 586–590. doi: 10.1126/science.1104885.

Pichoff, S. and Lutkenhaus, J. (2002) ‘Unique and overlapping roles for ZipA and FtsA in septal ring assembly in Escherichia coli’, *EMBO Journal*. doi: 10.1093/emboj/21.4.685.

Pichoff, S. and Lutkenhaus, J. (2005) ‘Tethering the Z ring to the membrane through a conserved membrane targeting sequence in FtsA’,

Molecular Microbiology, 55(6), pp. 1722–1734. doi: 10.1111/j.1365-2958.2005.04522.x.

Pichoff, S. and Lutkenhaus, J. (2007) 'Identification of a region of FtsA required for interaction with FtsZ', *Molecular Microbiology*, 64(4), pp. 1129–1138. doi: 10.1111/j.1365-2958.2007.05735.x.

Ptacin, J. L. *et al.* (2014) 'Bacterial scaffold directs pole-specific centromere segregation', *Proceedings of the National Academy of Sciences of the United States of America*, 111(19). doi: 10.1073/pnas.1405188111.

Ptomyces, S. and Chater, K. F. (1993) 'Genetics of Differentiation in Introduction : Differentiation As a Normal Aspect of', *Proteins*, pp. 685–713.

Ramamurthi, K. S. and Losick, R. (2009) 'Negative membrane curvature as a cue for subcellular localization of a bacterial protein', *Proceedings of the National Academy of Sciences*, 106(32), pp. 13541–13545. doi: 10.1073/pnas.0906851106.

Ramm, B., Heermann, T. and Schwille, P. (2019) 'The E. coli MinCDE system in the regulation of protein patterns and gradients', *Cellular and Molecular Life Sciences*. Springer International Publishing, 76(21), pp. 4245–4273. doi: 10.1007/s00018-019-03218-x.

Reimold, C. *et al.* (2013) 'Motion of variable-length MreB filaments at the bacterial cell membrane influences cell morphology', *Molecular Biology of the Cell*, 24(15), pp. 2340–2349. doi: 10.1091/mbc.e12-10-0728.

Rioseras, B. *et al.* (2018) ' Quantitative Proteome and Phosphoproteome Analyses of Streptomyces coelicolor Reveal Proteins and Phosphoproteins Modulating Differentiation and Secondary Metabolism ', *Molecular & Cellular Proteomics*, 17(8), pp. 1591–1611. doi: 10.1074/mcp.ra117.000515.

Rowlett, V. W. and Margolin, W. (2015) 'The Min system and other nucleoid-independent regulators of Z ring positioning', *Frontiers in*

Microbiology, 6(MAY), pp. 1–10. doi: 10.3389/fmicb.2015.00478.

Santos-Beneit, F. *et al.* (2017) 'A mechanism for FtsZ-independent proliferation in Streptomyces', *Nature Communications*. Springer US, 8(1), pp. 1–8. doi: 10.1038/s41467-017-01596-z.

Schoenemann, K. M., Vega, D. E. and Margolin, W. (2020) 'Peptide linkers within the essential ftsZ membrane tethers zipA and ftsA are nonessential for cell division', *Journal of Bacteriology*, 202(6). doi: 10.1128/JB.00720-19.

Scholefield, G. *et al.* (2011) 'Spo0J regulates the oligomeric state of Soj to trigger its switch from an activator to an inhibitor of DNA replication initiation', *Molecular Microbiology*, 79(4), pp. 1089–1100. doi: 10.1111/j.1365-2958.2010.07507.x.

Schwedock, J. *et al.* (1997) 'Assembly of the cell division protein FtsZ into ladder-like structures in the aerial hyphae of Streptomyces coelicolor', *Molecular Microbiology*, 25(05), pp. 847–858. doi: 10.1111/j.1365-2958.1997.mmi507.x.

Sen, B. *et al.* (2019) 'Specific amino acid substitutions in sheet S2 of FtsZ cause spiraling septation and impair assembly cooperativity in Streptomyces.', *submitted to Molecular Microbiology*. doi: 10.1111/mmi.14262.

Sharp, M. D. and Pogliano, K. (2003) 'The Membrane Domain of SpoIIIE Is Required for Membrane Fusion during', 185(6), pp. 1–4. doi: 10.1128/JB.185.6.2005.

Shedlovskiy, D., Shcherbik, N. and Pestov, D. G. (2017) 'One-step hot formamide extraction of RNA from Saccharomyces cerevisiae', *RNA Biology*. Taylor & Francis, 14(12), pp. 1722–1726. doi: 10.1080/15476286.2017.1345417.

Shih, Y. L. and Zheng, M. (2013) 'Spatial control of the cell division site

by the Min system in Escherichia coli', *Environmental Microbiology*, 15(12), pp. 3229–3239. doi: 10.1111/1462-2920.12119.

Sieger, B. *et al.* (2013) 'The lipid II flippase RodA determines morphology and growth in Corynebacterium glutamicum', *Molecular Microbiology*, 90(5), pp. 966–982. doi: 10.1111/mmi.12411.

Sigle, S. *et al.* (2015) 'Synthesis of the spore envelope in the developmental life cycle of Streptomyces coelicolor', *International Journal of Medical Microbiology*. Elsevier GmbH., 305(2), pp. 183–189. doi: 10.1016/j.ijmm.2014.12.014.

Sogues, A. *et al.* (2020) 'Essential dynamic interdependence of FtsZ and SepF for Z-ring and septum formation in Corynebacterium glutamicum', *Nature Communications*. Springer US, 11(1). doi: 10.1038/s41467-020-15490-8.

Sun, N. and Wong, K. (no date) 'Small molecules targeting at the bacterial cell division protein FtsZ as potential antimicrobial agents'.

Szwedziak, P. *et al.* (2012) 'FtsA forms actin-like protofilaments', *EMBO Journal*, 31(10), pp. 2249–2260. doi: 10.1038/emboj.2012.76.

Tocheva, E. I. *et al.* (2011) 'Long helical filaments are not seen encircling cells in electron cryotomograms of rod-shaped bacteria', *Biochemical and Biophysical Research Communications*. Elsevier Inc., 407(4), pp. 650–655. doi: 10.1016/j.bbrc.2011.03.062.

Tonthat, N. K. *et al.* (2013) 'SlmA forms a higher-order structure on DNA that inhibits cytokinetic Z-ring formation over the nucleoid', *Proceedings of the National Academy of Sciences*, 110(26), pp. 10586–10591. doi: 10.1073/pnas.1221036110.

Touzain, F. *et al.* (2011) 'DNA motifs that sculpt the bacterial chromosome', *Nature Reviews Microbiology*. Nature Publishing Group, 9(1), pp. 15–26. doi: 10.1038/nrmicro2477.

Tripathy, S. and Sahu, S. K. (2019) 'FtsZ inhibitors as a new genera of antibacterial agents', *Bioorganic Chemistry*. Elsevier, 91(July), p. 103169. doi: 10.1016/j.bioorg.2019.103169.

Vicente, M. *et al.* (2002) 'Role of the Carboxy Terminus of Escherichia coli FtsA in Self-Interaction and Cell Division', *Journal of Bacteriology*, 182(22), pp. 6366–6373. doi: 10.1128/jb.182.22.6366-6373.2000.

Wang, L. and Lutkenhaus, J. (1998) 'FtsK is an essential cell division protein that is localized to the septum and induced as part of the SOS response', *Molecular Microbiology*, 29(3), pp. 731–740. doi: 10.1046/j.1365-2958.1998.00958.x.

Wang, S. B. *et al.* (2009) 'Domains involved in the in vivo function and oligomerization of apical growth determinant DivIVA in Streptomyces coelicolor', *FEMS Microbiology Letters*, 297(1), pp. 100–109. doi: 10.1111/j.1574-6968.2009.01678.x.

Weiss, D. S. (2004) 'Bacterial cell division and the septal ring', *Molecular Microbiology*, 54(3), pp. 588–597. doi: 10.1111/j.1365-2958.2004.04283.x.

Willemse, J. *et al.* (2011) 'Positive control of cell division: FtsZ is recruited by SsgB during sporulation of Streptomyces', *Genes and Development*, 25(1), pp. 89–99. doi: 10.1101/gad.600211.

Wissel, M. C. and Weiss, D. S. (2004) 'Genetic Analysis of the Cell Division Protein FtsI (PBP3): Amino Acid Substitutions that Impair Septal Localization of FtsI and Recruitment of FtsN', *Journal of Bacteriology*, 186(2), pp. 490–502. doi: 10.1128/JB.186.2.490-502.2004.

Wu, L. J. *et al.* (2009) 'Noc protein binds to specific DNA sequences to coordinate cell division with chromosome segregation', *EMBO Journal*. Nature Publishing Group, 28(13), pp. 1940–1952. doi: 10.1038/emboj.2009.144.

Wu, L. J. and Errington, J. (2004) 'Coordination of cell division and

chromosome segregation by a nucleoid occlusion protein in Bacillus subtilis', *Cell*, 117(7), pp. 915–925. doi: 10.1016/j.cell.2004.06.002.

Wu, L. J. and Errington, J. (2011) 'Nucleoid occlusion and bacterial cell division', *Nature Reviews Microbiology*. Nature Publishing Group, 10(1), pp. 8–12. doi: 10.1038/nrmicro2671.

Zakrzewska-Czerwinska, J. *et al.* (2011) 'Replisome Trafficking in Growing Vegetative Hyphae of Streptomyces coelicolor A3(2)', *Journal of Bacteriology*, 193(5), pp. 1273–1275. doi: 10.1128/jb.01326-10.